

Università degli Studi di Salerno
Department of Chemistry and Biology



Ph.D Course in “Chemistry” – XXX Cycle

Ph.D Thesis in Chemistry

2016-2017

SUPRAMOLECULAR SCAFFOLDS FOR BIOMIMETIC CATALYSIS

Doctorate Student: Pellegrino La Manna

Tutor

Dr. Margherita De Rosa

Co-tutors

Prof. Placido Neri

Prof. Annunziata Soriente

(Università degli Studi di Salerno)

Dr. Maria Grazia Letizia Consoli

(ICB-CNR CATANIA)

Ph.D Coordinator

Prof. Gaetano Guerra

“Non è la conoscenza, ma l’atto di imparare; non il possesso, ma l’atto di arrivarci, che dà la gioia maggiore. Quando ho chiarito ed esaurito un argomento, mi ci allontano, per tornare nell’oscurità; l’uomo non soddisfatto è così strano, che se ha completato una struttura non ce la fa a restarci in pace, ma deve iniziarne un’altra. Immagino che si debba sentire così il conquistatore del mondo che, quando un regno è stato a malapena conquistato, si lancia subito verso un altro”.

[Carl Friedrich Gauss]

To my wonderful family

INDEX

List of Figures.....	iii
List of Abbreviations.....	xi
Abstract.....	xii
1. Introduction: Biomimetic Catalysis.....	1
1.1 Amino acids and Oligopeptides as Biomimetic Catalysts.....	3
1.2 Thiourea based Catalysts as Biomimetic Catalysts.....	6
1.3 Cyclodextrins, Cucurbiturils and Calixarenes as Biomimetic Catalysts.....	10
1.4 Metal Organic Frameworks as Biomimetic Catalysts.....	21
1.5 Molecularly Imprinted Polymers as Biomimetic Catalysts.....	22
1.6 Self-assembled Capsules as Biomimetic Catalysts.....	24
2. On Water Vinylogous Mukaiyama Aldol Reaction promoted by calixarene based catalysts.....	35
2.1 Aldol Reaction.....	35
2.2 Mukaiyama Aldol Reaction.....	38
2.3 Vinylogous Mukaiyama Aldol Reaction.....	39
2.4 On Water Catalysis.....	43
2.5 Results and Discussions.....	50
2.5.1 On Water VMAR promoted by Calixarene based Catalysts.....	50
2.6 CONCLUSIONS.....	78
3. Asymmetric 1,3-dipolar cycloaddition of nitrones to α,β-unsaturated aldehydes promoted by a self-assembled hexameric resorcinarene capsule.....	80
3.1 1,3-Dipolar Cycloadditions.....	80
3.1.1 1,3-DC: Synthesis of Isoxazolidines from Nitrones.....	84
3.2 Results and Discussion.....	88
3.3 CONCLUSIONS.....	96

4. Friedel-Crafts alkylation inside a self-assembled hexameric resorcinarene capsule.....	97
4.1 Friedel-Crafts alkylation.....	97
4.2 Results and Discussion.....	101
4.3 CONCLUSIONS.....	109
5. Experimental Section.....	110
5.1 General experimental conditions.....	110
5.2 General procedure for On Water catalysis of VMAR in presence of thioureidocalixarene catalysts.....	112
5.3 General procedure for On water catalysis of VMAR in presence of aminocalixarene catalysts.....	121
5.4 General procedures for the asymmetric 1,3 DC of nitrones to α,β -unsaturated aldehydes promoted by hexameric resorcinarene capsule.....	139
5.5 General procedures for the FC alkylation inside a self-assembled resorcinarene capsule.....	150

LIST OF FIGURES

Figure 1. Hydrophobic pocket of an enzyme.

Figure 2. Left, mechanism for a common aldol reaction.

Figure 3. *L*-proline and its most exploited derivatives in organocatalysis.

Figure 4. 1,8-biphenylenediol.

Figure 5. First example of cynchona alkaloid based organocatalyst.

Figure 6. Diarilyurea organocatalyst exploited by Curran *et al.* for the Claisen rearrangement of 6-methoxy allyl vinyl ether.

Figure 7. Schreiner's *N,N'*-bis[3,5-bis(trifluoromethyl)phenyl]thiourea.

Figure 8. Jacobsen's polymer-bound thiourea.

Figure 9. An example of enzymatic, bifunctional catalysis.

Figure 10. In red, Takemoto's bifunctional thiourea.

Figure 11. Left, Ricci's thiourea; right, Connon's thiourea.

Figure 12. Lateral view (left), upper view (middle) and chemical structure (right) of CB[6]

Figure 13. Upper, chemical structures of α -, β - and γ -CDs; bottom, related stilized representations of the macrocycles.

Figure 14. Upper, chemical structure and description of the faces of β -CD.

Figure 15. γ -CD based derivative exploited for biomimetic catalysis.

Figure 16. Organometallic complex designed by Breslow and co-workers for the mimicking of P450 enzyme.

Figure 17. Mimicking of chymotrypsin based on a β -CD derivative.

Figure 18. Some members of calixarenes family.

Figure 19. Left, a calix crater; right, structure of *p*-*tert*-butylcalix[4]arene.

Figure 20. Conformations of *p*-*tert*-butylcalix[4]arene.

Figure 21. Calix[4]arene derivative exploited for vancomycin mimics.

Figure 22. Calix[4]arene adorned with *N*-acetyl-D-glucosamine groups used to mimicking lectin.

Figure 23. Calixarene derivative synthesized by Gutsche and co-workers in the purpose of mimicking aldolase enzyme.

Figure 24. Calix[4]arene with azacrowns subunits employed in the cleavage of phosphodiester.

Figure 25. Imprinting of appropriate cavities in a cross-linked polymer by a template (in red) with three different functional groups.

Figure 26. Template for a MIP mimicking a transaminase enzyme.

Figure 27. Fujita and co-workers self-assembled capsule.

Figure 28. Structure of the $[\text{Ga}_4\text{L}_6]^{12-}$ complex.

Figure 29. Nitschke's iron metal cage.

Figure 30. Dimeric capsule (right) formed by self-assembly of molecule to the left.

Figure 31. Rebek's cylindrical capsule.

Figure 32. Left, chemical structure of resorcin[4]arene.

Figure 33. Mechanism proposed by Tiefenbacher for the iminium catalyzed reduction inside the capsule.

Figure 34a. Effect of the proline structure on the organocatalyzed reduction of α,β -unsaturated aldehydes inside and outside the resorcinarene capsule.

Figure 34b. Differences on the organocatalyzed reduction of α,β -unsaturated aldehydes inside and outside the resorcinarene capsule, changing the substrates, by Tiefenbacher group.

Figure 35. Hypothesis formulated by Tiefenbacher for the different selectivity inside the resorcinarene hexameric capsule.

Figure 36. Chemical structures of Atorvastatin (left), Tacrolimus (center) and Discodermolide (right).

Figure 37. Condensation of glyceraldehyde-3-phosphate with dihydroxyacetone phosphate.

Figure 38. Addition of oxaloacetic acid to acetyl-coenzyme A.

Figure 39. Cleavage of fructose 1,6 biphosphate to give glyceraldehyde-3-phosphate.

Figure 40. Mechanism for aldol reaction, in acidic conditions (upper) and in basic conditions (bottom).

Figure 41. From left to right: Carreira's, Yamamoto's and Corey's catalysts.

Figure 42. Comparison between a VMAR and a *normal* aldol reaction.

Figure 43. Comparison between metal and silyl enolate in the attack position for the VMAR.

Figure 44. VMAR between a dioxinone derivative and aldehydes promoted by Sato and Kaneko catalyst.

Figure 45. Carreira's catalyst for addition of dienolates to aldehydes.

Figure 46. Evans Cu-pybox ligand based catalysts.

Figure 47. VMAR with α -ketoesters promoted by a Cu-sulfoximine catalyst.

Figure 48. Examples of hydrogen bonding catalysis of VMAR. Catalysts employed are placed in blue frames.

Figure 49. From left to right: Feng's and Terada's catalysts.

Figure 50. From left to right: chemical structures of salinipyrone A and castanospermine.

Figure 51. Upper, from left to right: rasfonin and trichostatin D; bottom: khafrefungin.

Figure 52. Model proposed by Marcus for the *on water* catalysis.

Figure 53. Diels-Alder cycloaddition between anthracene-9-carbinol and *N*-ethylmaleimide.

Figure 54. Differences in the catalysis of Passerini reaction when performed in presence of water and in dichloromethane.

Figure 55. Diels-Alder (top) and nucleophilic opening of the epoxide performed by Sharpless group under *on water* conditions at concentration about 0.2 M.

Figure 56. The model proposed by Beattie *et al.*

Figure 57. Solvent studies for Mukaiyama aldol reaction between 2-(trimethylsilyloxy)furan and pyruvic aldehyde dimethyl acetal.

Figure 58. *On water* catalysis between nitrostyrene and dimethylmalonate.

Figure 59. Catalysts exploited for VMAR under *on water* conditions.

Figure 60. Plausible catalytic cycle for the VMAR catalyzed by calixarene derivatives **1** and **4**.

Figure 61. Different views of the optimized structure of **7a**⋅**1** complex obtained by molecular mechanics calculation (AMBER force field).

Figure 62. Proposed transition state model for the *on water* VMAR of **4** and **6** with α -ketoester **7a**.

Figure 63. Optimized structures of the: (a) **7a**⋅**4**, (b) **7b**⋅**4**, (c) **7c**⋅**4**, (d) **7d**⋅**4** complexes obtained by molecular mechanics calculations (AMBER force field).

Figure 64. Structure of screened catalysts **3**, **10**, **11a**, **11b**, **12**.

Figure 65. Plausible catalytic cycle for VMAR catalyzed by calixarene catalyst **10**.

Figure 66. Optimized structures of the **7a-c**·**10** complexes obtained by molecular mechanics calculations (AMBER force field).

Figure 67. Plausible catalytic cycle for VMAR catalyzed by calixarene **10**.

Figure 68. (a and b) Minimized structures (molecular mechanics calculations, AMBER force field) of the **7i**·**10** and **7j**·**10** complexes.

Figure 69. The *p*-substitution on the phenyl ring in **8b**, **8g**, **8h** and **8i** regulates the solid state self-assembly of γ -butenolides in helices, columns of self-assembled dimers or linear chains

Figure 70. A spiro-sugar isoxazolidine scaffold as polyfunctional building block for peptidomimetics design.

Figure 71. Allyl and allenyl anion types of dipoles for 1,3-DC.

Figure 72. A series of common dipoles and dipolarophiles for 1,3-DC.

Figure 73. Possible mechanisms for the 1,3-DC.

Figure 74. The three main mode in which FMO interact in 1,3-DC.

Figure 75. *Endo* and *exo* transition states for the 1,3-DC between nitron and electron-poor alkenes.

Figure 76. The pairs of enantiomers for *endo* and *exo* regioisomers resulting from the 1,3-DC between electron-poor alkenes and nitrones.

Figure 77. Examples of natural products in which isoxazolidine moiety (in blue) occurs.

Figure 78. 3,5-cycloadduct resulting from an inverse-electron-demand cycloaddition.

Figure 79. The eight stereoisomers originating from the 1,3-DC of nitrones with unsaturated aldehydes.

Figure 80. MacMillan's imidazolidinones. Left: first generation; right: second generation.

Figure 81. Self-assembly of resorcinarene **14** in water saturated CDCl_3 to give capsule **15**.

Figure 82. 3D pictures of the complex **16a** and **21** \subset **15**.

Figure 83. Proposed mechanism for the 1,3-DC between **16a** and **17a** inside the cage **15**.

Figure 84. A series of pesticides and fragrance of industrial relevance.

Figure 85. Some diarylalkane-based pharmaceuticals.

Figure 86. Some isolated natural product with indole framework.

Figure 87. Mechanism for the FC reaction of benzene with alkyl chlorides catalyzed by AlCl_3 .

Figure S1. Plot of the chemical shift of NH proton of catalyst **1** (3.2 mM in 0.5 mL CDCl_3 at 298 K) versus $[\mathbf{7a}]/10^{-3}$ at 25 °C in CDCl_3 .

Figure S2. Plot of the chemical shift of NH proton of catalyst **1** (3.2 mM in 0.5 mL CDCl_3 at 298 K) versus $[\mathbf{7b}]/10^{-3}$ at 25 °C in CDCl_3 .

Figure S3. Up: kinetics of the VMAR between ketoester **7a**, silyloxyfuran **6** and catalyst **10** in presence of several organic solvents; bottom: graphical comparison between reaction performed *on water* and *in organic solvents*.

Figure S4. Recycling experiments for the reaction between **6** and **7a** promoted by **10**.

Figure S5. Plot of δ (ppm) for ArHNH₂ proton of **10** as a function of the concentration of **7a** (CDCl₃, 298 K, 400 MHz).

Figure S6. Plot of δ (ppm) for ArHNH₂ proton of **10** as a function of the concentration of **7i** (CDCl₃, 298 K, 400 MHz).

Figure S7. Titration of **10** with **7a**.

Figure S8. Titration of **10** with **7i**.

Figure S9. Ellipsoid plots at 50% probability for γ -hydroxybutenolides **8b** (a), **8g** (b), **8h** (c), **8i** (d) and **8k** (e).

Figure S10. Relevant regions of ¹H NMR spectrum (400 MHz, CDCl₃, 298 K) showing: *L*-proline encapsulated (**20e**) (bottom); crotonaldehyde (**17a**) inside the capsule (middle), mixture of **20e** and **17a** (top).

Figure S11. DOSY NMR (600 MHz, CDCl₃, 298 K) of the capsule **15** at left and of the solution containing capsule **15** and crotonaldehyde **17a** at right.

Figure S12. DOSY NMR (600 MHz, CDCl₃, 298 K) of capsule **15** and iminium species **21**.

Figure S13. NOESY NMR (400 MHz, 298 K, CDCl₃) of the capsule **15** and iminium species **21**.

Figure S14. Selected expansions of NOESY NMR spectrum in **Figure S13**. Exchange peaks between aldehyde **17a** *outside* and *inside* the capsule **15** (top) and aldehyde **17a** and iminium species **21** (bottom) are visible.

Figure S15. Relevant region of NOESY NMR (400 MHz, CDCl₃, 298 K), d₈ = 250 ms, spectrum of the mixture of capsule **15** and **28**.

Figure S16. Relevant region of NOESY NMR (400 MHz, CDCl₃, 298 K), d₈ = 250 ms, spectrum of mixture of capsule **15** and **28**.

Figure S17. Relevant region of COSY NMR experiment performed on the mixture of capsule **15** and **28**. As can be seen, the pattern of peaks present in the range 5.1-5.6 ppm shows couplings involving two sets of protons.

Figure S18. Relevant region of NOESY NMR (600 MHz, CDCl₃, 298 K) experiment performed on the mixture of capsule **15** and benzyl chloride (**29**). As can be seen, an exchange peak involving benzylic protons is visible (indicated with blue star).

Figure S19. NOESY NMR (600 MHz, CDCl₃, 298 K), d8 = 250 ms, performed on the solution of resorcinarene capsule **15** and *N*-methylpyrrole (**28**).

Figure S20. DOSY NMR (600 MHz, CDCl₃, 298 K) of the solution of resorcinarene capsule **15** and *N*-methylpyrrole (**28**).

Figure S21. ¹H NMR (400 MHz, CDCl₃, 298 K) of the solution containing hexameric resorcinarene capsule **15**, *N*-methylpyrrole (**28**) and benzyl chloride (**29**) (in the same ratio used in the model reaction).

Figure S22. NOESY NMR (400 MHz, CDCl₃, 298 K), d8 = 250 ms, of the mixture of benzyl chloride (**29**) and *N*-methylpyrrole (**28**) in presence of the capsule **15**.

Figure S23. Plot of data for the product inhibition experiments summarized in **Tables S11-14**.

Figure S24. ¹H NMR Spectrum (300 MHz, CDCl₃, 298 K) of the solution (inhibition experiment) containing **28** (1.5 eq), **29** (1 eq) and capsule **15** (0.52 eq) in presence of NEt₄•BF₄ (10 eq respect to the resorcinarene capsule, 0.84 mmol).

LIST OF ABBREVIATIONS

BINAP	2,2'-Bis(diphenylphosphino)-1,1'-binaphthyl
Bn	benzyl
br	broad
Bu ^t	<i>tert</i> -butyl
CB	CUCURBITURYL
CD	CYCLODEXTRIN
CH ₂ Cl ₂	dichloromethane
CH ₃ OH	methanol
CN	cyano
DC	DIPOLAR CYCLOADDITION
d	doublet
dd	double doublet
DMSO	dimethylsulfoxide
dr	diastereoisomeric ratio
ee	enantiomeric excess
eq.	equivalent(s)
ESI	Electrospray Ionization
FC	FRIEDEL-CRAFTS
FMO	Frontier Molecular Orbital
H ₂ O	water
HOMO	Higher Occupied Molecular Orbital
HRMS	High Resolution Mass Spectrometry
LUMO	Lower Unoccupied Molecular Orbital
MIP	MOLECULARLY IMPRINTED POLYMERS

<i>m/z</i>	atomic mass unit per charge
MOF	METAL ORGANIC FRAMEWORK
NEt ₄ •BF ₄	Tetraethylammonium Tetrafluoroborate
NMR	Nuclear Magnetic Resonance
<i>o</i>	ortho
<i>p</i>	para
Ph	phenyl
Pr	propyl
s	singlet
t	triplet
TADDOL	$\alpha,\alpha,\alpha',\alpha'$ -tetraaryl-1,3-dioxolan-4,5-dimethanol
Tf	triflate
TFA	trifluoroacetic acid
THF	tetrahydrofuran
THT	tail to head
TMS	trimethylsilyl
VMAR	VINYLOGOUS MUKAIYAMA ALDOL REACTION

Abstract

This PhD thesis is concerned with the design, synthesis and the characterization of supramolecular scaffolds for biomimetic catalysis. Development of new organocatalytic systems based upon well-designed calix[4]arene derivatives was made and their application for on water catalysis of the Vinylogous Mukaiyama Aldol Reaction (VMAR) was explored. The obtained results showed that combination of high hydrophobicity and synthetic versatility of calixarene macrocycles can be exploited for a kind of catalysis which permits the use of mild conditions and the choice of a reaction medium, water, different from organic solvents which are largely employed for the synthesis of fine chemicals and are responsible of large energy usage and industrial pollution. So, calixarene macrocycles can be exploited to develop new environmentally oriented catalytic approaches. The target molecules bear a butenolide moiety substituted at γ position; this moiety represents a recurring motif in several compounds displaying a wide range of biological activities. Moreover, thanks to the presence of functional groups typically involved in processes of molecular recognition through weak interactions, like hydroxyl and carbonyl functionalities, these products exhibit interesting features in their solid state assembly, showing that playing on non covalent interactions could be a good opportunity to build supramolecular architectures resembling the natural ones.

Resorcin[4]arene self-assembled capsules were applied to catalyze the 1,3-dipolar cycloaddition between nitrones and unsaturated aldehydes and Friedel-Crafts reaction between aromatic (heteroaromatic) compounds and benzyl chloride. In both cases, the results indicated that resorcin[4]arene hexameric capsule is able to catalyze complex reaction thanks to its recognition and Brønsted acidity. The encapsulation of reagents into a confined environment, in the case of 1,3-dipolar cycloaddition, has made possible to obtain isoxazolidines with a certain grade of control on regio- and stereo-selectivity; in addition, nanoconfinement and hydrogen

bonding by OH groups of the resorcinarene subunits allowed Friedel Crafts alkylation with a wide range of electrophiles. Products from 1,3-dipolar cycloaddition and benzylated products from Friedel-Crafts alkylation are, on different levels, a viable building block for preparation of natural compounds and in medicinal chemistry.

Considering these results, it's reasonable to think that mimicking at a certain level the *modus operandi* of natural enzymes can represent a turning point in the developing of new pathways in the field of the organocatalysis. Particularly, an enzyme-like catalysis can be obtained by exploiting calixarene hydrophobic cavity and their ability to recognize and to discriminate different substrates based on non-covalent interactions (particularly hydrogen bonding), or by making use of self-assembled resorcin[4]arene capsules.

1. Introduction: Biomimetic Catalysis

1.1 Biomimetic catalysis

Biomimetic catalysis is only a part of a melting pot composed by several areas of chemistry and named *biomimetic chemistry*¹. The latter term was forged in 1972 by Breslow² to enlighten the effort made by chemists to apply informations furnished by biological models to common chemical systems and so to denote a border zone between biology and chemistry in which not only chemistry takes inspiration from biology, but also these two latter communicate and influence themselves. This large set ranges from the development and the study of novel supramolecular architectures thought to be considered artificial enzymes³, also in order to gain better understanding of the working principles of natural enzymes, product of an evolution process lasted billion of years, until to the production of new, *bioinspired*, materials with fascinating properties resembling those natural ones.

As a part of biomimetic chemistry, biomimetic catalysis refers to a certain kind of chemistry which has, as one of its declared goals, catalysis of chemical reactions through the mimicking of key features of enzymes⁴. A growing interest has been focused on this research field, considering that chemical reactions catalyzed by enzymes show remarkable rate acceleration, high stereoselectivity (both regio-, diastereo- and enantioselectivity), low waste generation, reduced energy consumption and can be performed under mild conditions⁵. Enzymes, generally, do their work in an aqueous environment, operating in the mixture of biomolecules inside the cell within narrow criteria and preserving the functionality and integrity of

¹ Marchetti, L.; Levine, M., *ACS Catal.*, **2011**, *1*, 1090.

² Breslow, R., *Chem. Soc. Rev.*, **1972**, *1*, 553.

³ Breslow, R., *Acc. Chem. Res.*, **1995**, *28*, 146.

⁴ Breslow, R., *Acc. Chem. Res.*, **1980**, *13*, 170.

⁵ Kuah, E.; Toh, S.; Yee, J.; Ma, Q.; Gao, Z., *Chem. Eur. J.*, **2016**, *22*, 8404.

biological systems in which they work by making use of their active site located inside a hydrophobic (Figure 1) pocket⁶. In this confined nanospace, a huge number of favorable interactions, especially non covalent, bind the right substrates and allow to these latter to acquire the appropriate orientation to react themselves.

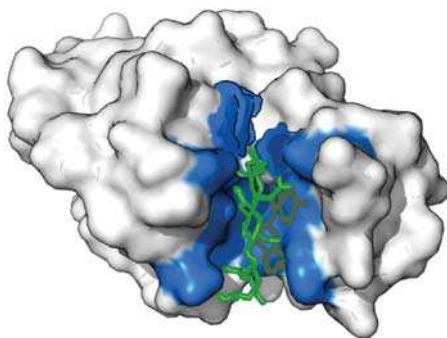


Figure 1. Hydrophobic pocket of an enzyme. Active site is highlighted in *blue*, while substrate in the site is highlighted in *green*.

So, trying to emulate the catalytic enzymatic performances gives opportunity to exploit water as reaction medium and to play with a plethora of functional groups in order to build an array of interactions which can work together to form nanosized reaction vessels which match the cooperativity and the versatility of the existing natural counterparts. As a result, molecules with various shapes, dimensions and functionalities were designed to answer typical issues of biomimetic catalysis and to overcome its own challenges. Also, it's possible to play with non covalent interactions in order to build new materials, with suitable properties to be utilized in crystal engineering⁷.

⁶ Kirby, J. A., *Angew. Chem. Int. Ed.*, **1996**, 35, 707.

⁷ Xia, Z., *Biomimetic Principles and Design of Advanced Engineering Materials*, Wiley, Hoboken, **2016**.

1.1 Amino acids and Oligopeptides as biomimetic catalysts

Initially, biomimetic catalysis was strictly linked to the organocatalysis⁸. Low molecular weight molecules were exploited to have a deeper insight on enzyme *modus operandi*. The first footsteps into biomimetic catalysis can be dated back to 1928, publication's year of *Analogies in the catalytic action of enzymes and definite organic substances* of the German chemist Wolfgang Langenbeck⁹. After three years, the use of amino acids as catalysts for the aldol reaction was reported¹⁰. From this point, advances were constant but slow and except for a few of cases (particularly L-proline)¹¹, it was not until the end of twentieth century that useful applications of organocatalysts were achieved. Nowadays, we have witnessed to a tremendous evolution of organocatalytic methods, in part due to the possibility of drastically reduce the amount of heavy metal ions contaminating final products and the environment and also to the increasing importance of concepts as *green chemistry*¹²

As basic building units and functional groups in nature and as the simplest, most economic and readily available source of chirality, it has been reasonable to think to employ amino acids as biomimetic catalysts. Bearing both acid and base groups, they can promote cooperatively chemical reactions, at some extent emulating enzymes. Moreover, ecotoxicity of these compounds is slow so strategies involving application of these molecules in several steps of synthesis of bioactive compounds is convenient.

Their first use in organocatalysis dates to 1931. Alanine was exploited by Fischer and Marshall to catalyzed aldol condensation. Later, in 1953, catalysis of Knoevenagel

⁸ *Asymmetric Organocatalysis: From Biomimetic Concepts to Applications in Asymmetric Synthesis* (eds Berkessel A. & Gröger H.), Wiley-VCH, Weinheim, **2005**.

⁹ Langenbeck, W., *Angew. Chem.*, **1928**, *41*, 740.

¹⁰ Fischer, F. G.; Marshall, A., *Chem. Ber.*, **1931**, *64*, 2825.

¹¹ Hajos, Z. G.; Parrish, D. R., *J. Org. Chem.*, **1974**, *39*, 1615.

¹² *Catalysis for Sustainability: Goals, Challenges, and Impacts*, (ed Umile T. P.), CRC Press, Boca Raton, **2015**.

reaction catalyzed by amino acids was investigated¹³, but the real turning point was in 1971, when Hajos, Parrish, Eder, Sauer, Wiechert exploited, with good results, L-proline as a catalyst for Robinson annulation of meso-trienones¹⁴ to give as a product the Wiechert-Mischer ketone. As we can see, the proposed reaction mechanism is similar to that of type I aldolase (Figure 2).

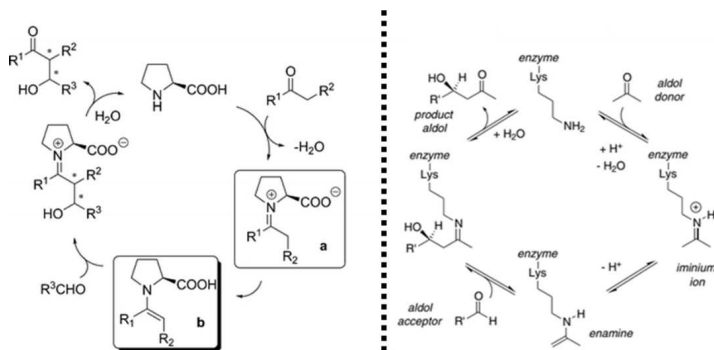


Figure 2. Left, mechanism for a common aldol reaction; right, mechanism for reaction catalyzed by aldolase type I.

The same catalyst was chosen to perform intermolecular aldol and Mannich reactions^{15,16}. Moreover, to gain more stereocontrol in some reactions, different research teams introduced modifications on the basic skeleton of the amino acid. For example, L-proline was functionalized with tetrazole and acylsulfonamide moieties to achieve a more efficient catalysis of Mannich and retro-Mannich reactions¹⁷. Probably, the most renowned derivative of the L-proline is the diarylprolinol silyl ether, which has allowed to boost up the enantioselectivity for many kind of reactions¹⁸. Usage of amino acids in catalysis is not limited to L-proline and its derivatives, although this latter represents one of the most successful and studied

¹³ Prout, F. S., *J. Org. Chem.*, **1953**, *18*, 928.

¹⁴ Eder, U.; Sauer, G.; Wiechert, R., *Angew. Chem. Int. Ed.*, **1971**, *10*, 496.

¹⁵ List, B.; Lerner, R. A.; Barbas III, C. F., *J. Am. Chem. Soc.*, **2000**, *122*, 2395.

¹⁶ List, B., *J. Am. Chem. Soc.*, **2000**, *122*, 9336.

¹⁷ Cobb, J. A. A.; Shaw, M. D.; Longbottom, D. A.; Gold, J. B.; Ley, S. V., *Org. Biomol. Chem.*, **2005**, *3*, 84.

¹⁸ Jensen, K. L.; Dickmeiss, G.; Jiang, H.; Albrecht, L.; Jørgensen, K. A., *Acc. Chem. Res.*, **2012**, *45*, 248.

organocatalysts and object of continuous design (Figure 3) : *L*-threonine derivatives are reported to catalyze *anti*-selective Mannich reaction in a purely aqueous system¹⁹; *L*-tyrosine was applied to the catalysis of the Knoevenagel condensation of arylaldehydes²⁰; *L*-cysteine based catalyst was found to be efficient to afford products of the enantioselective Rauhut-Currier reaction²¹; a green method for the self condensation of aldehydes has been successfully accomplished exploring catalytic activity of *L*-lysine²² and, eventually, all the naturally occurring α -amino acids were exploited to obtain cyclic carbonates via coupling of carbon dioxide with epoxides²³.

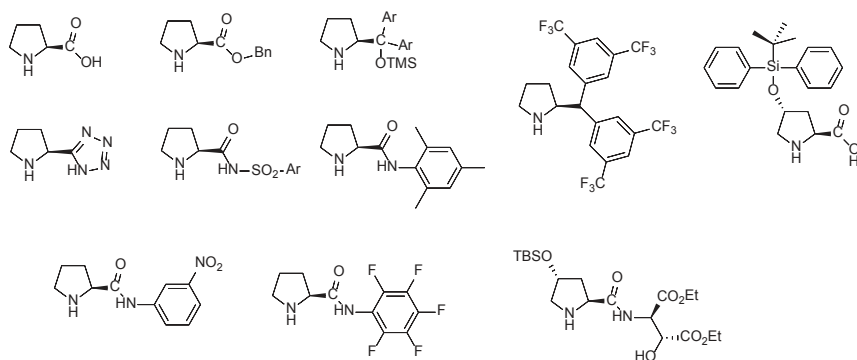


Figure 3. *L*-proline and its most exploited derivatives in organocatalysis.

A straightforward evolution to the utilization of repertoire of single amino acids is represented by peptides. Increasing number of amino acids residues can be a plan to getting close to the mimicking of natural enzymes and synthesis of artificial ones; in fact, the extraordinary degrees of stereoselectivity showed by enzymes is due to the presence in the active site of *multiple* amino acids arrayed in a specific

¹⁹ Cheng, L.; Wu, X.; Lu, Y., *Org. Biomol. Chem.*, **2007**, *5*, 1018.

²⁰ Thirupathi, G.; Venkatanarayana, M.; Dubey, P. K.; Kumari, Y. B., *Org. Chem. Int.*, **2012**, *1*

²¹ Miller, J. S.; Aroyan, C. E., *J. Am. Chem. Soc.*, **2007**, *129*, 256.

²² Watanabe, Y.; Sawada, K.; Hayashi, M., *Green Chem.*, **2010**, *12*, 384.

²³ Qi, C.; Jiang, H.; Wang, Z.; Zou, B.; Yang, S., *Synlett*, **2007**, *2*, 255.

manner²⁴. One of the challenges offered by their use in organocatalysis lies in the difficulty in predicting the conformation of even di- or tri-peptides²⁵, consequently a rational design of a peptide based catalyst remains not an easy issue, partially made less complicated via employment of combinatorial chemistry and novel screening methods. First remarkable example of their application in organocatalysis goes back to 1979, when Oku, Ito and Inoue reported the first asymmetric hydrocyanation of benzaldehyde to give mandelonitrile with a 90% of enantiomeric excess thanks to the catalytic activity showed by a synthetic dipeptide, *cyclo-L-Hys-L-Phe*²⁶. One year after, in 1980, highly stereoselective epoxidation of chalcones was performed by poly[(*S*)-alanine]²⁷. Epoxidations were also performed by aspartic acid-containing peptides²⁸. Regarding C-C bond forming reactions, in addition to the aforementioned hydrocyanation reaction, peptides were adopted to catalyze Michael²⁹, aldol³⁰ and Friedel-Crafts reactions³¹. A cornerstone in the field is surely represented by the work of Miller³², who, in 1998, succeeded to catalyze kinetic resolution of alcohols thanks to a tripeptide containing 3-(1-imidazolyl)-(*S*)-alanine as the *N*-terminal amino acid.

1.2 Thiourea based Catalysts as Biomimetic Catalysts

Hydrogen bonding is of great importance for the realization of the structures of biological macromolecules and it behaves as a medium by which transmission of

²⁴ Davie, E. A. C.; Mennen, S. M.; Xu, Y.; Miller, J. S., *Chem. Rev.* **2007**, *107*, 5759.

²⁵ Wennemers, H., *Chem. Commun.*, **2011**, *47*, 12036.

²⁶ Oku, J.; Ito, N.; Inoue, S., *Makromol. Chem.*, **1979**, *180*, 1089.

²⁷ Juliá, S.; Masana, J.; Vega, J. C., *Angew. Chem. Int. Ed.*, **1980**, *19*, 929.

²⁸ Gorka, P.; Jakobsche, C. E.; Miller, S. J., *J. Am. Chem. Soc.*, **2007**, *129*, 8710.

²⁹ Xu, Y.; Zou, W.; Sundén, H.; Ibrahim, I.; Córdova, A., *Adv. Synth. Catal.*, **2006**, *348*, 418.

³⁰ Tang, Z.; Yang, Z.-H.; Cun, L.-F.; Gong, L.-Z.; Mi, A.-Q.; Jiang, Y.-Z., *Org. Lett.*, **2004**, *6*, 2285.

³¹ Akagawa, K.; Yamashita, T.; Sakamoto, S.; Kudo, K., *Tetrahedron Lett.*, **2009**, *50*, 5602.

³² Miller, S. J.; Copeland, G. T.; Papaioannou, N.; Horstmann, T. E.; Ruel, E. M., *J. Am. Chem. Soc.*, **1998**, *120*, 1629.

information occurs in nature³³. This is especially true if we consider its fundamental contribution in the base pairing of nucleic acids³⁴, in molecular recognition³⁵ (above all anion recognition) and in the operating of enzymes³⁶.

First milestones in hydrogen bonding catalysis were laid in 1980s, when Hine group found that conformationally rigid 1,8-biphenylenediol (Figure 4) was able to catalyze reaction of phenyl glycidyl ether with diethylamine through nucleophilic activation by two hydrogen bonds³⁷.

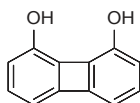


Figure 4. 1,8-biphenylenediol.

During the same decade, Hiemstra and Wynberg³⁸ reported an asymmetric conjugate addition reaction catalyzed by cinchona alkaloids carrying free hydroxyl moieties (Figure 5).

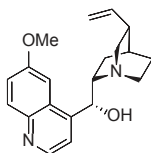


Figure 5. First example of cinchona alkaloid based organocatalyst.

Next important step was made by Curran³⁹, who discovered that a diarylurea (Figure 6) catalyzed dipolar Claisen rearrangement by dual hydrogen bonding.

³³ Brancato, G.; Coutrot, F.; Leigh, D. A.; Murphy, A.; Wong, J. K. Y.; Zerbetto, F.; *Proc. Natl. Acad. Sci.*, **2002**, *99*, 4967.

³⁴ Jeffrey, G. A.; Saenger, W. *Hydrogen Bonding in Biological Structures*, Springer, Berlin, **1991**.

³⁵ *Hydrogen Bonded Supramolecular Structures*, (eds Li, Z.-T. & Wu, L.-Z.) Springer, Berlin, **2015**.

³⁶ Jacobsen, E. N.; Knowles, R. R., *Proc. Natl. Acad. Sci.*, **2010**, *107*, 20678.

³⁷ Hine, J.; Linden, S. M.; KanagasaBapathy, V. M., *J. Am. Chem. Soc.*, **1985**, *107*, 1082.

³⁸ Hiemstra, H.; Wynberg, H., *J. Am. Chem. Soc.*, **1981**, *103*, 417.

³⁹ Curran, P. D.; Kuo, L. H., *Tetrahedron Lett.*, **1995**, *36*, 6647.

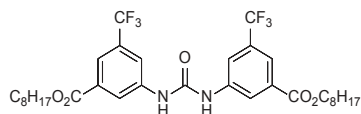


Figure 6. Diaryliurea organocatalyst exploited by Curran *et al.* for the Claisen rearrangement of 6-methoxy allyl vinyl ether.

Subsequently, in 2001, Schreiner *et al.*⁴⁰ showed that a thiourea based catalyst bearing electron withdrawing substituents (Figure 7) was effective in Diels Alder reaction. The same catalyst resulted also effective in acetalization of various aliphatic and aromatic carbonyl compounds⁴¹, due to stabilization of oxyanion intermediates: the anion recognition of thiourea functionality was further highlighted in 2007, when biomimetic reduction of conjugated nitroalkene was performed thanks to ability of thiourea of recognize nitro group⁴².

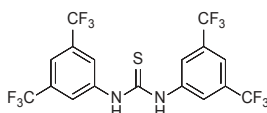


Figure 7. Schreiner's *N,N'*-bis[3,5-bis(trifluoromethyl)phenyl]thiourea.

A few years before, Jacobsen *et al.* designed a general and enantioselective catalyst for the Strecker reaction, based on a thiourea framework derivatized with a salicylidene imine (Figure 8) functionality⁴³.

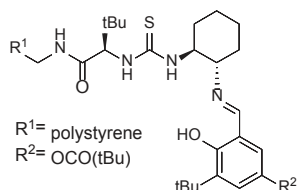


Figure 8. Jacobsen's polymer-bound thiourea.

⁴⁰ Schreiner, P. R.; Wittkopp, A., *Org. Lett.*, **2002**, 4, 217.

⁴¹ Kotke, M.; Schreiner, P. R., *Tetrahedron*, **2006**, 62, 434.

⁴² Zhang, Z.; Schreiner, P. R., *Synthesis*, **2007**, 16, 2559.

⁴³ Sigman, S. M.; Jacobsen, E. N., *J. Am. Chem. Soc.*, **1998**, 120, 4901.

A logical evolution of catalytic systems shown above was represented by the introduction of *bifunctional* catalysts, containing a nucleophile activating functionality (Lewis or Brønsted base)⁴⁴. They resemble natural enzymes thanks to their ability to activate nucleophile and electrophile simultaneously (Figure 9). The most known case is maybe represented by Takemoto's thiourea⁴⁵, designed to bear a tertiary amine group (Figure 10) in order to promote the enantioselective Michael reaction of malonates to nitroolefines. Tertiary amine functionality was also incorporated in Jacobsen's thiourea, exploited with success in cyanosilylation of ketones⁴⁶. Simple tertiary amine moiety was replaced by binaphthyl-derived tertiary amine by Wang *et al* and their organocatalyst was found to efficiently perform Morita-Baylis-Hilman reactions⁴⁷. In the same year, Ricci *et al.* proposed a chiral thiourea derivative with an additional hydroxy-group and it was employed in Friedel-Crafts alkylation of nitroalkenes with indoles⁴⁸. Later, Connon *et al.* introduced a thiourea based cinchona alkaloid (Figure 11) catalyst⁴⁹. Other organocatalysts were developed, playing on the tunability of N-substituents in terms of basicity and structure and even now many efforts are conducted on this research field^{50,51}.

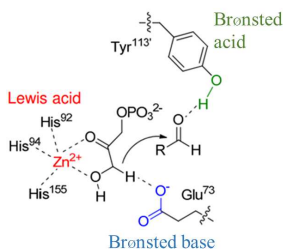


Figure 9. An example of enzymatic, bifunctional catalysis.

⁴⁴ Dixon, D. J., *Beilstein J. Org. Chem.*, **2016**, *12*, 1079.

⁴⁵ Okino, T.; Hoashi, Y.; Takemoto, Y., *J. Am. Chem. Soc.*, **2003**, *125*, 12672.

⁴⁶ Fuerst, D. E.; Jacobsen, E. N., *J. Am. Chem. Soc.*, **2005**, *127*, 8964.

⁴⁷ Wang, J.; Li, H.; Yu, X.; Zu, L.; Wang, W., *Org. Lett.*, **2005**, *7*, 4293.

⁴⁸ Herrera, P. R.; Sgarzani, V.; Bernardi, L.; Ricci, A., *Angew. Chem. Int. Ed.*, **2005**, *44*, 6576.

⁴⁹ McCooey, S. H.; Connon, S. J., *Angew. Chem. Int. Ed.*, **2005**, *44*, 6367.

⁵⁰ Cao, C.-L.; Ye, M.-C.; Sun, X.-L.; Tang, Y., *Org. Lett.*, **2006**, *8*, 2901.

⁵¹ Yamaoka, Y.; Miyabe, H.; Takemoto, Y., *J. Am. Chem. Soc.*, **2007**, *129*, 6686.

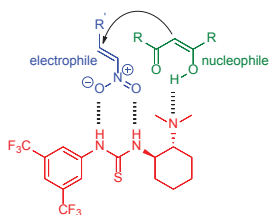


Figure 10. In red, Takemoto's bifunctional thiourea. It can be seen that the catalyst bears a thiourea moiety to activate the electrophile (in blue) and a basic tertiary amine moiety to activate the nucleophile (in green).

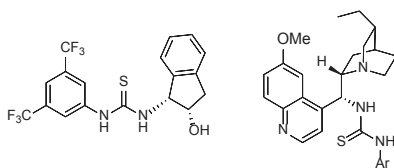


Figure 11. Left, Ricci's thiourea; right, Connon's thiourea.

1.3 Cyclodextrins, Cucurbiturils and Calixarenes as Biomimetic Catalysts

The active site of enzymes, responsible for their high control in regio- and stereoselectivity of chemical reactions, is buried inside an hydrophobic pocket, where stabilization of reactants and assumption of a fitting orientation or conformation occurs. If we consider supramolecular systems provided with hydrophobic cavities of suitable dimensions and able to recognize selectively the reactants, we can look at them as possible candidates to mimic natural enzymes to some extent.

Cucurbiturils (CB[n]) are macrocycles being the product condensation reaction between formaldehyde and glycoluril⁵². The glycoluril subunits are bound in a ring

⁵² Lagona, J.; Mukhopadhyay, P.; Chakrabarti, S.; Isaacs, L., *Angew. Chem. Int. Ed.*, **2005**, *44*, 4844.

like arrangement via methylene bridges with a very rigid structure, if compared to other kind of macrocycles. Resemblance of the macromolecules with a pumpkin (belonging to the *cucurbitaceae* family) gives the name to them (Figure 12). They possess not only a hydrophobic cavity, but also two negatively charged carbonyl lined portals of great importance for molecular recognition. Indeed, these two distinctive elements act together in order to permit to the CB[n] to efficiently recognize both transition metal cations and moieties with hydrophobic and cationic character⁵³, like cadaverine. In addition, also amino acids and short peptides are recognized by CB[n]⁵⁴



Figure 12. Lateral view (left), upper view (middle) and chemical structure (right) of CB[6].

CB[n] are able to promote various photochemical and thermochemical reactions with an interesting increase in stereoselectivity and rate enhancement⁵⁵. Cucurbit[6]uril (CB6) has been showed to be able to catalyze 1,3-dipolar cycloaddition between alkynes and alkyl azides⁵⁶; cucurbit[7]uril (CB7) has been employed to perform a stereoselective [4+4] photodimerization of 2-aminopyridine hydrochloride⁵⁷; actually, cucurbit[8]uril (CB8) has been exploited to promote photodimerization of *trans*-cinnamic acids⁵⁸. Furthermore, it's noteworthy to observe that inclusion complexes with macrocyclic hosts, among which CB[n], have shown a moderate increase in pka of the complexed guests and this feature has

⁵³ Barrow, J. S.; Kasera, S.; Rowland, M. J.; Del Barrio, J.; Scherman, O. A., *Chem. Rev.* **2015**, *115*, 12320.

⁵⁴ Buschmann, H. J.; Mutihac, L.; Mutihac, R. C.; Schollmeyer, E., *Thermochim. Acta*, **2005**, *430*, 79.

⁵⁵ Assaf, K. I.; Nau, W. M., *Chem. Soc. Rev.*, **2015**, *44*, 394.

⁵⁶ Mock, W. L.; Irra, T. A.; Wepsiec, J. P.; Adhya, M., *J. Org. Chem.*, **1989**, *54*, 5302.

⁵⁷ Wang, R.; Yuan, L.; Macartney, D. H., *J. Org. Chem.*, **2006**, *71*, 1237.

⁵⁸ Pattabiraman, M.; Natarajan, A.; Kaanumalle, L. S.; Ramamurthy, V., *Org. Lett.*, **2005**, *7*, 529.

been proved a key point to promote protonation of included molecules. Especially, it has been found that CB[n] catalyze acid hydrolysis of oximes, amides and carbamates⁵⁹. Despite of all these results, application of CB[n] to biomimetic catalysis is limited by difficulties in functionalization of the surface of the macrocycle and to their limited solubility in common solvents, if compared to cyclodextrins (CDs). Some attempt has been made to derivatize CBs; in particular CB[6] was successfully derivatized to make them more soluble in water and organic solvents starting from condensation of cyclohexanoglycoluril building block with formaldehyde⁶⁰.

CDs are a class of structurally similar compounds made up of cyclic oligosaccharides of amylose consisting of, generally, a number of glucopyranose subunits between 6 and 8 (Figure 13)⁶¹.

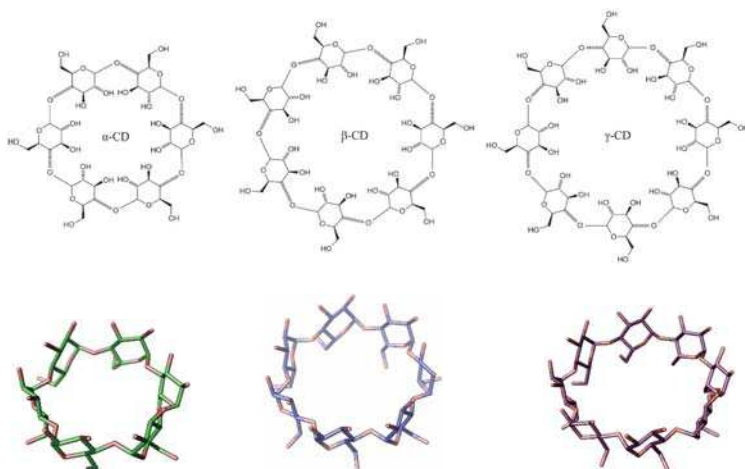


Figure 13. Upper, chemical structures of α -, β - and γ -CDs; bottom, related stylized representations of the macrocycles.

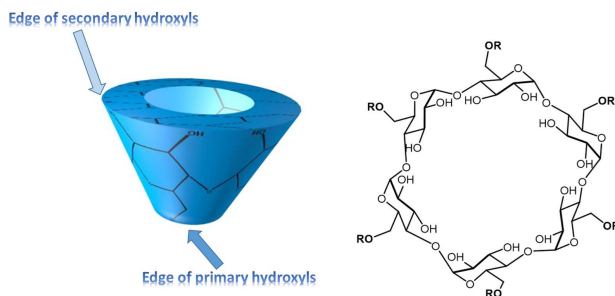
⁵⁹ Klöck, C.; Dsouza, R. N.; Nau, W. M., *Org. Lett.*, **2009**, *11*, 2595.

⁶⁰ Lee, J. W.; Samal, S.; Selvapalam, N.; Kim, H.-J.; Kim, K., *Acc. Chem. Res.*, **2003**, *36*, 621.

⁶¹ Crini, G., *Chem. Rev.*, **2014**, *114*, 10940.

CDs were prepared by an enzymatic process, in which starch is treated with a set of enzymes. This hydrolysis process leads to the formation of dextrans, which, by cyclodextrin glycosyl transferase enzyme are cleaved and at the two ends of the cleaved fragment are linked to produce a CD. Purification of the mixture of α -, β - and γ - CDs can be performed on the basis of the solubility in water (β -CD is obtained from crystallization in water, while α and β are purified through an expensive chromatographic process); or by adding the appropriate complexing agent and subsequent filtration, as these macrocycles easily form solid host-guest inclusion complexes. Alternatively, it's possible to exploit dedicated enzyme to produce the chosen macromolecule.

CDs have a toroidal shape ring. It's possible discriminate two edges: a primary face, narrower, composed from primary hydroxyl groups of sugar residues and a secondary face, wider, constituted from secondary hydroxyl moieties (Figure 14).



Cyclodextrins properties.

Property	α -Cyclodextrin	β -Cyclodextrin	γ -Cyclodextrin
Number of glucopyranose units	6	7	8
Molecular Weight (g/mol)	972	1135	1297
Solubility in water at 25°C (% w/v)	14.5	1.85	23.2
Outer Diameter (Å)	14.6	15.4	17.5
Cavity Diameter (Å)	4.7-5.3	6.0-6.5	7.5-8.3
Height of torus (Å)	7.9	7.9	7.9
Cavity Volume (Å ³)	174	262	427

Figure 14. Upper, chemical structure and description of the faces of β -CD. Bottom, table of CDs properties.

These hydroxyl moieties provide a hydrophilic outer surface giving CDs good solubility in water, whereas the hydrophobic cavity permits encapsulation of several guests thanks to the hydrophobic effect. This feature, along with the presence of well-designed procedure to introduce many functionalities (including derivatization of hydroxyl moieties) and their easy availability, makes these macrocycles attractive for various applications, which range from pharmaceutical⁶² (drug delivery systems) to cosmetic⁶³ and food flavor preservation⁶⁴.

Catalytic use of CDs is very extensive. They have been exploited as ligands in organometallic chemistry for the hydrogenation of unsaturated acids⁶⁵ and asymmetric oxidation of thioanisole⁶⁶, in hydrolysis of phenylacetates⁶⁷, Diels-Alder reactions⁶⁸, 1,3-dipolar cycloaddition⁶⁹, Suzuki cross-coupling reactions⁷⁰, reduction of α -ketoesters⁷¹, oxidative cleavage of aziridines or epoxides⁷², Strecker reaction⁷³, addition of thiols to alkenes⁷⁴, regulation of Fries rearrangement of phenyl acetate⁷⁵, as phase transfer catalysts (PTC) for deoxygenation of allylic alcohols⁷⁶, epoxidation⁷⁷, oxidation and hydrosilylation of olefins⁷⁸.

Involvement of CDs in enzyme mimicking also is huge. Breslow and co-workers proposed a thiamine pyrophosphate-dependent enzyme mimic linking a thiazolium

⁶² Loftsson, T.; Brewster, M. E., *J. Pharm. Pharmacol.*, **2010**, *62*, 1607.

⁶³ Buschmann, H. J.; Schollmeyer, E., *J. Cosmet. Sci.*, **2002**, *53*, 185.

⁶⁴ Marques, H. M. C., *Flavour Fragr. J.*, **2010**, *25*, 313.

⁶⁵ Lee, J.-T.; Alper, H., *Tetrahedron Lett.*, **1990**, *31*, 1941.

⁶⁶ Shen, H. M.; Ji, H. B., *Tetrahedron Lett.*, **2012**, *53*, 3541.

⁶⁷ VanEtten, R. L.; Clowes, G. A.; Sebastian, J. F.; Bender, M. L., *J. Am. Chem Soc.*, **1967**, *89*, 3253.

⁶⁸ Schneider, H.-J.; Sangwan, N. K., *Angew. Chem. Int. Ed. Engl.*, **1987**, *26*, 896.

⁶⁹ Meyer, A. G.; Easton, C. J.; Lincoln, S. F.; Simpson, G. W., *Chem. Commun.*, **1997**, 1517.

⁷⁰ Hapiot, F.; Lyskawa, J.; Tilloy, S.; Bricout, H.; Monflier, E., *Adv. Synth. Catal.*, **2004**, *346*, 83.

⁷¹ Pinel, C.; Gendreau-Diaz, N.; Br  h  ret, A.; Lemaire, M., *J. Mol. Catal. A.: Chem.*, **1996**, *112*, L157

⁷² Surendra, K.; Krishnaveni, N. S.; Reddy, M. A.; Nageswar, Y. V. D.; Rao, K. R., *J. Org. Chem.*, **2003**, *68*, 9119.

⁷³ Surendra, K.; Krishnaveni, N. S.; Mahesh, A.; Rao, K. R., *J. Org. Chem.*, **2006**, *71*, 2532.

⁷⁴ Krishnaveni, N. S.; Surendra, K.; Rao, K. R., *Chem. Commun.*, **2005**, *0*, 669.

⁷⁵ Ohara, M.; Watanabe, K., *Angew. Chem. Int. Ed. Engl.*, **1975**, *14*, 820.

⁷⁶ Lee, J. T.; Alper, H., *Tetrahedron Lett.*, **1990**, *31*, 4101.

⁷⁷ Ganeshpуре, P. A.; Satish, S. J., *J. Chem. Soc., Chem. Commun.*, **1988**, 981.

⁷⁸ Lewis, L. N.; Sumpter, C. A.; Stein, J., *J. Inorg. Organomet. Polymers*, **1996**, *6*, 123.

ring (Figure 15) to β - and γ -CDs⁷⁹. Similarly, the same group attached a pyridoxamine moiety to CDs in order to emulate the activity of enzymes having as coenzymes pyridoxamine or pyridoxal phosphate. A manganese-porphyrin complex with four β -CDs substituents (Figure 16) was synthesized by Breslow and co-workers with the aim of mimicking P450 enzymes⁸⁰; β -CD was functionalized by Bender and co-workers with imidazole to obtain an efficient enzyme model of chymotrypsin⁸¹ (Figure 17).

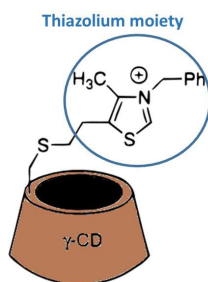


Figure 15. γ -CD based derivative exploited for biomimetic catalysis.

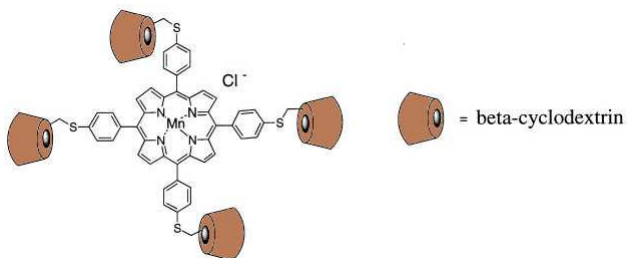


Figure 16. Organometallic complex designed by Breslow and co-workers for the mimicking of P450 enzyme.

⁷⁹ Breslow, R.; Dong, D. S., *Chem. Rev.*, **1998**, *98*, 1997.

⁸⁰ Breslow, R.; Huang, Y.; Zhang, X.; Yang, J., *Proc. Natl. Acad. Sci. USA*, **1997**, *94*, 11156.

⁸¹ Bender, M. L., *J. Inclusion Phenom.*, **1984**, *2*, 433.

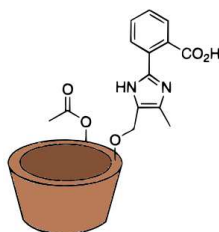


Figure 17. Mimicking of chymotrypsin based on a β -CD derivative.

Calixarenes are macrocycles (Figure 18) belonging to the cyclophane class⁸². The term *calixarene* was coined in 1975 by Gutsche, because of the resemblance of the tetramer derivative with a *calix crater* (Figure 19), a kind of vase in ancient Greece.

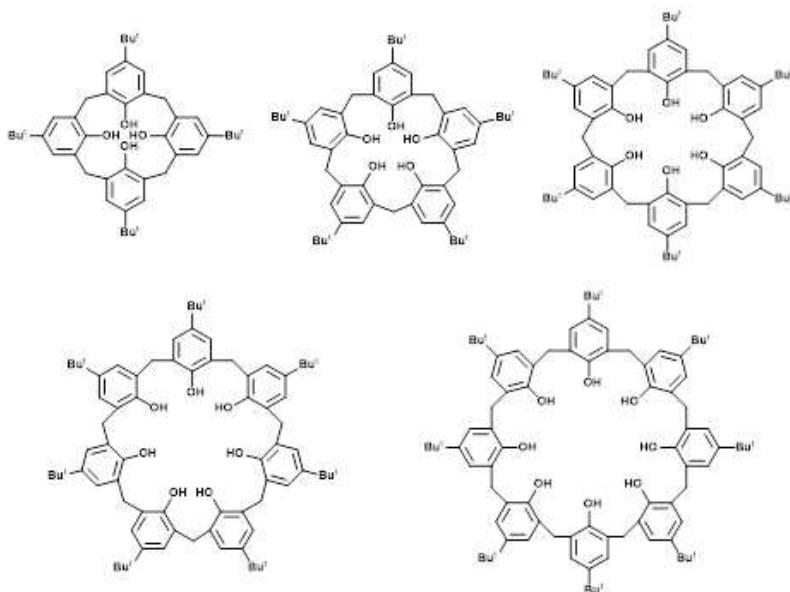


Figure 18. Some members of calixarenes family.

As a convention, the number of phenolic units composing the macrocycle is reported in square bracket.

⁸² Gutsche, C. D., *Calixarenes: An Introduction*, Royal Society of Chemistry, Cambridge, 2008.



Figure 19. Left, a *calix crater*; right, structure of *p-tert-butylcalix[4]arene*.

From a structural point of view, calixarenes display an *upper rim* (wider) and a *lower rim* (narrower).

Their synthesis can occur according to two approaches: a one-step approach, explored mainly by Gutsche and co-workers, and a multi-step approach, studied by Kammerer and Bohmer and co-workers.

In the one-step approach, useful to obtain symmetric calixarene, a condensation reaction between *p-tert-butylphenol* and formaldehyde in basic environment occurs, followed by dissolution in the appropriate solvent. Depending on the reaction conditions, it is possible to obtain different products: when NaOH is utilized as a base and diphenyl ether as solvent, *p-tert-butylcalix[4]arene* is the preferred product, but when KOH and *p-xylene* are used, *p-tert-butylcalix[6]arene* is the preferred one. Furthermore, if NaOH and xylene are exploited, *p-tert-butylcalix[8]arene* is achieved. In the multi-step approach, useful to build dissymmetric macromolecules, different subunits were synthesized apart, and in a final reaction these subunits are joined.

Their conformational properties have been largely studied. Calix[n]arenes are tridimensional structures capable of adopting different equilibrium conformations. For *p-tert-butylcalix[4]arene* for example, four conformations are possible, with the first one having an hydrophobic cavity: cone, partial cone, 1,3-alternate and 1,2-alternate (Figure 20).



Figure 20. Conformations of *p*-*tert*-butylcalix[4]arene. From left to right: cone, partial cone, 1,2-alternate and 1,3-alternate.

Several strategies for functionalization of the upper rim and the lower rim are accessible⁸³. Hydroxyl groups at the lower rim are easily susceptible to *O*-alkylation or *O*-acylation. Upper rim shows a different picture: rings of the calixarene are activated so they can undergo electrophilic substitution, but in this case the *tert*-butyl moiety must be removed. The scope is achieved through a retro Friedel-Crafts reaction with AlCl₃ as the catalyst in toluene. This enables more paths to derivatize the macrocycle and makes them highly tunable for a wide range of applications⁸⁴. Since cavities are preformed and well organized, these macrocycles have been exploited as hosts, because versatility of moieties bounded at the rims and possibility to exploit hydrophobic, CH- π , π - π and cation- π interactions with the hydrophobic aromatic cavity. This combination of features has motivated many research groups to utilize them as scaffold for building bio-inspired molecular receptors⁸⁵ for selective recognitions of cations^{86,87}, anions⁸⁸ and neutral guests⁸⁹.

Building artificial receptors has been a challenge which has attracted great interest.

A notable example is represented by mimics of vancomycin, an antibiotic glycopeptide which binds to a peptide sequence of cell wall of Gram positive bacteria inhibiting its growth. Calix[4]arene bearing at the upper rim peptide

⁸³ *Calixarenes 2001*, (eds Asfari, Z.; Böhmer, V.; Harrowfield, J.; Vicens, J.; Saadiou, M.), Springer, Berlin, **2001**.

⁸⁴ Böhmer, V., *Angew. Chem. Int. Ed.*, **1995**, *34*, 713.

⁸⁵ Sansone, F.; Baldini, L.; Casnati, A.; Ungaro, R., *New J. Chem.*, **2010**, *34*, 2715.

⁸⁶ Ghidini, E.; Ugozzoli, F.; Ungaro, R.; Harkema, S.; El-Fadl, A. A.; Reinhoudt, D. N., *J. Am. Chem. Soc.*, **1990**, *112*, 6979.

⁸⁷ Arduini, A.; Demuru, D.; Pochini, A.; Secchi, A., *Chem. Commun.*, **2005**, *0*, 645.

⁸⁸ Troisi, F.; Russo, A.; Gaeta, C.; Bifulco, G.; Neri, P., *Tetrahedron Lett.*, **2007**, *48*, 7986.

⁸⁹ Haino, T.; Matsumura, K.; Harano, T.; Yamada, K.; Saijyo, Y.; Fukazawa, Y., *Tetrahedron*, **1998**, *54*, 12185.

moieties linked by 1,3,5-diethylene triamine⁹⁰ were synthesized (Figure 21) and the macrocycles was found to efficiently recognize alanine dipeptides used as a model of bacterial peptidoglycan branch. Moreover, some of the calixarene derivatives showed biological activity very similar to that of vancomycin. Consoli *et al.* designed a series of macrocycles for mimicking lectin⁹¹, derivatizing calix[4]arenes at the upper rim with several glycosylthioureido groups (Figure 22) able to perform hydrogen bonding.

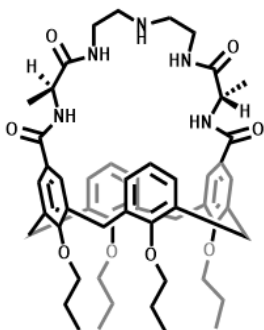


Figure 21. Calix[4]arene derivative exploited for vancomycin mimics.

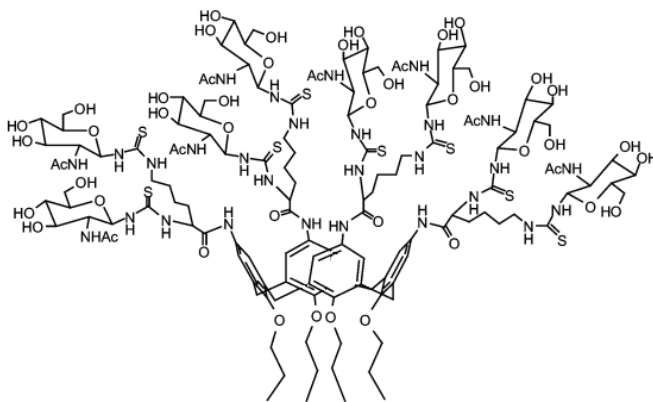


Figure 22. Calix[4]arene adorned with N-acetyl-D-glucosamine groups used to mimicking lectin.

⁹⁰ Casnati, A.; Fabbri, M.; Pelizzi, N.; Pochini, A.; Sansone, F.; Ungaro, R.; Di Modugno, E.; Tarzia, G., *Bioorg. Med. Chem. Lett.*, **1996**, *6*, 2699.

⁹¹ Consoli, G. M. L.; Cunsolo, F.; Geraci, C.; Sgarlata, V., *Org. Lett.*, **2004**, *6*, 4163.

Binding to DNA was also studied: a calix[4]arene with dodecyl chains at the lower rim and amino groups at the upper rim was synthesized and its ability to bind DNA was analyzed⁹².

In the field of gene delivery, calix[4]arenes derivatized with guanidinium groups were designed, showing interesting properties in the recognition and in the binding of the plasmid DNA⁹³.

Synthesis of aldolase enzymes mimic was an old but always formidable challenge which fascinated the scientists. The first cornerstone was represented by the attempt of Gutsche and co-workers⁹⁴; despite of hard synthetic work made, no significative results were obtained (Figure 23). Synthesis of hydrolase enzymes mimic was also exploited: in 2005, a model of phosphodiesterase mimic was proposed⁹⁵. Calix[4]arenes with a growing number of azacrown subunits linked at the upper rim and complexing cations Zn^{2+} or Cu^{2+} were synthesized⁹⁶; derivative with three azacrown subunits gave good results (Figure 24)

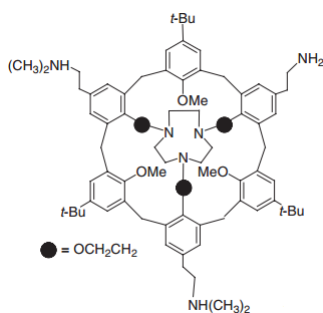


Figure 23. Calixarene derivative synthesized by Gutsche and co-workers in the purpose of mimicking aldolase enzyme.

⁹² Rodik, R. V.; Anthony, A.-S.; Kalchenko, V. I.; Méli, Y.; Klymchenko, A. S., *New J. Chem.*, **2015**, *39*, 1654.

⁹³ Rullaud, V.; Siragusa, M.; Cumbo, A.; Gygax, D.; Shahgaldian, P., *Chem. Commun.*, **2012**, *48*, 12186.

⁹⁴ Matthews, S. E.; Beer, P. D., *Calixarene in the Nanoworld*, (eds Vicens, J.; Harrowfield, J.), Springer, Berlin, **2006**.

⁹⁵ Baldini, L.; Cacciapaglia, R.; Casnati, A.; Mandolini, L.; Salvio, R.; Sansone, F.; Ungaro, R., *J. Org. Chem.*, **2012**, *77*, 3381.

⁹⁶ Cacciapaglia, R.; Casnati, A.; Mandolini, L.; Reinhoudt, D. N.; Salvio, R.; Sartori, A.; Ungaro, R., *J. Am. Chem. Soc.*, **2006**, *128*, 12322.

Attempts to emulate other enzymes were made: calix[4]arenes carrying several imidazole moieties at the upper rim as trans-acyl-transferase mimics were reported⁹⁷; carbonic anhydrase enzyme mimics based on calix[4]arene podands bearing two or four histidine or glycine groups at the upper rim were proposed⁹⁸.

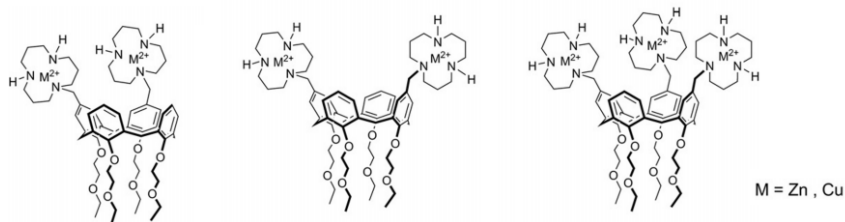


Figure 24. Calix[4]arene with azacrowns subunits employed in the cleavage of phosphodiesteres.

1.4 Metal Organic Frameworks as Biomimetic Catalysts

Metal organic frameworks (MOFs) are a class of porous hybrid polymeric materials, consisting of metal ions linked together by organic bridging ligands, forming a 3D structure⁹⁹. These materials seem to be successful to combine the convenient properties of inorganic materials with those of the organic ones in order to achieve a new porous material with the desired properties. Tunability concerns not only the nature of organic and inorganic parts, but also the porosity and the surface area, generally very high (up to 10,000 m²/g). From the point of view of the biomimetic catalysis, all these features represent a serious advantage, because it's possible to tailor MOFs in order to make an appropriate environment, e.g. to build a model for the active site of an enzyme¹⁰⁰.

⁹⁷ Dospil, G.; Schatz, J., *Tetrahedron Lett.*, **2001**, 42, 7837.

⁹⁸ Molard, Y.; Bureau, C.; Lopez, H. P.; Lamartine, R.; de Vains, J. B. R., *Tetrahedron Lett.*, **1999**, 40, 6383.

⁹⁹ Zhou, H.-C.; Long, J. R.; Yaghi, O. M., *Chem. Rev.*, **2012**, 112, 673.

¹⁰⁰ Gu, Z.-Y.; Park, J.; Raiff, A.; Wei, Z.; Zhou, H.-C., *ChemCatChem.*, **2014**, 6, 67.

MOFs can be exploited either as the truly biomimetic catalyst, or like a skeleton which contains the catalytic sites mimicking some enzyme like activity and thus forming an heterogeneous biomimetic catalyst, whose advantages consist in a better recovery and recycling of the catalyst and in an increase of the dispersion of the active sites leading to an improvement in the catalytic efficiency¹⁰¹.

Porphyrins and metalloporphyrins have been encapsulated or, in some case, have been utilized as ligands to construct MOFs¹⁰², in order to mimicking heme proteins like hemoglobin or cytochrome P450 or construct model of natural light harvesting systems¹⁰³. γ -CDs have been exploited to synthesize the so called *edible* MOFs¹⁰⁴. Development in this field is still at the beginning and further efforts are necessary.

1.5 Molecularly Imprinted Polymers as Biomimetic Catalysts

Molecular imprinting is a process by which a proper molecule is used as a template for the design and the synthesis of structures made by copolymerization of cross-linked monomers with appropriate functional groups¹⁰⁵. As a result, after removal of the molecular template, a shell structure is obtained, with cavities which show complementarity in size, shape and in interactions with the original template (Figure 25).

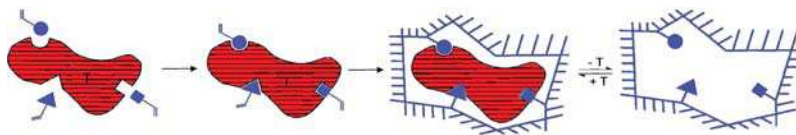


Figure 25. Imprinting of appropriate cavities in a cross-linked polymer by a template (in red) with three different functional groups.

¹⁰¹ Farrusseng, D.; Aguado, S.; Pinel, C., *Angew. Chem. Int. Ed.*, **2009**, *48*, 7502.

¹⁰² Zhao, M.; Ou, S.; Wu, C.-D., *Acc. Chem. Res.*, **2014**, *47*, 1199.

¹⁰³ Wang, J.-L.; Wang, C.; Lin, W., *ACS Catal.*, **2012**, *2*, 2630.

¹⁰⁴ Smaldone, R. A.; Forgan, R. S.; Furukawa, H.; Gassensmith, J. J.; Slawin, A. M. Z.; Yaghi, O. M.; Stoddart, J. F. *Angew. Chem. Int. Ed.* **2010**, *49*, 8630.

¹⁰⁵ Chen, L.; Wang, X.; Lu, W.; Wu, X.; Li, J., *Chem. Soc. Rev.*, **2016**, *45*, 2137.

In this way, a very efficient and selective molecular recognition is obtained, as a consequence of imprinting a memory of the molecular template during the process of building. Although molecularly imprinted polymers (MIPs) exhibit this significant key feature and for this reason they have found application in many areas, they also display a large shortcoming¹⁰⁶: binding sites are highly specific but their distribution is very heterogeneous, both in number and in size, leading to lower catalytic capabilities than biological counterparts and to a distribution of binding site affinities. Nevertheless, good results are achieved in enzyme mimics exploiting MIPs. Using the appropriate template monomer¹⁰⁷, MIPs with chiral cavities were made and were used to catalyze biomimetic synthesis of amino acids from glycine, with 36% ee.

A transaminase mimic¹⁰⁸ was obtained using the molecule in Figure 26 as a template for MIPs. The template in this case resembles transition state of the reaction. Conversion of phenylpyruvic acid to phenylalanine was obtained with a 32% *L*-ee, being the catalytic sites of the MIPs chiral. Other MIPs were designed as nanoreactors¹⁰⁹ to catalyze 1,3-dipolar cycloaddition.

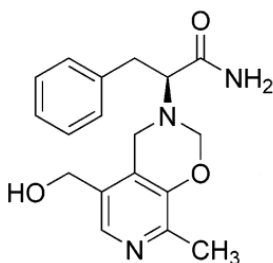


Figure 26. Template for a MIP mimicking a transaminase enzyme.

¹⁰⁶ Vasapollo, G.; Del Sole, R.; Mergola, L.; Lazzoi, M. R.; Scardino, A.; Scorrano, S.; Mele, G., *Int. J. Mol. Sci.*, **2011**, *12*, 5908.

¹⁰⁷ Wulff, G.; Vietmeier, J., *Makromol. Chem. Macromol. Chem. Phys.*, **1989**, *190*, 1727.

¹⁰⁸ Svenson, J.; Zheng, N.; Nicholls, A., *J. Am. Chem. Soc.*, **2004**, *126*, 8554.

¹⁰⁹ Zhang, H.; Piacham, T.; Drew, M.; Patek, M.; Mosbach, K.; Ye, L., *J. Am. Chem. Soc.*, **2006**, *128*, 4178.

1.6 Self-assembled Capsules as Biomimetic Catalysts

Amongst the declared goals of the supramolecular chemistry, surely the understanding of how common, macroscopic, chemical principles can change when molecules are confined and allowed to react into nanoscale spaces¹¹⁰ plays a key role. On this basis, hard work has been done to develop complex supramolecular structure to be considered, like natural enzymes, a sort of nanoreactors¹¹¹, which thanks to their shape, size and local environment could be exploited to walk new paths regarding activity and selectivity of known chemical processes and could be able to get a deeper insight into reactivity of molecules into well-defined and nanoscopic spaces.

Self-assembly can be considered an ubiquitous process inside living beings; our biological world, as we know it, was born by a self-assembly of few building blocks¹¹², so we can deduce that it's a simple and efficient strategy to build well organized structures: complex supramolecular structures can also be built linking many subunits by covalent bonds, but this implies complicated stepwise synthesis, that rarely results in a convenient approach. Non covalent interactions which can be utilized in self-assembly include hydrogen bonding interactions, hydrophobic interactions and metal-ligand interactions.

Self-assembled capsules are defined as *receptors with enclosed cavities that are formed by the reversible non covalent interaction of two or more, not necessarily identical, subunits*¹¹³. They have forged a large role because playing on reversible non covalent interactions permits flexibility and dynamicity, regarding both

¹¹⁰ Petrosko, S. H.; Johnson, R.; White, H.; Mirkin, C. A., *J. Am. Chem. Soc.*, **2016**, *138*, 7443.

¹¹¹ *Organic Nanoreactors: From Molecular to Supramolecular Organic Compounds*, (eds Sadjadi, S.), Academic Press, Cambridge, **2016**.

¹¹² Lehn, J.-M., *Science*, **2002**, *295*, 2400.

¹¹³ Conn, M. M.; Rebek, Jr.J., *Chem. Rev.*, **1997**, *97*, 1647.

encapsulation of substrates and release of the products, typical of their biological counterparts and needed in catalysis¹¹⁴.

In self-assembled capsules based on metal-ligand interactions¹¹⁵, ligands can be one-dimensional components which arrange themselves in two-dimensional structures following interactions with transition metals, or two dimensional components which are assembled in three-dimensional aggregates.

A cornerstone in metal-ligand self-assembled capsules was represented by the work of Fujita group, which synthesized self-assembled nanocages with tetrahedral symmetry composed of six Pd(II) ions held together by four diverging tridentate organic ligands (Figure 27)¹¹⁶. The positive charge of the whole structure makes it high soluble in water. Diels-Alder reaction between anthracenes and phtalimide was performed in this nanoreactor¹¹⁷.

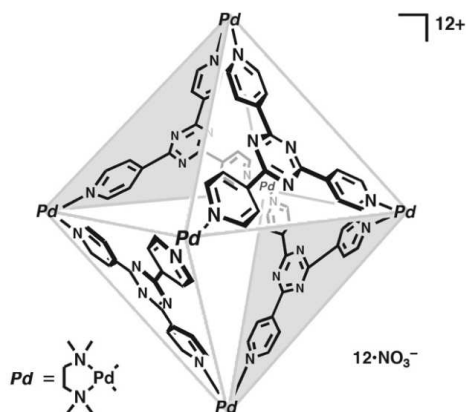


Figure 27. Fujita and co-workers self-assembled capsule.

¹¹⁴ Yoshizawa, M.; Klosterman, J. K.; Fujita, M., *Angew. Chem. Int. Ed.*, **2009**, *48*, 3418.

¹¹⁵ Brown, J. C.; Toste, F. D.; Bergman, R. G.; Raymond, K. N., *Chem. Rev.*, **2015**, *115*, 3012.

¹¹⁶ Fujita, M.; Oguro, D.; Miyazawa, M.; Oka, H.; Yamaguchi, K.; Ogura, K., *Nature*, **1995**, *378*, 469.

¹¹⁷ Yoshizawa, M.; Tamura, M.; Fujita, M., *Science*, **2006**, *312*, 251.

Raymond and Bergman described a chiral tetrahedral $[\text{Ga}_4\text{L}_6]^{12-}$ complex (Figure 28), where the ligand (L) consisted of 1,5-bis(2,3-dihydroxybenzamido)naphthalene¹¹⁸. The cage was intensively studied and it was found that in water the aggregate is effective to trap cationic guests such as tropylium cation¹¹⁹, phosphonium species¹²⁰, metal complexes¹²¹ and preferentially encapsulated protonated amines¹²². This supramolecular structure showed to be able to catalyze Aza-Cope rearrangements¹²³, allylic alcohols isomerization¹²⁴, hydroalkoxylation¹²⁵ and Nazarov cyclization¹²⁶. For Aza-Cope rearrangement, iminium intermediate is stabilized inside the capsule and after left the cage, hydrolysis of iminium species occurs. In the case of Nazarov cyclization, problem of product inhibition was resolved adding to the reaction mixture maleimide, which readily reacted with product of the cyclization to give a Diels-Alder adduct.

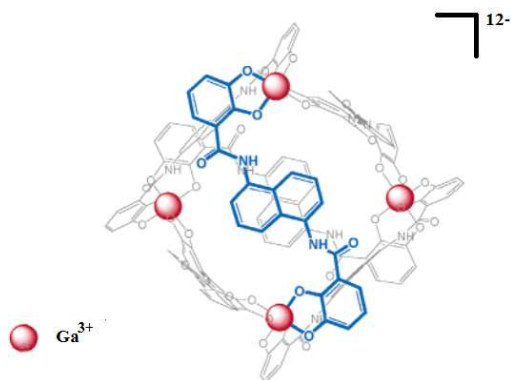


Figure 28. Structure of the $[\text{Ga}_4\text{L}_6]^{12-}$ complex.

¹¹⁸ Caulder, L. D.; Brückner, C.; Powers, R. E.; König, S.; Parac, T. N.; Leary, J. A.; Raymond, K. N., *J. Am. Chem. Soc.*, **2001**, *123*, 8923.

¹¹⁹ Brumaghim, J. L.; Michels, M.; Pagliero, D.; Raymond, K. N., *Eur. J. Org. Chem.*, **2004**, *24*, 5115.

¹²⁰ Ziegler, M.; Brumaghim, J. L.; Raymond, K. N., *Angew. Chem. Int. Ed.*, **2000**, *39*, 4119.

¹²¹ Fiedler, D.; Bergman, R. G.; Raymond, K. N., *Angew. Chem. Int. Ed.*, **2006**, *45*, 745.

¹²² Fiedler, D.; Leung, D. H.; Bergman, R. G.; Raymond, K. N., *Acc. Chem. Res.*, **2005**, *38*, 349.

¹²³ Brown, C. J.; Bergman, R. G.; Raymond, K. N., *J. Am. Chem. Soc.*, **2009**, *131*, 17530.

¹²⁴ Leung, D. H.; Bergman, R. G.; Raymond, K. N., *J. Am. Chem. Soc.*, **2007**, *129*, 2746.

¹²⁵ Wang, Z. J.; Brown, C. J.; Bergman, R. G.; Raymond, K. N.; Toste, F. D., *J. Am. Chem. Soc.*, **2011**, *133*, 7358.

¹²⁶ Hastings, C. J.; Bergman, R. G.; Raymond, K. N., *J. Am. Chem. Soc.*, **2010**, *132*, 6938.

Nitschke group also prepared tetrahedral $[M_4L_6]^{6-}$ cages, but with Fe^{2+} ions¹²⁷ instead of Ga^{3+} . The iron metal cage (Figure 29), in terms of recognition, had a different behavior respect to $[Ga_4L_6]^{12-}$ cage, because cationic species are not encapsulated, both due to lower charge of the complex and to bigger shielding of the charge of Fe ions by their ligands. This example can be considered a borderline case, since opening and closing of the cage can take place both through coordinative bonds (N-Fe) and dynamic covalent bonds (C=N). Interestingly, these cages turned out to be able to catalyze a multistep transformation of furan, dioxygen and nitromethane¹²⁸.

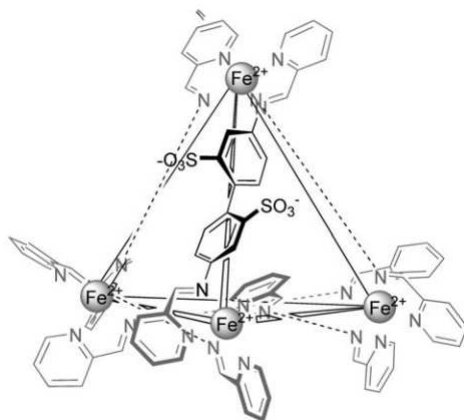


Figure 29. Nitschke's iron metal cage.

Self-assembled hydrogen-bonding based capsules started to become notorious with pseudospherical capsule of Rebek¹²⁹, in 1995, based on a tetraurea moiety capable to self-assembly. This aggregate (Figure 30) proved to be, in 1998, able to catalyze Diels-Alder reactions through reversible encapsulation¹³⁰.

¹²⁷ Mal, P.; Schultz, D.; Beyeh, K.; Rissanen, K.; Nitschke, J. R., *Angew. Chem. Int. Ed.*, **2008**, *47*, 8297.

¹²⁸ Salles Jr., A. G.; Zarra, S.; Turner, R. M.; Nitschke, J. R., *J. Am. Chem. Soc.*, **2013**, *135*, 19143.

¹²⁹ Valdés, C.; Spitz, U. P.; Kubik, S. W.; Rebek, J., *Angew. Chem. Int. Ed. Engl.*, **1995**, *34*, 1885.

¹³⁰ Kang, J.; Santamaria, J.; Hilmersson, G.; Rebek, Jr. J., *J. Am. Chem. Soc.*, **1998**, *120*, 7389.

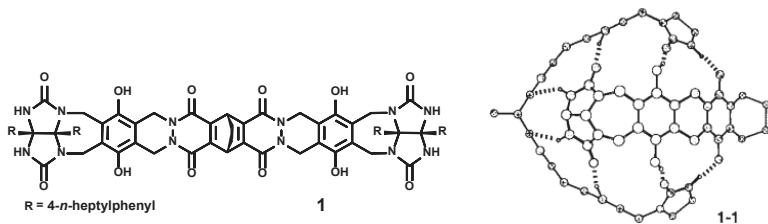


Figure 30. Dimeric capsule (right) formed by self-assembly of molecule to the left.

He also synthesized a resorcin[4]arene derivative able to self-assembly to give a cylindrical capsule (Figure 31), whose halves were held together by a seam of eight bifurcated hydrogen bonding¹³¹. The array of π bonds due to the presence of aromatic rings is responsible for the creation of a layer of negative charge that surrounds the space in the capsule. Little molecules like toluene and xylene are easily encapsulated; also long guests such as terphenyl chains or combinations of ethane and naphthalene fill properly the interior space of the capsule.

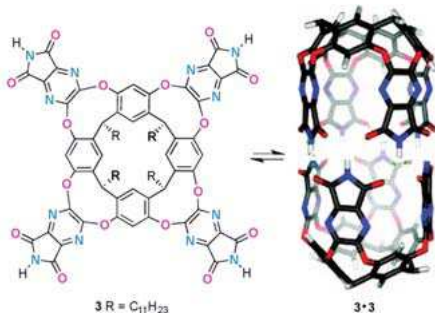


Figure 31. Rebek's cylindrical capsule.

Another significant example and largely studied supramolecular system is the aggregate which is obtained by self-assembly (Figure 32) of six C-undecyl-resorcin[4]arene subunits¹³².

¹³¹ Heinz, T.; Rudkevich, D. M.; Rebek, Jr. J., *Nature*, **1998**, 394, 764.

¹³² MacGillivray, L. R.; Atwood, J. L., *Nature*, **1997**, 389, 469.



Figure 32. Left, chemical structure of resorcin[4]arene; middle, representation of the same resorcin[4]arene; right, representation of the hexameric resorcin[4]arene capsule.

The structure of resorcin[4]arene is similar to that of calix[4]arene but it is achieved by condensation in acidic environment of resorcinol with the proper aldehyde in ethanol¹³³. When aldehyde is sufficiently long, the supramolecule is conformationally stable and its solubility in organic solvents is highly increased.

Atwood and MacGillivray found that resorcin[4]arene in crystal state formed a racemic mixture of pseudospherical hexamers in which each water molecule forms three hydrogen bonds with OH groups of three resorcin[4]arene units, while each resorcinarene unit forms hydrogen bonding with other four resorcinarenes. This pseudospherical aggregate has a cavity of 1375 Å³. This arrangement was also observed in water saturated organic solvents (chloroform, benzene) by Cohen group¹³⁴ by diffusion NMR experiments performed on C-undecyl-resorcin[4]arene; from six to eight molecules of solvent (chloroform or benzene) can be accommodated¹³⁵ inside the cavity. Alcohols could also be encapsulated¹³⁶ and generally, polar small molecules such as carboxylic acids and sugars¹³⁷. Furthermore, Rebek and Shivanyuk demonstrated that, through cation-π interactions with

¹³³ (a) Hoegberg, A. G. S., *J. Am. Chem. Soc.*, **1980**, *102*, 6046; (b) Hoegberg, A. G. S., *J. Org. Chem.*, **1980**, *45*, 4498.

¹³⁴ Avram, L.; Cohen, Y., *J. Am. Chem. Soc.*, **2002**, *124*, 15148.

¹³⁵ Shivanyuk, A.; Rebek, Jr. J., *J. Am. Chem. Soc.*, **2003**, *125*, 3432.

¹³⁶ Slovak, S.; Cohen, Y., *Chem. Eur. J.*, **2012**, *18*, 8515.

¹³⁷ Salem, T. E.; Baruch, I.; Avram, L.; Cohen, Y.; Palmer, L. C.; Rebek, Jr. J., *Proc. Natl. Acad. Sci. USA*, **2006**, *103*, 12296.

electron rich aromatic walls, the capsule encapsulated quaternary ammonium salts¹³⁸.

Many steps forward were made by Tiefenbacher and co-workers. They showed that also tertiary amines, albeit not protonated and so unable to make hydrogen bonding, could be efficiently encapsulated inside the capsule. It was shown that these neutral guests were protonated¹³⁹ inside the hexameric aggregate and that this protonation caused encapsulation. A series of experiments revealed that hexameric resorcin[4]arene capsules acted as a Brønsted acid, with pKa value approximately of 5.5-6. This is due to the extensive delocalization of negative charge on the whole aromatic framework.

The same group reported the use of the hexameric assemble as a biomimetic catalyst in the cyclization of terpenes¹⁴⁰. The capsule was able to catalyze tail to head (THT) cyclization reaction like cyclase enzymes¹⁴¹. Other notable examples of catalytic applications of hexameric resorcinarene capsule concern about hydration of aromatic alkynes¹⁴² (also in combination with encapsulation of Au complexes), 1,3-dipolar cycloaddition of diazoacetate esters¹⁴³, sulfoxidation of thioethers¹⁴⁴, isomerization of epoxides¹⁴⁵, intramolecular hydroalkoxylation of unsaturated alcohols¹⁴⁶. A *teflon-footed* resorcinarene capable to self-assembly to give hexameric capsule in fluorinated solvents was also synthesized using a fluorinated aldehyde¹⁴⁷; Shimizu group demonstrated that this capsule exhibited improved

¹³⁸ Shivanyuk, A.; Rebek, Jr. J., *Proc. Natl. Acad. Sci. USA*, **2001**, *98*, 7662.

¹³⁹ Zhang, Q.; Tiefenbacher, K., *J. Am. Chem. Soc.*, **2013**, *135*, 16213.

¹⁴⁰ Zhang, Q.; Tiefenbacher, K., *Nat. Chem.*, **2015**, *7*, 197.

¹⁴¹ Christianson, D. W., *Chem. Rev.*, **2006**, *106*, 3412.

¹⁴² La Sorella, G.; Sporni, L.; Ballester, P.; Strukul, G.; Scarso, A., *Catal. Sci. Technol.*, **2016**, *6*, 6031.

¹⁴³ La Sorella, G.; Sporni, L.; Strukul, G.; Scarso, A., *ChemCatChem*, **2015**, *7*, 291.

¹⁴⁴ La Sorella, G.; Sporni, L.; Strukul, G.; Scarso, A., *Adv. Synth. Catal.*, **2016**, *358*, 3443.

¹⁴⁵ Caneva, T.; Sporni, L.; Strukul, G.; Scarso, A., *RSC Adv.*, **2016**, *6*, 83505.

¹⁴⁶ Catti, L.; Tiefenbacher, K., *Chem. Commun.*, **2015**, *51*, 892.

¹⁴⁷ Shimizu, S.; Kiuchi, T.; Pan, N., *Angew. Chem. Int. Ed.*, **2007**, *46*, 6442.

properties compared to previously described resorcinarene capsule due to fluorophobic effect¹⁴⁸ and was able to catalyze Diels-Alder reaction¹⁴⁹.

A last but not less important example was represented by iminium catalyzed reduction of unsaturated aldehydes¹⁵⁰, which can be seen as an imine reductase mimic. Tiefenbacher and co-workers started from the study of the organocatalytic reduction of α,β unsaturated aldehydes with Hantzsch ester using as catalysts many kinds of proline derivatives.

Influence of the encapsulation of substrates was evaluated above all in terms of difference of enantioselectivity (Δee) performing reactions in presence or without 26% mol of capsule. In fact, acceleration of reaction was not observed, as hexameric capsule separates iminium species from the nucleophile (Figure 33).

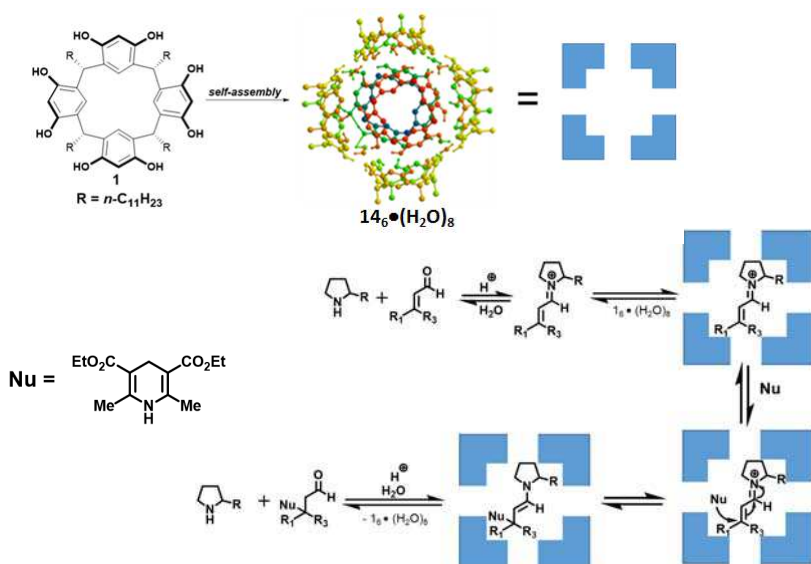


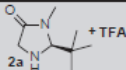
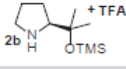
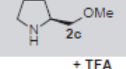
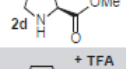
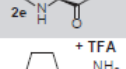
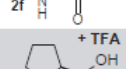
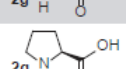
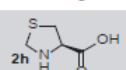
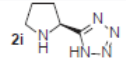
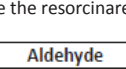
Figure 33. Mechanism proposed by Tiefenbacher for the iminium catalyzed reduction inside the capsule.

¹⁴⁸ Berger, R.; Resnati, G.; Metrangolo, P.; Weber, E.; Hulliger, J., *Chem. Soc. Rev.*, **2011**, *40*, 3496.

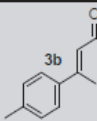
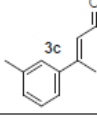
¹⁴⁹ Shimizu, S.; Usui, A.; Sugai, M.; Suematsu, Y.; Shirakawa, S.; Ichikawa, H., *Eur. J. Org. Chem.*, **2013**, *22*, 4734.

¹⁵⁰ Bräuer, T. M.; Zhang, Q.; Tiefenbacher, K., *Angew. Chem. Int. Ed.*, **2016**, *55*, 7698.

Figure 34a. Effect of proline structure on the organocatalyzed reduction of α,β -unsaturated aldehydes

Entry	Catalyst	Capsule	Yield (%)	ee (%)	Δee (%)
1	 + TFA	No	66 ± 5	5 ± 2 (R)	4
		Yes	72 ± 15	1 ± 0 (R)	
2	 + TFA	No	41 ± 3	52 ± 2 (R)	5
		Yes	51 ± 7	47 ± 4 (R)	
3	 + TFA	No	54 ± 1	35 ± 1 (R)	35
		Yes	52 ± 12	0 ± 2	
4	 + TFA	No	65 ± 8	9 ± 1 (R)	31
		Yes	61 ± 13	22 ± 0 (S)	
5	 + TFA	No	92 ± 4	2 ± 0 (R)	32
		Yes	72 ± 2	30 ± 0 (S)	
6	 + TFA	No	41 ± 2	3 ± 2 (S)	45
		Yes	54 ± 3	48 ± 1 (S)	
7	 + TFA	No	69 ± 3	23 ± 0 (S)	44
		Yes	79 ± 1	67 ± 0 (S)	
8		No	27 ± 0	9 ± 2 (S)	65
		Yes	93 ± 1	74 ± 0 (S)	
9		No	22 ± 7	3 ± 1 (S)	43
		Yes	85 ± 1	46 ± 0 (S)	
10		No	82 ± 3	10 ± 1 (R)	51
		Yes	78 ± 5	41 ± 1 (S)	

inside and outside the resorcinarene capsule.

Entry	Aldehyde	Capsule	Yield (%)	ee (%)	Δee (%)
1		No	26 ± 2	9 ± 2 (S)	9
		Yes	67 ± 2	18 ± 1 (S)	
2		No	37 ± 2	20 ± 5 (S)	41
		Yes	89 ± 3	61 ± 1 (S)	

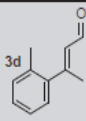
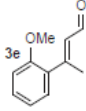
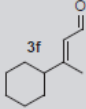
3	 3d	No	10 ± 1	19 ± 2 (R)	92
		Yes	12 ± 0	73 ± 1 (S)	
4	 3e	No	26 ± 12	9 ± 1 (S)	69
		Yes	96 ± 4	78 ± 2 (S)	
5	 3f	No	73 ± 1	37 ± 1 (S)	26
		Yes	89 ± 8	63 ± 1 (S)	

Figure 34b. Differences on the organocatalyzed reduction of α,β -unsaturated aldehydes inside and outside resorcinarene capsule, changing the substrates, by Tiefenbacher group¹⁵⁰.

When proline with a sterically shielding group in α position was involved, low difference between reaction without and with capsule was noted. Higher Δe_e was observed when *L*-proline derivatives with hydrogen bonding donor or acceptor abilities were utilized and the better outcomes were obtained with *L*-proline, probably as a consequence of the directioning ability of carboxylic group of the catalyst (Figure 34).

A series of control experiments were carried out to assess the role of the capsule. When a large Hantzsch ester was involved in the reaction in presence of the capsule, a slower conversion and a reduced Δe_e were noted, accordingly to a reaction performed outside the capsule. In fact, while iminium species can enter inside the capsule, the large Hantzsch ester doesn't fit inside so the reaction can occur only outside the hexameric aggregate. Very similar results were achieved when a large catalyst or a large aldehyde were exploited. Evidence that strong modulation of enantiomeric excess occurs inside the capsule is also furnished by performing the reaction in presence of an inhibitor, a dicationic species recognized very well by the supramolecular structure such as hexamethonium bromide. Reaction carried out in presence of this salt results in very low Δe_e . Actually, also a control experiment

adding dimethylsulfoxide (DMSO), a competitor for hydrogen bonding and an agent causing disassembly of the hexameric capsule, was performed, resulting in no difference in terms of enantioselectivity. To explain these significant results, Tiefenbacher and co-workers proposed a model in which iminium species was bounded to the inner wall of the capsule cavity by cation- π interactions with the less hindered face (Figure 35).

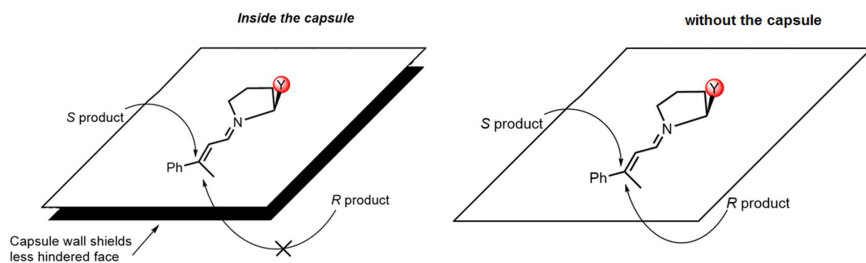


Figure 35. Hypothesis formulated by Tiefenbacher for the different selectivity showed by organocatalysed reduction of unsaturated aldehydes inside the resorcinarene hexameric capsule and without the capsule.

2. On Water Vinylogous Mukaiyama Aldol Reaction promoted by calixarene catalysts

2.1 Aldol reaction

Aldol reaction is, without doubt, one of the most studied and widely explored reactions of organic chemistry¹⁵¹. It is utilized, for example, for the synthesis of pharmaceuticals, like tetracycline antibiotics and immunosuppressants (Figure 36)¹⁵², and methyl isobutyl ketone¹⁵³.

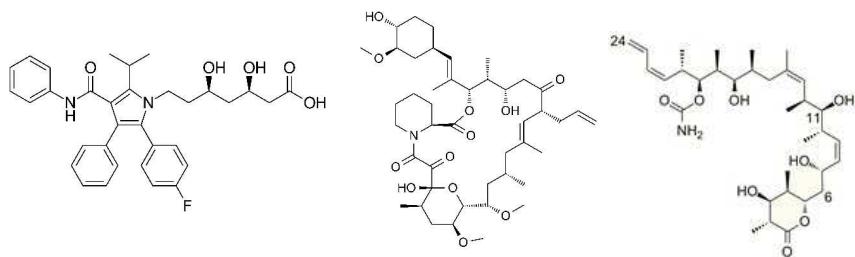


Figure 36. Chemical structures of Atorvastatin (left), Tacrolimus (center) and Discodermolide (right).

Described by Wurtz and Borodin in 18th century¹⁵⁴, it can be considered a cornerstone in the sum of C-C bond forming reactions. In nature, aldol reaction represents an efficient way to operate some useful transformations catalyzed by enzymes named *aldolases*: condensation of glyceraldehyde-3-phosphate with dihydroxyacetone phosphate to give fructose-1,6-biphosphate (Figure 37), in gluconeogenesis; addition of acetylcoenzyme A to oxaloacetic acid (Figure 38), in the

¹⁵¹ *Modern Aldol Reactions*, Vol. I and Vol. II, (ed Mahrwald, R.), Wiley-VCH, Weinheim, 2008.

¹⁵² Schetter, B.; Mahrwald, R., *Angew. Chem. Int. Ed.*, 2006, 45, 7506.

¹⁵³ Weissermel, K.; Arpe, H.-J., *Industrial Organic Chemistry*, Fourth Edition, Wiley-VCH, Weinheim, 2008.

¹⁵⁴ (a) Wurtz, C. A., *J. Prakt. Chem.*, 1872, 5, 457; (b) Von Richter, reporting condensation between pentanal and heptanal performed by Borodin, A.; Von Richter, V., *Ber. Dtsch. Chem. Ges.*, 1869, 2, 552.

first step of Krebs's cycle; cleavage (Figure 39) of 1,6 phosphate diester of fructose in glycolysis (a retro-aldol condensation)¹⁵⁵.

The mechanism of the aldol reaction is illustrated below (Figure 40). It can be carried out both under basic and acid conditions. A nucleophilic enolate or enol attacks electrophilic substrate, forming a β -hydroxy-carbonyl compound. Often, same conditions lead to a further step with removal of a water molecule, named *condensation*, to give an α,β -unsaturated compound.

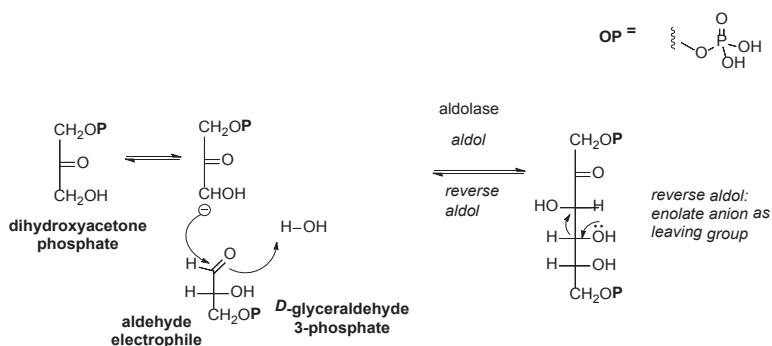


Figure 37. Condensation of glyceraldehyde-3-phosphate with dihydroxyacetone phosphate.

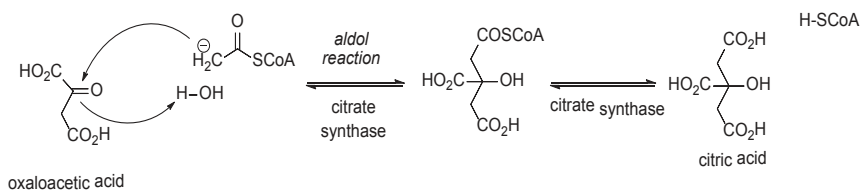


Figure 38. Addition of oxaloacetic acid to acetyl-coenzyme A.

¹⁵⁵ Dewick, P. M., *Essentials of Organic Chemistry: For Students of Pharmacy, Medicinal Chemistry and Biological Chemistry*, Wiley-VCH, Weinheim, 2006.

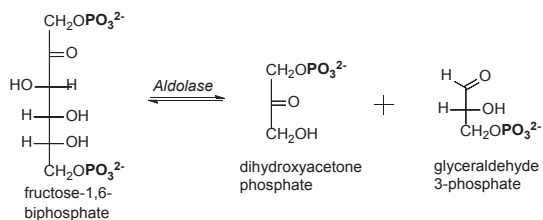


Figure 39. Cleavage of fructose 1,6-bisphosphate to give glyceraldehyde-3-phosphate and dihydroxyacetone phosphate

Electrophilic substrates are not limited to aldehydes but can also be 1,2 dicarbonyl compounds; similarly, enolizable compounds can include not only ketones, but also other molecules with aptitude to be enolizable, like esters and various 1,3 dicarbonyl compounds or equivalents.

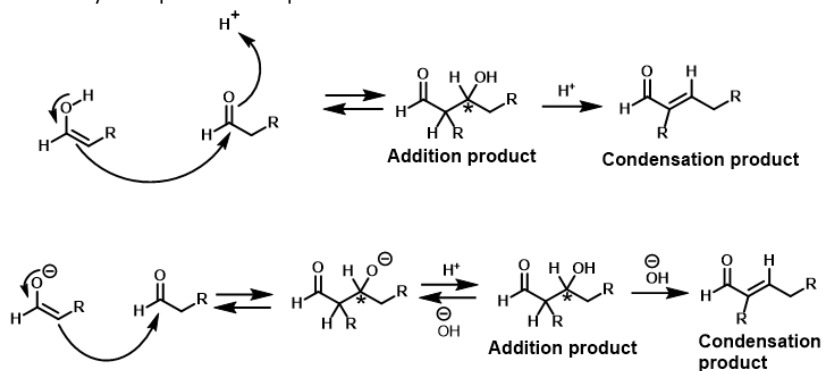


Figure 40. Mechanism for aldol reaction, in acidic conditions (upper) and in basic conditions (bottom). It's possible to make two new stereogenic centers by aldol addition.

Since aldol reaction can lead to generation of stereocenters (Figure 40), several studies were conducted to optimize stereoselectivity in the asymmetric version of the reaction. Two general approaches were developed¹⁵⁶, one using chiral catalysts¹⁵⁷ and the other which exploits stereoinduction by placing chiral moieties (chiral auxiliaries) into substrate framework¹⁵⁸.

¹⁵⁶ Machajewski, T. D.; Wong, C.-H., *Angew. Chem. Int. Ed.*, **2000**, 39, 1352.

¹⁵⁷ Trost, M. B.; Brindle, C. S., *Chem. Soc. Rev.*, **2010**, 39, 1600.

¹⁵⁸ Gnas, Y.; Glorius, F., *Synthesis*, **2006**, 12, 1899.

2.2 Mukaiyama Aldol Reaction

With the aim to gain a close control on the stereoselectivity, different approaches were developed, involving control of the enolate geometry. For this reason, many attempts, with success, were made: lithium¹⁵⁹, boron¹⁶⁰, and other metal enolates¹⁶¹, oxazolidinones and *L*-proline¹⁶² were used. Although, these methods suffered of several drawbacks.

In 1973, Mukaiyama and co-workers exploited as latent and stable enolates preformed silyl enolates using TiCl_4 as the catalyst in stoichiometric amount¹⁶³. The first catalytic version of this reaction was performed by Reetz group¹⁶⁴, exploiting Al and Ti-based catalysts. Later, Mukaiyama introduced Sn-based catalysts with improved performances¹⁶⁵. Further developments were made by Corey¹⁶⁶, Yamamoto¹⁶⁷ and, to conclude, Carreira¹⁶⁸ (Figure 41).

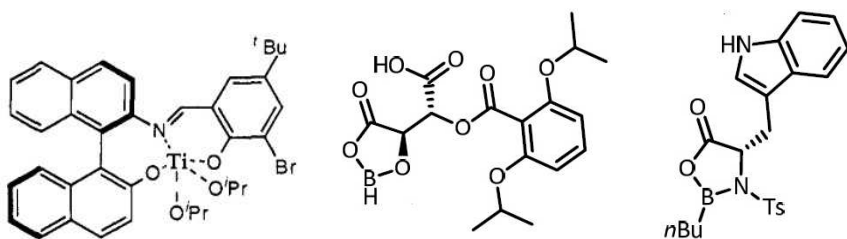


Figure 41. From left to right: Carreira's, Yamamoto's and Corey's catalysts.

¹⁵⁹ Kleschick, W. A.; Buse, C. T.; Heathcock, C.H., *J. Am. Chem. Soc.*, **1977**, *99*, 247.

¹⁶⁰ Evans, D. A.; Nelson, J. V.; Vogel, E.; Taber, T. R., *J. Am. Chem. Soc.*, **1981**, *103*, 3099.

¹⁶¹ (a) Yoshikawa, N.; Yamada, Y. M. A.; Das, J.; Sasai, H.; Shibasaki, M., *J. Am. Chem. Soc.*, **1999**, *121*, 4168; (b) Trost, B. M.; Ito, H., *J. Am. Chem. Soc.*, **2000**, *122*, 12003.

¹⁶² List, B.; Lerner, R. A.; Barbas III, C. F., *J. Am. Chem. Soc.*, **2000**, *122*, 2395.

¹⁶³ Mukaiyama, T.; Narasaka, K.; Banno, K., *Chem. Lett.*, **1973**, 1011.

¹⁶⁴ Reetz, M. T.; Kyung S.-H.; Bolm, C.; Zierke, T., *Chem. Ind.*, **1986**, 824.

¹⁶⁵ Kobayashi, S.; Uchiro, H.; Fujishita, Y.; Shiina, I.; Mukaiyama, T., *J. Am. Chem. Soc.*, **1991**, *113*, 4247.

¹⁶⁶ Corey, J. E.; Cywin, C. L.; Roper, T. D., *Tetrahedron Lett.*, **1992**, *33*, 6907.

¹⁶⁷ Furuta, K.; Maruyama, T.; Yamamoto, H., *J. Am. Chem. Soc.*, **1991**, *113*, 1041.

¹⁶⁸ Carreira, E. M.; Singer, R. A.; Lee, W., *J. Am. Chem. Soc.*, **1994**, *116*, 8837.

2.3 Vinylogous Mukaiyama Aldol reaction

In 1926, Claisen introduced the concept of vinylogy to explain the acidic properties of acetylacetone and related ketoaldehydes¹⁶⁹; this concept was taken up again by Fuson in 1935¹⁷⁰ and extended to describe the transmission of electronic effects through a conjugated organic bonding system. Many kinds of reactions were redrafted in a vinylogous fashion, as, from a synthetically point of view, this allows to introduce more carbon atoms at once^{171,172}. Mukaiyama aldol reaction followed the same fate: in 1975, Mukaiyama and Ishida proposed a vinylogous extension of the Mukaiyama aldol reaction¹⁷³. Using a crotonaldehyde derived silyl enol ether, cinnamaldehyde dimethyl acetal and TiCl_4 as a catalyst, they added four carbon atoms in a single operation instead of two to the carbonyl compound, as normally occurs for the aldol reaction (Figure 42).

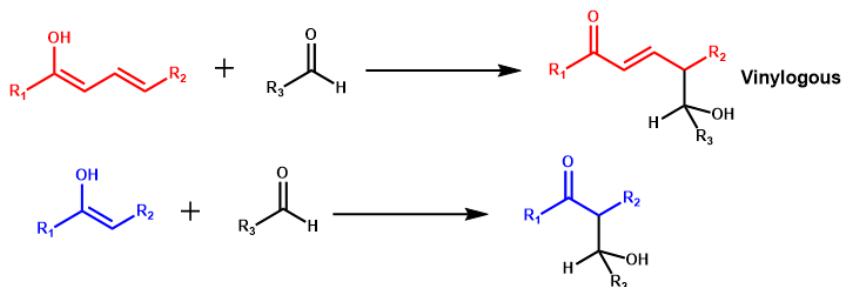


Figure 42. Comparison between a VMAR and a *normal* aldol reaction.

Not only possibility of rapidly increase in few steps the length of a carbon chain raised interest, but also issues linked to the regioselectivity: an α -adduct and a γ -adduct are possible. Nevertheless, usually, with silyl enolates the γ -adduct is the preferred one, unlike metal dienolates, which promote the formation of α -adduct

¹⁶⁹ Claisen, L., *Ber. Dtsch. Chem. Ges.*, **1926**, 59, 144.

¹⁷⁰ Fuson, R., *Chem. Rev.*, **1935**, 16, 1.

¹⁷¹ Casiraghi, G.; Zanardi, F.; Appendino, G.; Rasso, G., *Chem. Rev.*, **2000**, 100, 1929.

¹⁷² Ratjen, L.; Garcia-Garcia, P.; Lay, F.; Beck, M. E.; List, B., *Angew. Chem. Int. Ed.*, **2011**, 50, 754.

¹⁷³ Mukaiyama, T.; Ishida, A., *Chem. Lett.*, **1975**, 319.

(Figure 43), due to issues concerning orbital coefficients and electrophilic susceptibilities¹⁷⁴.

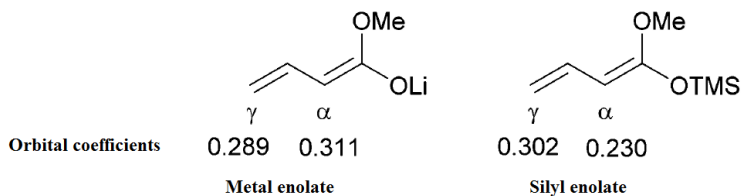


Figure 43. Comparison between metal and silyl enolate in the attack position for VMAR.

First investigation of an enantioselective catalytic version of the Vinylogous Mukaiyama Aldol Reaction (VMAR) was in 1994, by Sato and Kaneko with an acyloxyborane complex as the catalyst¹⁷⁵ (Figure 44).

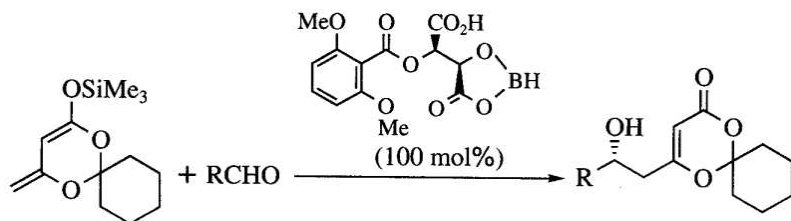


Figure 44. VMAR between a dioxinone derivative and aldehydes promoted by Sato and Kaneko catalyst.

Despite the hard attempts, their system showed some drawbacks. Further improvements were made by Carreira group¹⁷⁶, which developed a catalytic system with high turnover and enantiocontrol thanks to the lability of the used ligands (Figure 45).

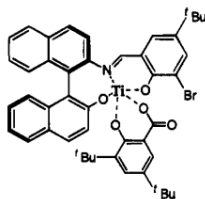


Figure 45. Carreira's catalyst for addition of dienolates to aldehydes.

¹⁷⁴ Denmark, S. E.; Heemstra, J. R.; Beutner, G. L., *Angew. Chem. Int. Ed.*, **2005**, *44*, 4682.

¹⁷⁵ Sato, M.; Sunami, S.; Sugita, Y.; Kaneko, C., *Chem. Pharm. Bull.*, **1994**, *42*, 839.

¹⁷⁶ Singer, R. A.; Carreira, E. M., *J. Am. Chem. Soc.*, **1995**, *117*, 12360.

Later, Evans and co-workers designed an efficient catalytic system for VMAR of acetoacetate and dioxinone based nucleophiles¹⁷⁷. A procedure designed specifically for open-chain silyloxy dienes was implemented firstly by Campagne group¹⁷⁸; later, Evans *et al.* developed a method for 1,3 bis(silyloxy)diene and silyloxyfurans relying on Cu-Pybox ligand (Figure 46) based catalyst¹⁷⁹.

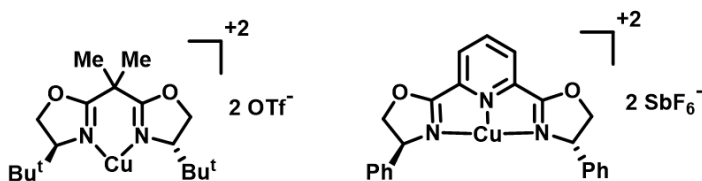


Figure 46. Evans Cu-pybox ligand based catalysts.

Frings *et al.* designed Cu-sulfoximine ligands (Figure 47) for VMAR with α -ketoesters¹⁸⁰.

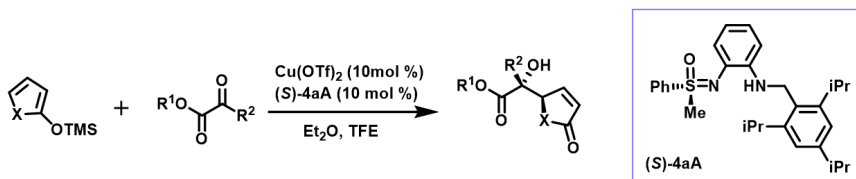


Figure 47. VMAR with α -ketoesters promoted by a Cu-sulfoximine catalyst.

A truly metal free approach was developed by Rawal and co-workers, which attempted, with good results, a hydrogen-bonding catalysis of the VMAR¹⁸¹. This idea was followed by other groups, which exploited thiourea based catalysts¹⁸² (Figure 48).

¹⁷⁷ Evans, D. A.; Fitch, D. M.; Smith, T. E.; Cee, V. J., *J. Am. Chem. Soc.*, **2000**, *122*, 10033.

¹⁷⁸ Bluet, G.; Campagne, J.-M., *J. Org. Chem.*, **2001**, *66*, 4293.

¹⁷⁹ Evans, D. A.; Kozlowski, M. C.; Murry, J. A.; Burgey, C. S.; Campos, K. R.; Connell, B. T.; Staples, R. J., *J. Am. Chem. Soc.*, **1999**, *121*, 669.

¹⁸⁰ Frings, M.; Atodiresel, I.; Wang, Y.; Runsink, J.; Raabe, G.; Bolm, C., *Chem. Eur. J.*, **2010**, *16*, 4577.

¹⁸¹ Gondí, V. B.; Gravel, M.; Rawal, V. H., *Org. Lett.*, **2005**, *7*, 5657.

¹⁸² (a) Zhu, N.; Ma, B.-C.; Zhang, Y.; Wang, W., *Adv. Synth. Catal.*, **2010**, *352*, 1291; (b) Singh, R. P.; Foxman, B. M.; Deng, L., *J. Am. Chem. Soc.*, **2010**, *132*, 9558.

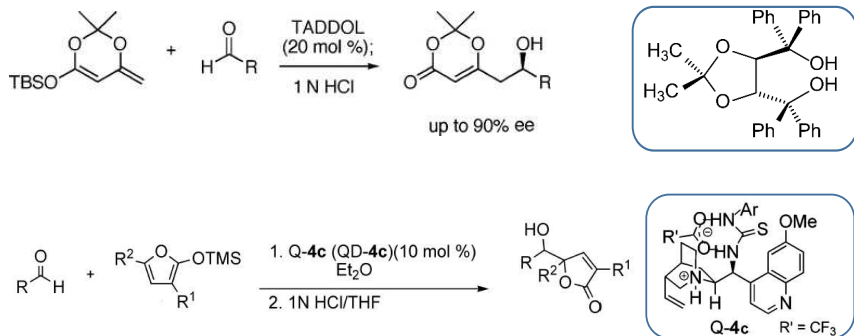


Figure 48. Examples of hydrogen bonding catalysis of VMAR. Catalysts employed are placed in blue frames.

A different approach, aimed to generate the enolate *in situ*, was developed by Feng and Terada groups¹⁸³ (Figure 49).

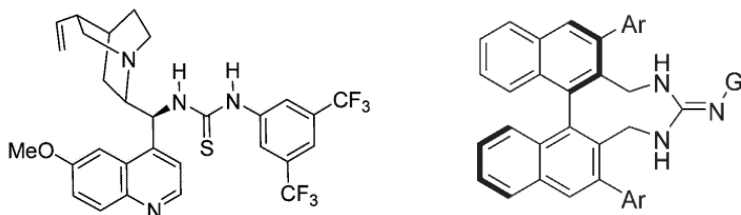


Figure 49. From left to right: Feng's and Terada's catalysts.

The interest toward VMAR is due mainly to the fact that this reaction is largely exploited for the synthesis of building blocks which make rapidly accessible complex frameworks which are recurrent in biologically relevant synthons (Figure 50). A noteworthy example is represented from polyketides and alkaloids¹⁸⁴; in fact, this reaction was also employed for synthesis of compounds (Figure 51) with therapeutic properties¹⁸⁵.

¹⁸³ (a) Yang, Y.; Zheng, K.; Zhao, J.; Shi, J.; Lin, L.; Liu, X.; Feng, X., *J. Org. Chem.*, **2010**, 75, 5382; (b) Ube, H.; Shimada, N.; Terada, M., *Angew. Chem. Int. Ed.*, **2010**, 49, 1858.

¹⁸⁴ Kalesse, M.; Cordes, M.; Symkenberg, G.; Lu, H.-H., *Nat. Prod. Rep.*, **2014**, 31, 563.

¹⁸⁵ Tatsuta, K.; Hosokawa, S., *Chem. Rev.*, **2005**, 105, 4707.

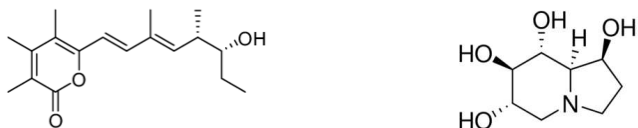


Figure 50. From left to right: chemical structures of salinipyron A and castanospermine.

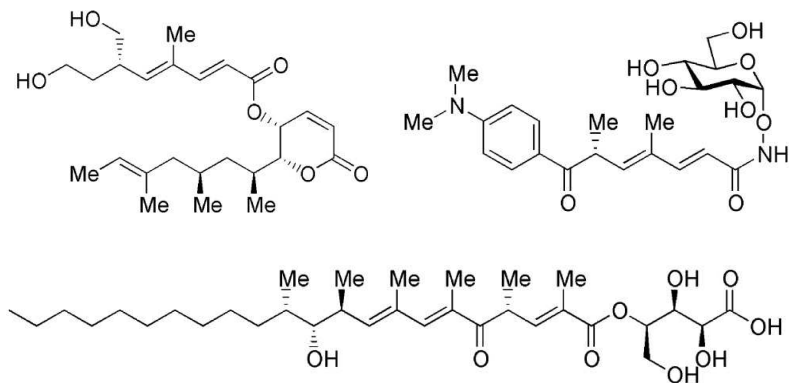


Figure 51. Upper, from left to right: rasfonin and trichostatin D; bottom: khafrefungin.

2.4 On Water Catalysis

In the perspective of building supramolecular scaffolds for biomimetic catalysis, an important opportunity is represented by the possibility of exploiting water as a medium in chemical reactions: water is fundamental for cells of living beings¹⁸⁶, because enzymatic catalysis takes place in an aqueous environment with few byproducts and generation of waste¹⁸⁷. Considering its involvement in organic catalysis is not just interesting from a conceptual point of view¹⁸⁸, as issues related to environmental sustainability are rising¹⁸⁹, chemistry is experiencing more attention to safer methods of production too. One of this issues is surely linked to

¹⁸⁶ Philip, B., *H₂O: A Biography of Water*, Orion Publishing, London, 2000.

¹⁸⁷ Chanda, A.; Fokin, V. V., *Chem. Rev.*, 2009, 109, 725.

¹⁸⁸ Simon, M.-O.; Li, C. -J., *Chem. Soc. Rev.*, 2012, 41, 1415.

¹⁸⁹ Matlack, A. S., *Introduction to Green Chemistry*, Marcel Dekker, New York, 2001.

the use of organic solvents, since they consume about 60% of the overall energy¹⁹⁰ and, if we restrict our considerations to Active Pharmaceutical Ingredient (API) manufacture, make up more than 80% of the material usage¹⁹¹.

Water has many advantages besides being environmentally friendly, in comparison to commonly employed organic solvents. It's less expensive, is not toxic or flammable and workups can result in less tedious procedures to execute¹⁹². Regardless of all these advantages, exploiting water as a medium for organic reactions has traditionally raised scepticism, principally for reasons related to reactivity, solubility and potential instability of reagents and/or catalysts to the point that in many cases water was considered a serious contaminant¹⁹³.

Moreover, water gives opportunity to exploit hydrophobic effect, that is *the tendency of non polar species to aggregate in water solution*¹⁹⁴ so as to decrease the hydrocarbon-water interfacial area. Studies on the feasibility of organic reactions on water are not new¹⁹⁵ but, since from the beginning, explanations on the role played by water were a bit ambiguous. Grieco reported a surprising acceleration for the Diels-Alder reactions and the Claisen rearrangement using water as solvent¹⁹⁶. Rideout and Breslow reported striking results from the study of the Diels-Alder reaction of cyclopentadiene with a series of dienophiles when it was performed in water¹⁹⁷, hinting that hydrogen bonding could play a considerable role, idea lately picked up again and extended by Marcus (Figure 52)¹⁹⁸.

¹⁹⁰ Szekely, G.; Jimenez-Solomon, M. F.; Marchetti, P.; Kim, J. F.; Livingston, A. G., *Green Chem.*, **2014**, *16*, 4440.

¹⁹¹ Constable, D. J. C.; Jimenez-Gonzales, C.; Henderson, R. K., *Org. Process. Res. Dev.*, **2007**, *11*, 133.

¹⁹² Riddick, J. A., *Organic Solvents: Physical Properties and Methods of Purification*, Wiley, New York, **1986**.

¹⁹³ Kobayashi, S.; Li, C.-J., *Science of Synthesis: Water in Organic Synthesis*, Eds. Kobayashi, S.; Carreira, E. M.; Decicco, C. P.; Fürstner, A.; Molander, G. A., Thieme, Stuttgart, **2012**.

¹⁹⁴ Breslow, R., *Acc. Chem. Res.*, **1991**, *24*, 159.

¹⁹⁵ Hopff, H.; Rautenstrauch, C. W., *US2262002*, **1939**.

¹⁹⁶ (a) Grieco P. A., Garner, P.; He, Z.-M., *Tetrahedron Lett.*, **1983**, *24*, 1897; (b) Grieco, P. A.; Brandes, E. B.; McCann, S.; Clark, J. D., *J. Org. Chem.*, **1989**, *54*, 5849.

¹⁹⁷ Rideout, D. C.; Breslow, R., *J. Am. Chem. Soc.*, **1980**, *102*, 7816.

¹⁹⁸ Jung, Y.; Marcus, R. A., *J. Am. Chem. Soc.*, **2007**, *129*, 5492.

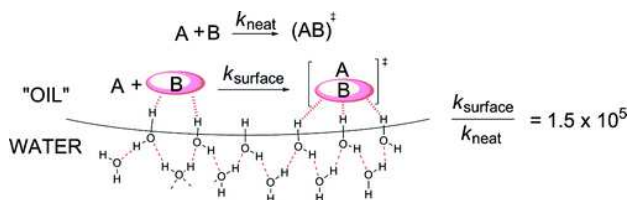


Figure 52. Model proposed by Marcus for the *on water* catalysis. At the interface between organic phase and water, every four water molecules, one has a OH group dangling and able to form hydrogen bonding with molecules in the organic phase.

Similar results were reported by Engberts in the Diels-Alder reaction between methyl vinyl ketone and cyclopentadiene¹⁹⁹. In particular, Breslow reported a remarkable effect on the cycloaddition between cyclopentadiene and acrylonitrile and between anthracene-9-carbinol and *N*-ethylmaleimide (Figure 53) and proposed that hydrophobic effect was responsible for this results.

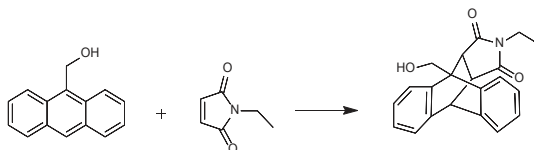


Figure 53. Diels-Alder cycloaddition between anthracene-9-carbinol and *N*-ethylmaleimide.

In the latter case, the cycloaddition rate was 2-fold slower in methanol than in isooctane and this was initially explained by the effect of hydrogen bonding that assists the binding of the dienophile to the diene in a non polar solvent, but this explanation was severely undermined when reaction rate using water was 65-fold faster than using methanol. Adding salting out agents, such as LiCl, that lower solubility of non polar compounds in water and increase their tendency to aggregate themselves too, increased reaction rate. In 2003, Pirrung performed, with significative results, Passerini (Figure 54) and Ugi reactions with water as a medium²⁰⁰. Later, he coined the term “on water” to describe reaction where

¹⁹⁹ Otto, S.; Blozkijl, W.; Engberts, J. B. F. N., *J. Org. Chem.*, **1994**, *59*, 5372.

²⁰⁰ Pirrung, M. C.; Das Sarma, K.; *J. Am. Chem. Soc.*, **2004**, *126*, 444.

reactants are insoluble in water and underlined how immiscibility of reactants with water was crucial for the reaction efficiency. He also noted the strict similarities between reactions performed on water and those performed under high pressure, as reagents are closer in transition state in both cases²⁰¹.

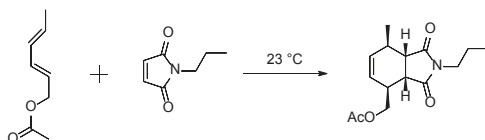
Solvent	Time (h)	Temperature (°C)	Conversion (%)	Yield (%)	Rate (%) (M ⁻² s ⁻¹)
CH ₂ Cl ₂	18	25	50	45	0.01
H ₂ O	3.5	25	100	95	0.18
1.0 M aq LiCl	0.8	25	100	95	2.86
2.5 M aq LiCl	0.3	25	100	95	nd
0.5 M aq glucose	2	25	100	94	1.29
1.0 M aq glucose	0.8	25	100	95	nd
H ₂ O	2	4	100	93	0.20
H ₂ O	5	50	100	91	0.10

Figure 54. Differences in the catalysis of Passerini reaction when performed in presence of water and in dichloromethane.

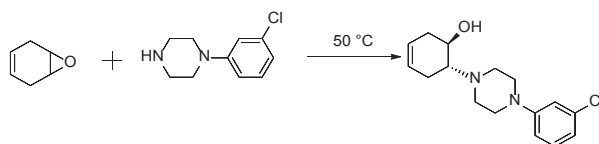
In 2005, Sharpless et al pointed out that much of the work of Breslow and Rideout was conducted in dilute homogeneous solutions (mM), so they performed Diels-Alder cycloadditions, opening of the epoxides and Claisen rearrangements (Figure 55) at high concentrations in aqueous suspension²⁰². Although results evidenced the role played by water observing dramatic enhancement in reaction rate, they concluded that “on water” strategy was effective, but reasons for the achieved results were not clear. According to Sharpless *et al.*, a careful attention should be put to rule out other possibilities, like a very limited solubility of the reactants in water or a catalysis occurring at the phase boundaries thanks to the dangling OH groups of water at the interface reactants/water.

²⁰¹ Pirrung, M. C.; Das Sarma, K.; Wang, J., *J. Org. Chem.*, **2008**, *73*, 8723.

²⁰² Narayan, S.; Muldoon, J.; Finn, M. G.; Fokin, V. V.; Kolb, H. C.; Sharpless, K. B., *Angew. Chem. Int. Ed.*, **2005**, *44*, 3275.



Solvent	Conc. [M]	Time to completion [h]	Yield [%]
toluene	1	144	79
CH ₃ CN	1	>144	43
MeOH	1	48	82
neat	3.69	10	82
H ₂ O	3.69	8	81



Solvent	Conc. [M]	t [h]	Yield [%]
toluene	1	120	<10
neat	3.88	72	76
EtOH	1	60	89
on H ₂ O	3.88	12	88

Figure 55. Diels Alder (top) and nucleophilic opening of the epoxide (bottom) performed by Sharpless group under *on water* conditions and concentration about 0.2 M.

Later, Beattie *et al* suggested, as explanation for *on water* catalysis, a simple acid mechanism facilitated by the strong adsorption of the hydroxide ion byproduct (Figure 56) at the oil-water interface²⁰³.

²⁰³ Beattie, J. K.; McErlean, C. S. P.; Phippen, C. B. W., *Chem. Eur. J.*, **2010**, *16*, 8972.

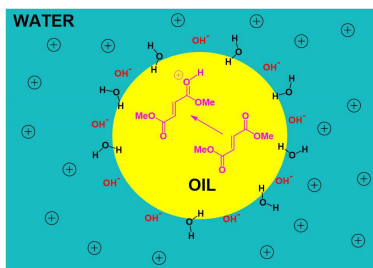


Figure 56. The model proposed by Beattie *et al.* Organic reactions on water are promoted by OH^- ions adsorbed at the interface oil-water. When a substrate S is activated by protonation, a hydroxide ion is formed and it is stabilized by a strong adsorption to the interface. If the equilibrium $\text{S} + \text{H}_2\text{O} \leftrightarrow \text{SH}^+ + \text{OH}^-$ is considered, it is easy to understand how removal of hydroxide ion by adsorption drives the protonation equilibrium of the substrate to right, justifying an acid catalysis mechanism even in neutral solutions.

Even if origins of the enhancement rate provoked by use of water have to be investigated yet, application of the “on water” approach has found more and more application in organocatalysis.

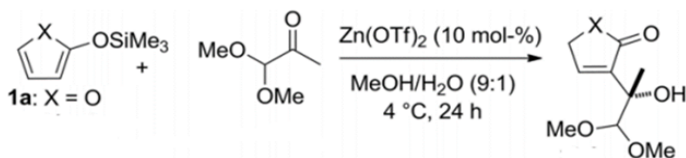
A mirable example of on water catalysis was embodied by Schreiner *et al.*, who first investigated the combined effects of *on water* and *traditional* non covalent catalysis for the opening of styrene oxide catalyzed by a thiourea based catalyst²⁰⁴, finding that non covalent interactions were amplified by hydrophobic effect. Similar results were also obtained by Rueping²⁰⁵, who studied asymmetric hydrogenation of quinolines catalyzed by Brønsted acid on water.

Another noteworthy example is the work of Woyciechowska and co-workers, who explored the effect of water in the Mukaiyama Aldol reaction of silyloxyfuran with aldehydes catalyzed by zinc triflate, achieving a general switch in regioselectivity respect to organic solvents (Figure 57). In details, they succeeded in yielding selectively α -substituted α,β -unsaturated- γ -lactones²⁰⁶.

²⁰⁴ Kleiner, C. M.; Schreiner, P. R., *Chem. Commun.*, **2006**, 0, 4315.

²⁰⁵ Rueping, M.; Theissmann, T., *Chem. Sci.*, **2010**, 1, 473.

²⁰⁶ (a) Woyciechowska, M.; Forcher, G.; Buda, S.; Mlynarski, J., *Chem. Commun.*, **2012**, 48, 11029; (b) Adamkiewicz, A.; Woyciechowska, M.; Mlynarski, J., *Eur. J. Org. Chem.*, **2016**, 16, 2897.



Entry	Solvent	Yield of α product 3a (%)	Yield of γ product 3b (%)
1	THF	n.d	45
2	<i>i</i> Pr	n.d	56
3	MeOH	30	10
4	THF/H ₂ O	44	13
5	MeOH/H₂O	75	6
6	<i>i</i> Pr/H ₂ O	44	15
7	DME/H ₂ O	38	28
8	Acetone/H ₂ O	33	12

Figure 57. Solvent studies performed by Woyciechowska and co-workers for Mukayama aldol reaction between 2-(trimethylsilyloxy)furan and pyruvic aldehyde dimethyl acetal. A more striking achievement was awarded by Bae and co-workers: investigating the performance of a cinchona-based squaramide catalyst in the Michael addition of malonates to nitroalkenes, they observed a notable increasing in reaction rate for the reaction performed under *on water* conditions²⁰⁷. Firstly, they examined a group of catalysts with different hydrophobicities performing reaction both on water (brine) and in organic solvents (Figure 58). As it can be seen, performances are better in brine than in organic solvents and better with more hydrophobic catalyst. The high increase in reaction rate allowed the authors to drastically reduce the amount of catalyst (from 1% mol to 0.01% mol) too.

²⁰⁷ Bae, H. Y.; Song, C. E., *ACS Catal.*, **2015**, *5*, 3613.

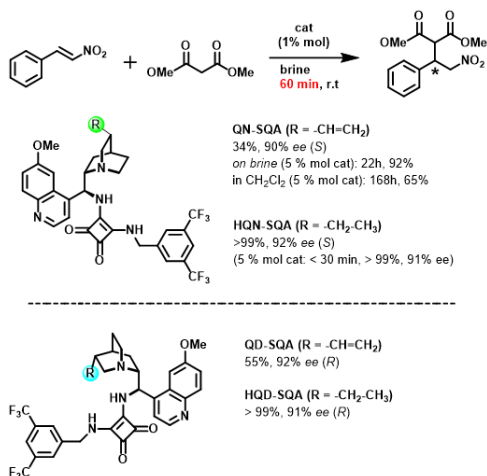


Figure 58. *On water* catalysis between nitrostyrene and dimethylmalonate with squaramide-based catalysts investigated by Bae and co-workers²⁰⁷.

2.5 Results and Discussion

2.5.1 On Water VMAR promoted by Calixarene based Catalysts

Since in the last years many efforts have been devoted to the development of environmentally oriented catalytic strategies, with a particular emphasis to the study of organic reactions in water as a medium, we decided to investigate the feasibility of VMAR, generally carried out in anhydrous organic solvents²⁰⁸, under *on water* conditions promoted by calixarene macrocycles as catalysts: we envisioned that remarkable hydrophobicity of calixarenes, little explored until now²⁰⁹, could result in a rate acceleration if used as catalysts under *on water* conditions. In addition, these supramolecular structures present an hydrophobic cavity which can

²⁰⁸ The following examples have been reported in which a mixture of water/organic solvents was used: (a) Battistini, L.; Dell'Amico, L.; Sartori, A.; Curti, C.; Pelosi, G.; Casiraghi, G.; Attanasi, O. A.; Favi, G.; Zanardi, F., *Adv. Synth. Catal.*, **2011**, 353, 1966; (b) Tian, H.; Chen, Y.; Wang, D.; Bu, Y.; Li, C., *Tetrahedron Lett.*, **2011**, 42, 1803.

²⁰⁹ Despite hydrophobicity of calixarene macrocycles, there are many examples of their use for *in water* catalysis: (a) Eymur, S.; Akceylan, E.; Sahin, O.; Uyanik, A.; Yilmaz, M., *Tetrahedron*, **2014**, 70, 4471; (b) Sayin, S.; Yilmaz, M., *RSC Adv.*, **2014**, 4, 2219; (c) Shimizu, S.; Shimada, N.; Sasaki, Y., *Green. Chem.*, **2006**, 8, 608.

be readily adorned with supramolecularly interacting groups, such as amide, urea, or thiourea moieties, which could be useful for the substrate recognition.

Thus, we carefully designed a series of calixarene derivatives (Figure 59) as ideal candidates to be employed as catalysts in VMAR between furanone **6** and α -ketoesters **7** (Scheme 1). This reaction constitutes a convenient strategy to synthesize functionalized γ -butenolides containing tertiary hydroxyl groups, as useful building blocks for biological and pharmaceutical products²¹⁰.

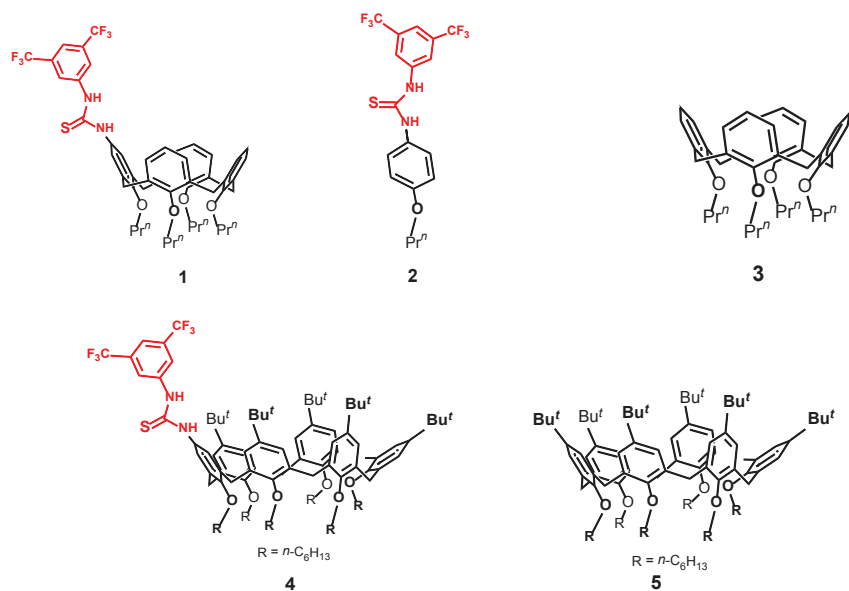
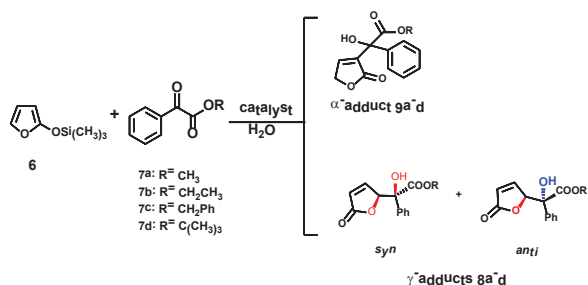


Figure 59. Catalysts exploited for VMAR under *on water* conditions.

²¹⁰ (a) Nicewicz, D. A.; Satterfield, D. A.; Schmitt, D. C.; Johnson, J. S., *J. Am. Chem. Soc.*, **2008**, *130*, 17281; (b) Hayashi, Y.; Yamaguchi, H.; Toyoshima, M.; Okado, K.; Toyo, T.; Shoji, M., *Chem. Eur. J.*, **2010**, *16*, 10150; (c) Grimaldi, M.; De Rosa, M.; Di Marino, S.; Scrima, M.; Posteraro, B.; Sanguinetti, M.; Fadda, G.; Soriente, A.; D'Ursi, M., *Biorg. & Med. Chem.*, **2010**, *18*, 7985; (d) De Rosa, M.; Zanfardino, A.; Notomista, E.; Wichelhaus, T. A.; Saturnino, C.; Varcamonti, M.; Soriente, A., *Eur. J. Med. Chem.*, **2013**, *69*, 779; (e) *Natural Lactones and Lactams*, (ed Janecki, T.), Wiley-VCH, Weinheim, **2013**.



Scheme 1. VMAR of TMSOF **6** with benzoylformates **7a-d**.

Initially, we chose as a model reaction the VMAR between 2-(trimethylsilyloxy)furan (TMSOF) **6** and methyl-benzoylformate **7a** (Scheme 1) to afford butenolide architectures **8** and **9**. We examined the feasibility of the reaction on-water without any catalyst at 30 °C (**entry 1**, **Table 1**). Because the reactants **6** and **7a** are insoluble in the reaction medium, a rapid and vigorous magnetic stirring was applied. Under these conditions, the reaction proceeded sluggishly yielding only the γ -adduct **8a** in poor yield after 24 h (Scheme 1).

Table 1. Catalyst and solvent screening for the VMAR of **7a** with **6** under on water conditions

Entry ^a	Catalyst	Medium	Conv. To 8a (%) ^b	Dr(<i>anti</i> / <i>syn</i>) ^c
1	-	H ₂ O	25	63/37
2	1	H ₂ O	50	60/40
3	1	CH ₂ Cl ₂	31	40/60
4	1	CH ₃ OH	15	48/52
5	1	THF	12	30/70
6	1	toluene	trace	Nd
7	2	H ₂ O	34	55/45
8	3	H ₂ O	23	50/50

^aAll reactions were carried out using 0.2 mmol of methyl-benzoylformate **7a**, 1.2 equiv. of **6**, 5.0 mol % of catalyst in 1 mL of medium at 30°C; t = 24h ^bDetermined by ¹H NMR analysis. ^cDetermined by ¹H NMR analysis according to literature data^{206,211,212}

²¹¹ Frings, M.; Atodiresel, I.; Runsink, J.; Raabe, G.; Bolm, C., *Chem. Eur. J.*, **2009**, *15*, 1566.

²¹² (a) Curti, C.; Battistini, L.; Ranieri, B.; Rassa, G.; Casiraghi, G.; Zanardi, F., *J. Org. Chem.*, **2011**, *76*, 2248; (b) Curti, C.; Battistini, L.; Zanardi, F.; Rassa, G.; Zambrano, V.; Pinna, L.; Casiraghi, G., *J. Org. Chem.*, **2010**, *75*, 8681.

Performing the reaction in the presence of catalyst **1** under identical conditions increased the conversion of **7a** to 50% after 24 h (entry 2, Table 1). An *anti/syn* ratio of 60/40 of the two diastereoisomers of γ -butenolide **8a** was determined by integration of their ^1H NMR signals while no trace of the α -adduct **9a** was observed. The stereochemical outcome of the VMAR in Scheme 1 can be explained through the models of the transition states proposed in Figure 61. The role of hydrogen bonds between thiourea and carbonyl groups is crucial for the activation of the substrate **7** (Figure 60a). Thus, the attack at the activated carbonyl group of **7a** from the front face of **6** (as drawn in Figure 60b) results favored thanks to the stabilization induced by C-H $\cdots\pi$ (see inset in Figure 60) interactions between methyl group of 2-(trimethylsilyloxy)furan **6** with aromatic walls of **1**.

Given these results, following a known protocol^{201,202,203}, we decided to compare the rate of the VMAR between **6** and **7a** under identical conditions but in different solvents. When the reaction was carried out in organic solvents, where either **6**, **7a**, and calixarene-catalyst **1** are completely soluble, lower conversions (entries 3-6, Table 1) were observed. These data explicitly suggest that calixarene-catalyst **1** is more active for VMAR under on-water conditions. It's noteworthy to observe that, in organic solvents, a switch of the stereoselectivity was obtained in favor of the *syn* adduct, with an *anti/syn* ratio of 40/60 and 30/70 in CH_2Cl_2 and THF (entries 3 and 5, Table 2), respectively.

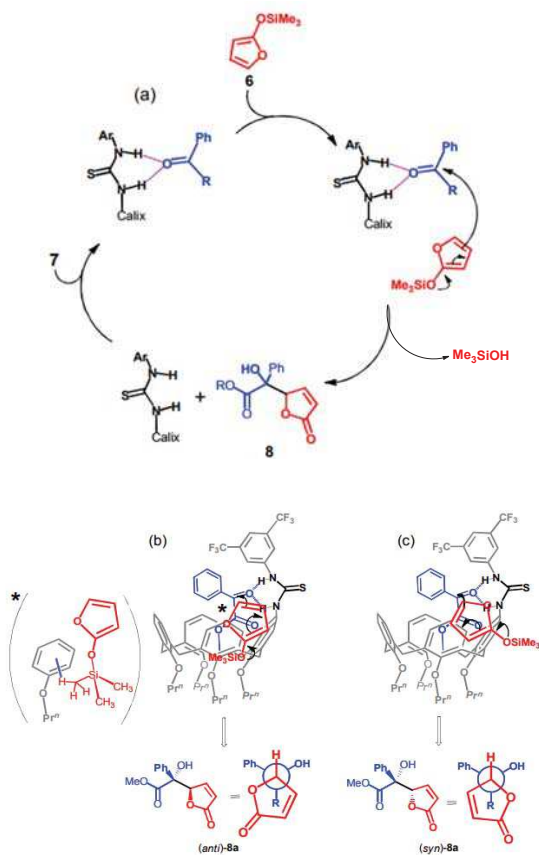


Figure 60. (a) Plausible catalytic cycle for the VMAR catalyzed by calixarene derivatives **1** and **4**. (b) and (c) Proposed transition states for the *on water* VMAR of **1** and **6** with α -ketoesters **7**.

With the aim of confirming the active role of the calix[4]arene framework for VMAR catalysis under on-water conditions, we performed the reaction between **6** and **7a** in H₂O in the presence of catalyst **2**, which could be considered the closest analog of **1** devoid of the calix-macrocyclic. Under analogous conditions (entry 7, Table 1) a 34 % of conversion was achieved. These results unequivocally demonstrated that the

hydrophobicity of the calixarene skeleton is critically important for the "on-water" catalysis of VMAR in Scheme 1.

Subsequently, we decided to investigate the role of the thiourea group in **1** in order to define its function for VMAR catalysis. When **6** and **7a** were vigorously stirred in H₂O at 30 °C for 24 h in the presence of calix[4]arene **3**²¹³, deprived of the thiourea group at the *exo*-rim, a conversion of 23 % (entry 8, Table 1) was obtained, significantly lower than that observed (50 %) under analogous condition in the presence of **1** (entry 2, Table 1). These results clearly show that the thiourea group actively contributes to accelerate the VMAR rate, likely thanks to its ability to recognize **7a** via H-bonding interactions.

To confirm this hypothesis, we investigated the binding affinity of **1** toward the substrate **7a** by ¹H NMR experiments in CDCl₃²¹⁴. (Figure S1 in Experimental Section). In details, a ¹H NMR titration was performed²¹⁵ in which the concentration of **1** was kept constant while the concentration of **7a** was varied. The addition of **7a** to the solution of **1** caused significant downfield shifts of the NMR signals of NH thiourea protons. This indicated that these groups were engaged in H-bonding interactions with the carbonyl group of **7a** (Figure 62) with a fast complexation equilibrium. A nonlinear least-squares fitting for a NH proton gives an association constant value of 600±70 M⁻¹ for the complexation of **7a** with **1**.

Molecular mechanics calculations (AMBER force field) indicated that calixarene **1** (blue colored in Figure 61) is able to complex α -ketoester **7a** (in yellow, Figure 61) by means of two H-bonds between the NH groups of **1** and the carbonyl group of **7a**. In addition, the methyl group of **7a** (in green, Figure 61) was nested into the aromatic

²¹³ Verboom, W.; Datta, S.; Asfari, Z.; Harkema, S.; Reinhoudt, D. N., *J. Org. Chem.*, **1992**, *57*, 5394.

²¹⁴ When more polar H-bonds competitors solvent such as CD₃CN and *d*₆-DMSO were used, no shift of the ¹H NMR signals of **1** was observed.

²¹⁵ Hirose, K. In *Analytical Methods in Supramolecular Chemistry* (ed. Schalley, C. A.), Wiley-VCH, Weinheim, **2007**, pp.17-54.

cavity of **1** establishing three stabilizing C-H \cdots π interactions (mean distance C-H \cdots π centroid = 2.91 Å).

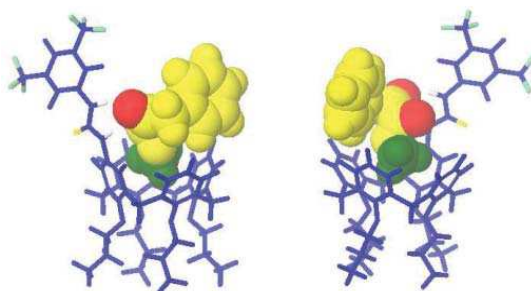


Figure 61. Different views of the optimized structure of **7a** \subset **1** complex obtained by molecular mechanics calculation (AMBER force field).

In order to optimize the reaction conditions, we studied the VMAR between **6** and **7a** under on-water conditions by changing temperature, reaction time, reagents molar ratio, calixarene catalyst, and stirring method.

By prolonging the reaction time between **6** and **7a** in the presence of **1**, from 24 to 48 h, no further improvement of the yield was observed (entry 3, Table 2). Interestingly, when the **7a/6** molar ratio was changed from 1.0/1.2 to 1.0/1.5, then a significant increase (entry 5, Table 2) of the conversion of **7a** was observed (66 % vs. 50 %). Moreover, an increase in the temperature of reaction shortened the reaction time from 24 to 14 h (entries 8 and 9, Table 2) leaving the selectivity unchanged.

Table 2. VMAR between 6 and 7a in presence of catalyst 1 at different conditions

Entry ^a	7a:6 ratio (equiv.)	T(°C)	t(h)	Conv. To 8a (%) ^b	Dr(anti/syn) ^c
1	1:1.2	30	14	35	59/41
2	1:1.2	30	24	50	60/40
3	1:1.2	30	48	51	60/40
4	1:1.5	30	14	46	60/40
5	1:1.5	30	24	66	60/40
6	1:1.5	30	48	65	55/45
7	1:1.8	30	24	53	57/43
8	1:1.5	50	24	66	59/41
9	1:1.5	50	14	66	60/40

^aAll reaction were carried out using 0.2 mmol of methyl-benzoylformate **7a**, 5.0 mol % of catalyst **1** in 1 mL of deionized water. ^bDetermined by ¹H NMR analysis. ^cDetermined by ¹H NMR analysis according to literature data^{206,211,212} The reactions were performed under rapid and vigorous magnetic stirring.

With these results in hand, we turned our attention to the calixarene-size. As recently reported²⁰⁷, the use of a more hydrophobic catalyst could result in a significant rate acceleration. On this basis, we synthesized the larger thioureido-calix[6]arene catalyst **4**, (see Experimental Section) bearing hydrophobic moieties at both the *exo* and *endo* rim, such as *tert*-butyl and *n*-hexyl groups, respectively. When the reaction was performed in the presence of catalyst **4**, an increase in the conversion up to 68 % in 14 h was observed (entry 3, Table 3), whereas calix[4]-catalyst **1** required a 24 h reaction time to obtain a 66 % of conversion (entry 2, Table 3), under the same conditions. This result clearly shows that by increasing the dimension of the calixarene-catalyst, and consequently its hydrophobicity, a significant increase of the VMAR rate occurs. In addition, an increase of the diastereoselectivity of VMAR between **6** and **7a** in the presence of **4** was observed with an *anti/syn* ratio of 80/20 for **8a**. Likely the presence of *tert*-butyl groups in **4** favors the attack of furanone **6** to the front face of **7a** (as drawn in Figure 62) thanks to the further stabilization induced by C-H... π interactions between *tert*-butyl groups of **4** and furan ring of **6** (inset in Figure 62).

Table 3. Catalyst and α -ketoester screening for the VMAR

Entry ^a	7	catalyst	t(h)	Conv. To 8 (%) ^b	Dr(anti/syn) ^c
1	7a	1	14	46	57/43
2	7a	1	24	66	54/46
3	7a	4	14	68	80/20
4	7a	4	24	72	70/30
5	7b	1	14	36	67/33
6	7b	4	14	18	57/43
7	7c	1	14	31	54/46
8	7c	4	14	36	50/50
9	7d	4	14	42	50/50

^aAll reactions were carried out using 0.2 mmol of methyl-benzoylformate **7a**, 1.5 equiv. of **6**, 5.0 mol % of catalyst in 1 mL of deionized water. ^bDetermined by ¹H NMR analysis. ^cDetermined by ¹H NMR analysis according to literature data^{206,211,212}. The reactions were performed under rapid and vigorous magnetic stirring.

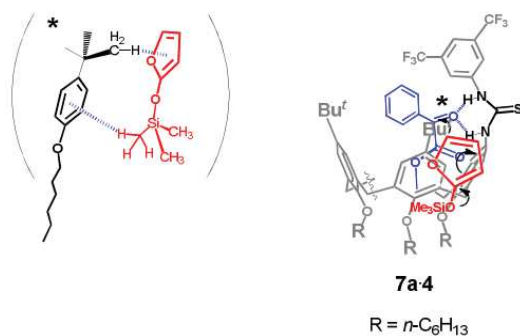


Figure 62. Proposed transition state model for the on water VMAR of **4** and **6** with α -ketoester **7a**.

Only slight changes in the conversion were obtained by prolonging the reaction time to 24 h (entry 4, Table 3). It is known that the stirring method affects the rate of organic reactions performed under on-water conditions²⁰³. Therefore, we decided to perform the VMAR between **6** and **7a** in the presence of **1** and **4** with a vortex stirring under otherwise identical conditions (at 30 °C, see Table 3). With this stirring method a 23 and 10 % of conversions of **7a** were observed after 14 h at 30 °C in the presence of catalysts **1** and **4** respectively, significantly lower with respect to the analogous magnetically stirred reactions (entries 1 and 3 in Table 3).

In analogy to **1**, the reaction between **6** and **7a** in the presence of **4** in organic solvents led to a dramatic decrease in the conversion percentages (Table 4) with respect to the on-water conditions. In these instances, an inversion of the VMAR diastereoselectivity was observed by switching from H₂O (*anti* favored) to organic solvent (*syn* favored).

Table 4. Solvent screening for the VMAR of **7a** and **6** in presence of catalyst **4**.

Entry ^a	Medium	Conv. To 8a (%) ^b	Dr(<i>anti</i> / <i>syn</i>) ^c
1	H ₂ O ^d	68	78/22
2	CH ₂ Cl ₂ ^d	39	32/68
3	CH ₃ OH	25	23/77
4	THF ^e	trace	nd
5	Toluene ^e	10	34/66

^aAll reactions were carried out using 0.2 mmol of methyl-benzoylformate **7a**, 1.2 equiv. of **6**, 5.0 mol % of catalyst **4** in 1 mL of medium at 30°C. ^bDetermined by ¹H NMR analysis. ^cDetermined by ¹H NMR analysis according to literature data^{206,211,212}. ^dDeionized water. ^eAnhydrous solvent.

Interestingly, these data indicated clearly that for both the catalysts **1** and **4** the *syn/anti* ratio observed for **8a** is closely related to the nature of the solvent more than the structure of the calix-catalyst. Probably, in water the C-H... π interactions between **7a** and the calixarene aromatic walls (see Figures 62 and 60b) are maximized, if compared with organic solvents, thus favoring the *anti* **8a** stereoisomer.

Finally, when the VMAR between **6** and **7a** was conducted in the presence of calix[6]-catalyst **5**²¹⁶, which was deprived of the thiourea group at the *exo*-rim, only a 26 % of conversion was obtained, with an *anti/syn* ratio of 60/40 for **8a**. Thus, in analogy to what observed for **3**, the H-bond recognition of **7a** by thiourea group implies an acceleration rate of VMAR.

At this point, we decided to focus our attention to the α -ketoester substrate in order to evaluate the influence of its structure on the VMAR rate. When α -ketoester **7b**, bearing an estereal ethyl group, was reacted with **6** in the presence of calix[4]arene-

²¹⁶ Gaeta, C.; Troisi, F.; Neri, P., *Org. Lett.*, **2010**, *12*, 2092.

based catalyst **1**, only a 36 % of conversion was obtained after 14 h (entry 5, Table 3), while under analogous conditions the methyl α -ketoester analogue **7a** was converted to 46 % (entry 1, Table 3). Probably, the lower catalytic efficiency of **1** toward **7b** is due to its lower affinity for the reactant. To confirm this assumption, we performed a binding study between **1** and **7b** by ^1H NMR spectroscopy. As for **7a**, an ^1H NMR titration²¹⁵ was performed in which the concentration of **1** was kept constant while the concentration of **7b** was varied (Figure S2 in the Experimental Section). By these data, an association constant of $150 \pm 30 \text{ M}^{-1}$ for the complexation of **7b** with **1** was calculated, a value significantly lower than that observed for the complexation of **7a** with **1** ($600 \pm 70 \text{ M}^{-1}$).

A close inspection of the optimized structure of **7a**·**1** complex (Figure 63a) suggests that probably the ethyl group of **7b** (its optimized structure is visible in Figure 63b) is too large to be effectively hosted into the calix-cavity and consequently this involves less hydrophobic contacts between reactant **7b** and catalyst **1**, which justify the observed lower catalytic efficiency.

The above results clearly indicated that the ability of calix catalyst **1** to accelerate VMAR under on-water condition is closely related to its recognition abilities toward the substrate **7**, thus implying a supramolecular control of this catalysis. In accordance with this conclusion, when the benzyl α -ketoester analogue **7c** was reacted with **6** in the presence of **1** only a 31 % of conversion was obtained. A similar trend was also observed with calix[6]arene-based catalyst **4**, whereby increasing the size of the alcoholic moiety of the α -ketoester substrate **7** leads to a decrease of the catalyst efficiency.

In order to rationalize these data we have performed molecular mechanics calculations with the purpose to investigate the structure of the complexes between the calix[6]arene catalyst **4** and the α -ketoester substrates **7**. Close inspection of the minimized (AMBER force field) structure (Figure 63a) of the complex between **4** and

methyl ester **7a** reveals that the methyl group of **7a** is included in the aromatic cavity of **4** optimally oriented to establish a C-H \cdots π interaction (distance C-H \cdots π centroid = 2.74 Å). In addition, H-bonds interactions were detected between the two NH groups of **4** and the carbonyl group of **7a** (Figure 63a), with a mean distance N \cdots O of 2.78 Å and a mean angle N-H \cdots O of 145.3°.

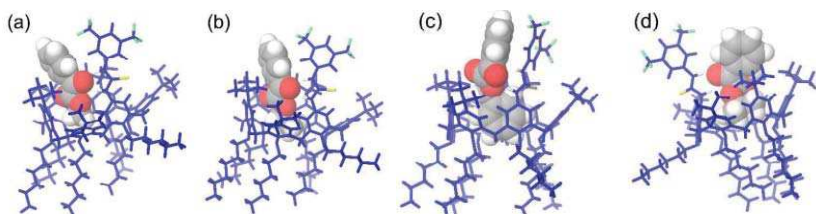


Figure 63. Optimized structures of the: (a) **7a**·**4**, (b) **7b**·**4**, (c) **7c**·**4**, (d) **7d**·**4** complexes obtained by molecular mechanics calculations (AMBER force field).

Interestingly, the H bonds in **7a**·**4** complex result shorter and stronger than those calculated for **7c**·**4** complex (Figure 63c) in which a mean distance N \cdots O of 2.87 Å and a mean angle N-H \cdots O of 139.9° were found. Based on these results, we can conclude that **4** has the strongest ability to activate the carbonyl of **7a** toward the nucleophilic attack of **6** compared to carbonyl group of **7c**. A close inspection of the minimized structure of the **7c**·**4** complex reveals that the benzyl group is hosted into the cavity of **4**, adopting an arrangement that facilitates the formation of C-H \cdots π and π \cdots π interactions (Figure 63c), but less favorable to the formation of hydrogen bonds between N-H groups of **4** and carbonyl moiety of **7c**. The data reported in Table 3 indicate a 42 % of conversion of **7d** after 14 h in presence of **4** a value higher than that observed for **7c** under analogous conditions. Also in this case the higher catalytic efficiency towards the substrate **7d** can be explained by the formation of stronger H bonds between thiourea group of **4** and carbonyl group of **7d**. In fact, examination of the minimized structure of the complex **7d**·**4** reveals the presence of

two H-bonds N-H...O=C with a mean distance of 2.82 Å shorter than that observed for **7c** (2.87 Å) and a mean angle N-H...O of 149.6°, more advantageous than the H-bond angle detected in **7c**·**4** complex (139.9°). In conclusion, analogously to catalyst **1** also for **4** the catalytic efficiency is closely related to the binding properties of the substrate **7** respect to the calixarene catalyst.

In summary, we have explored the application of calixarene macrocycles as catalysts for a vinylogous Mukaiyama aldol reaction (VMAR) under on water conditions. We have found that the rate acceleration of the VMAR is closely related to the hydrophobicity of the calixarene skeleton and to its ability to recognize the α -ketoester via H-bonding interactions with the thiourea group.

Following these results, we have hypothesized that, thanks to the amplification commonly observed under on water conditions, it was probable that even weaker H-bonds donor groups could be able to catalyze organic reactions. Thus, we designed as organocatalysts the simple aminocalix[4]arene derivatives **10**²¹⁷ and **12**²¹⁸ (Figure 64) bearing weak H-bond donor NH₂ groups.

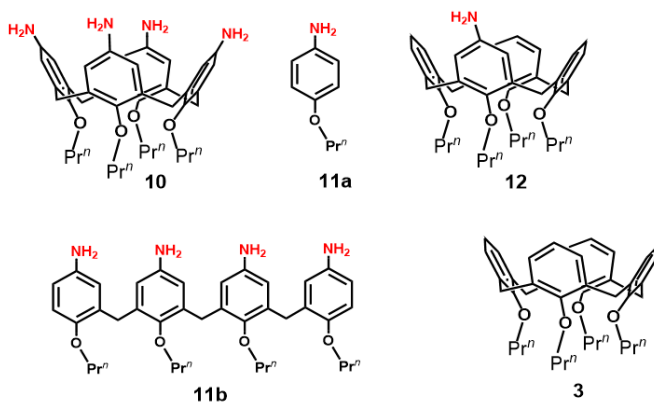
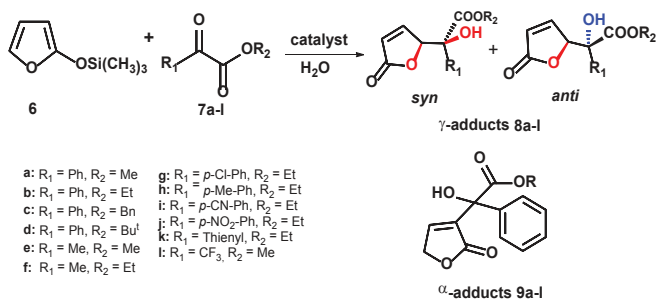


Figure 64. Structure of screened catalysts **3**, **10**, **11a**, **11b**, **12**.

²¹⁷ Jakobi, R. A.; Böhmer, V.; Gruttner, C.; Kraft, D.; Vogt, W., *New J. Chem.*, **1996**, *20*, 493.

²¹⁸ Wageningen, A. M. A., Snip, E.; Verboom, W.; Reinhoudt, D. N.; Boerrigter, H., *Liebigs Ann. Recueil*, **1997**, 2235.

As a model reaction to study the catalytic activity of tetraminocalix[4]arene **10** under "on-water conditions", the VMAR of 2-(trimethylsilyloxy)furan **6** with α -ketoesters **7a-l** was chosen (Scheme 2 and Table 5).



Scheme 2. VMAR between 2-(trimethylsilyloxy)furan **6** and α -ketoesters **7a-l**.

Firstly, we started investigating the influence of the medium on the reaction rate acceleration and on the stereo- regioselectivity between **6** and **7a** in the presence of catalyst **10** (Table 5). Interestingly, using water as medium for 4 hours (entry 3, Table 5), a nearly quantitative conversion (99 %) of **7a** to the γ -adduct **8a** was observed, with a *syn/anti* ratio of 63/37, while no trace of the α -adduct **9a** was detected. Under these conditions, the reactants **6** and **7a** and the catalyst **10** were insoluble, so the suspension was vigorously stirred magnetically. When the above on water VMAR was performed in the absence of catalyst **10**, 28 % of conversion to **8a** was observed after 14 h (entry 1, Table 5), with a switch of the stereoselectivity in favor of the *anti* adduct (*syn/anti* ratio of 32/68). This result clearly indicated that the presence of **10** accelerates the rate of conversion of **6** and **7a** to **8a** thanks to the combined effects of hydrophobic interactions with the calix[4]arene skeleton, and H-bonding interactions with the NH₂ groups of catalyst **10**.

Table 5. Solvent screening for the VMAR of **6** with **7a**.

Entry ^[a]	Catalyst	Medium	Time (h)	Conversion to 8a [%] ^[b]	Dr (<i>anti/syn</i>) ^[c]
1	-	H ₂ O ^[d]	14	28	68/32
2	10	H ₂ O ^[d]	2	74	33/67
3	10	H ₂ O ^[d]	4	99	37/63
4	10	CH ₂ Cl ₂ ^[e]	14	50	48/52
5	10	Toluene ^[e]	14	43	31/69
6	10	THF ^[e]	14	64	50/50
7	10	CH ₃ OH ^[e]	14	70	65/35
8	10	D ₂ O	2	34	34/66
9	10	H ₂ O ^[f]	4	37	21/79
10	11a	H ₂ O	4	48	38/62
11	11a	H ₂ O ^{[d],[g]}	14	65	40/60
12	11b	H ₂ O ^[d]	4	30	60/40
13	12	H ₂ O ^{[d],[g]}	14	77	54/46
14	3	H ₂ O ^[h]	24	23	50/50

[a] General conditions: **7a** (0.23 mmol, 1 eq), **6** (0.34 mmol, 1.5 eq) and 5.0 mol % of catalyst in 1 mL of medium at 30°C and under rapid and vigorous magnetic stirring. [b] Determined by ¹H NMR analysis. [c] Determined by ¹H NMR analysis according to literature data^{206,211,219}. [d] Deionized water. [e] Anhydrous solvent. [f] The reaction was performed using reciprocal shaker with an agitation speed= 1400 rpm. [g] The reaction was performed in the presence of 20 mol % of catalyst. [h] See reference 220. [i] Catalyst was recovered and reused for five consecutive runs; under these reaction conditions without appreciable changes in the yield and diastereoselectivity.

The stereochemical outcome of the above VMAR (Scheme 2) can be rationalized through the model of the transition state (**1**) proposed in Figure 65). It is very likely that the H-bonds (in red in Figure 65) between the amino group of **10** and the carbonyl group of **7a** in the complex **7a**•**10** play a key role in the activation of the substrate. Thus, the attack at the activated carbonyl group of **7a** from the front (as drawn in Figure 65) face of **6** is favored, probably thanks to the stabilization of the ternary complex **6**•**10**•**7a**, (see the proposed model obtained by molecular

²¹⁹ Wang, Y.; Xing, F.; Xue, M.; Du, G.-F.; Guo, X.-H.; Huang, K.-W.; Dai, B., *Synthesis*, **2016**, 48, 79.

²²⁰ De Rosa, M.; La Manna, P.; Soriente, A.; Gaeta, C.; Talotta, C.; Neri, P., *RSC Adv.*, **2016**, 6, 91846.

mechanics calculations, Figure 65) induced by a multipoint recognition of **6** and **7a** via H-bonds (see Figure 65).

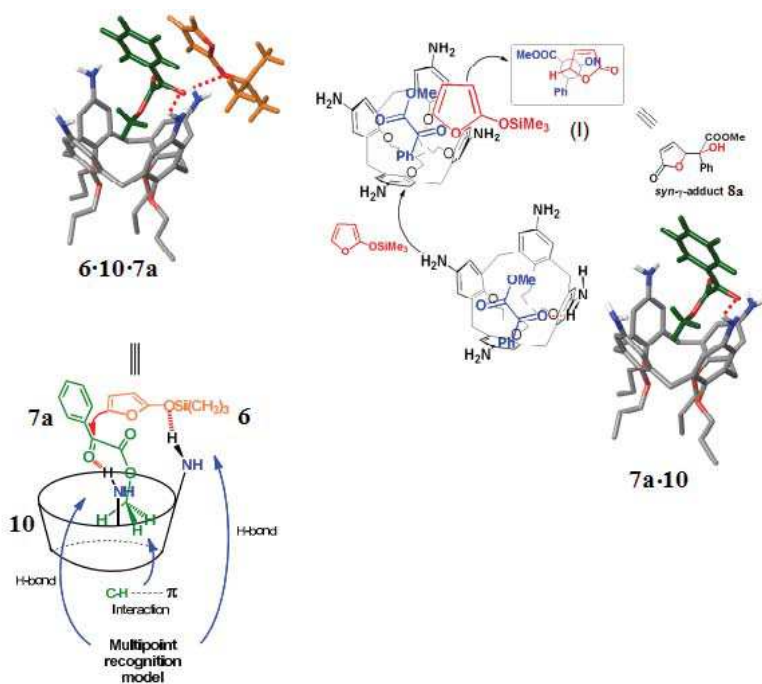


Figure 65. Plausible catalytic cycle for VMAR catalyzed by calixarene catalyst **10**. (a) Model of the complex **7a·10** obtained by molecular mechanics calculations (AMBER force field). (b) Model of the ternary complex **6·10·7a** obtained by molecular mechanics calculations and multipoint recognition model proposed for the activation of the substrate **7a**. (c) Proposed transition states for the on-water VMAR of **6** and **7a** catalyzed by **10**. (b and c) In green α -ketoester **7a**, in orange 2-(trimethylsilyloxy)furan **6**, the dotted lines in red indicate H-bonds.

In particular, we propose a ternary complex **6·10·7a** in which an amino group of **10** establishes a H-bond with the carbonyl group of **7a**, while a proximal NH₂ group forms an H-bond with the silyloxy group of **6** (see multipoint model in Figure 66). Some interesting examples in which the amino groups are effective H-bond donating groups in organocatalytic processes have been previously reported in the

literature²²¹. We have previously reported²²⁰ that when **6** and **7a** were suspended in water and stirred in the presence of *p*-H-calix[4]arene **3**, a conversion of 23 % to **8a** was observed after 24 h (entry 14, Table 5), which is significantly lower than that obtained in the presence of *p*-NH₂-calix[4]arene **10** (99 %, entry 3, in Table 5). These results clearly support the hypothesis that the weakly H-bond interacting NH₂ groups of **10** are very effective in the catalysis of the VMAR in Scheme 2 under on-water conditions. To confirm our hypothesis about the presence of H-bonding interactions between **10** and **7a**, we performed ¹H NMR titration experiments in CDCl₃. In details, the concentration of **10** was kept constant while the concentration of **7a** was varied (see Figure S5 in the Experimental Section).

The addition of **7a** to the solution of **10** caused a slight downfield shifts of the NMR signal of the aromatic hydrogen atoms in *ortho* to NH₂ groups of **10** (Figure S7 in the Experimental Section). This indicated that the NH₂ groups were engaged in H-bonding interactions with the carbonyl group of **7a** (Figure 66) with a fast complexation equilibrium. A nonlinear least-squares fitting for the ArH signal gave an association constant value of $35 \pm 5 \text{ M}^{-1}$ for the complexation of **7a** with **10** in accordance with the weak H-bond donating abilities of the NH₂ groups. Similar results were obtained with substrate **7i** (Figure S6 and Figure S8 in the Experimental Section) with an association constant value of $78 \pm 7 \text{ M}^{-1}$. Finally, we have performed DFT calculations²²² with the aim to evaluate the H-bond strength between the NH₂ groups of **10** and the carbonyl groups of **7a**. In details, the H-bond strengths were estimated through the magnetically induced currents adopting a computational protocol recently reported²²³. The DFT calculation at the B3LYP/6-31G* level of theory, indicated an energy value of 2.5 kcal/mol for the Calix–NH–H···O=C(Ph)COOMe H-bond; a value significantly lower (< 1 kcal/mol) was found for

²²¹ Sakakura, A.; Kazuhiko, K.; Ishihara, K., *Org. Lett.*, **2006**, *8*, 2229.

²²² DFT calculations were performed by Prof. R. Zanasi and Dr. G. Monaco.

²²³ (a) Fliegl, H.; Lehtonen, O.; Sundholm, D.; Kaila, V. R. I., *Phys. Chem. Chem. Phys.*, **2011**, *13*, 434; (b) Monaco, G.; Della Porta, P.; Jablonski, M.; Zanasi, R., *Phys. Chem. Chem. Phys.*, **2015**, *17*, 5966.

the H-bonding interaction between NH₂ group of **10** and carbonyl ester of **7a**. In conclusion, DFT calculations indicated that the H-bonding interaction between the amino group of **10** and the ketone carbonyl group of **7a** is classifiable as a weak H-bonding interaction²²⁴.

Performing the VMAR between **6** and **7a** in the presence of **10** as catalyst in organic solvents (see also Figure S3 in the Experimental Section), such as CH₂Cl₂ (entry 4, Table 5), toluene (entry 5, Table 5), or THF (entry 6, Table 5), lead to a decrease in the conversion of **7a** to **8a**, exactly to 50, 43, and 64 %, after 14 h, respectively, thus supporting the concept of hydrophobic amplification. Furthermore, another supporting evidence was obtained by performing the VMAR between **6** and **7a** in the presence of **10** in D₂O as medium. Under these conditions (entry 8, Table 5) a 34 % of conversion of **7a** to **8a** was observed after 2 h. This lower efficiency with respect to H₂O (99 % after 4 h) can be ascribed to the higher viscosity of D₂O (about 20 %), which reduces the mixing efficiency and consequently the hydrophobic effect²⁰⁷. The role played by the calix[4]arene scaffold on the catalytic efficiency was also investigated. In particular, when the VMAR between **6** and **7a** was conducted in the presence of the monomeric counterpart **11a**²²⁵ as catalyst under on-water conditions, then a 48 % of conversion to **8a** was obtained after 4 h (entry 10, Table 5) and a slight improvement was observed with prolonged reaction times (entry 11, Table 5), indicating a significantly lower catalytic efficiency with respect to **10** (99 % after 4 h). Additionally, it is interesting that the use of the linear tetramer **11b**²²⁶ as catalyst was considerably less efficient than **10**, under the same reaction conditions, leading to a conversion similar to that obtained in the absence of any catalyst (30 % after 4h, entry 12, Table 5). Clearly, this latter result highlights the importance of the calixarene cavity and indicates that the catalytic efficiency of **10** is also related to the

²²⁴ Steiner, T., *Angew. Chem. Int. Ed.*, **2002**, *41*, 48.

²²⁵ Ho, I.T.; Chu, J. H.; Chung, W. S., *Eur. J. Org. Chem.*, **2011**, 1472.

²²⁶ Matthews, S. E.; Saadioui, M.; Böhmer, V.; Barbosa, S.; Arnaud-Neu, F.; Schwing-Weill, M.-J.; Garcia Carrera, A.; Dozol, J.-F., *J. Prakt. Chem.*, **1999**, *341*, 264.

preorganization of the catalyst²²⁷. In fact, differently by the conformationally mobile catalyst **11b**, the calix[4]arene **10**, as is known²¹⁷, is blocked (preorganized) in the cone-structure and in this way facilitating the formation of H-bond interactions between the amino-groups at the *upper rim* of **10** and the substrate, according to the multipoint recognition model proposed in Figure 66.

In addition, when the reaction was performed in the presence of 20 % of catalyst **12** (Figure 64), bearing a single amino group at the calix[4]arene *upper rim*, the aldol adduct **8a** was obtained in 77 % after 14 h, while 5 % of **10** is already sufficient to give a 99 % of conversion after 4 h (entries 13 and 3, Table 5). The results strongly suggest that, in accordance with the multipoint recognition model proposed in Figure 66, two adjacent amino-groups strongly promote the reaction.

With the aim to optimize the reaction conditions, we studied the VMAR between **6** and **7a** in the presence of **10** under on-water conditions by changing the reaction time, the percentage of catalyst, and the temperature. By shortening the reaction time from 4 to 2 h, a drop in the yield from 99 to 74 % was observed (entry 1, Table 6). A lower percentage of catalyst **10** led to a worsening of conversion to **8a** (80 % after 14 h, entry 3 in Table 6). Analogously, an increase of the reaction temperature from 30 to 50 °C led to a lower conversion (53 % after 14 h, entry 6 in Table 6).

It has been reported that the protonation of the amino groups in 2,2'-diamino-1,1'-binaphthyl organocatalyst leads to an improvement of the catalytic efficiency of a Diels-Alder reaction between α -acyloxyacroleins with cyclic dienes because the ammonium group is a stronger H-bond donor than the amino group²²¹. Prompted by these results, we studied the catalytic efficiency of **10** toward the VMAR in Scheme 2 in the presence of acid co-catalysts (entries 7–10, Table 6). From our screening, it was clear that the combination of catalyst **10** with acid additives (entries 7-10, Table

²²⁷ As is known by the preorganization principle introduced by Cram, the more highly hosts are preorganized and more stable will be their host-guest complexes, see: Cram, D. J., *Angew. Chem. Int. Ed. Engl.*, **1988**, 27, 1009.

6) did not give any improvements, likely because the formation of anilinium species leads to an higher cation hydration and/or water-solubility of **10**.

Table 6. Optimization of the deionized water volume for the VMAR and comparison with reaction performed in presence of additives.

Entry ^[a]	10 (mol%)	Additive (mol %)	T (°C)	Conversion to 8a [%] ^[b]	Dr (<i>anti/syn</i>) ^[c]	V (mL)
1 ^[d]	5	-	30	74	33/67	1
2	5	-	30	99	37/63	1
3 ^[e]	2.5	-	30	80	53/47	1
4	5	-	30	66	30/70	0.5
5	5	-	30	68	36/64	1.5
6 ^[e]	5	-	50	53	31/69	1
7 ^[e]	5	CF ₃ COOH (10)	30	traces	nd	1
8	5	PhCOOH (10)	30	82	36/64	1
9	5	PhCOOH (20)	30	83	38/62	1
10 ^[e]	5	HCl (10)	30	traces	nd	1

^[a]General conditions: All reactions were carried out using **7a** (0.23 mmol, 1 eq.), **6** (0.34 mmol, 1.5 eq.) and 5.0 mol % of catalyst **10** in 1 mL of medium at 30°C and under rapid and vigorous magnetic stirring and stopped, if not specified, after 4 h. ^[b]Determined by ¹H NMR analysis. ^[c] Determined by ¹H NMR analysis according to literature data.^{211,219} Reaction time: 2 h. ^[e] Reaction time: 14 h.

Finally, the catalytic efficiency of tetraminocalix[4]arene **10** toward the VMAR in Scheme 2 was compared with that of Cu(OTf)₂, recently reported²¹¹ and largely exploited. The reaction between **7a** and **6** (1.5 equiv) in presence of Cu(OTf)₂ (5.0 % mol, in 1 mL of water at 30 °C under rapid and vigorous magnetic stirring) showed a moderate catalytic efficiency with a conversion of 48 % after 4 h significantly lower than that achieved using tetraminocalix[4]arene catalyst **10** (99% after 4h, entry 3,

Table 5). Furthermore, using $\text{Cu}(\text{OTf})_2$ a reversal of diastereoselectivity was obtained: *syn/anti* ratio of 21/79 was achieved, compared to 63/37 in the presence of the catalyst **10**. Thus, this result points out the potentialities of calixarene organocatalyst under on-water conditions in terms of high efficiency and stereoselectivity. Then, the influence of the amount of water was also evaluated, since it is known that under on water conditions, the amount of water provides the medium for an efficient mixing of the reactants, but it does not affect their effective concentrations²²⁸. When the VMAR was conducted in the presence of **10** and of a smaller amount of water (0.5 vs. 1.0 mL) a lower conversion to obtained after 14 h (entry 4, Table 6). A similar lower conversion to **8a** was observed by increasing the amount of water to 1.5 mL (entry 5, Table 6). Thus, our experiments showed that the optimized conditions for the VMAR in Scheme 2 are: 1 mL of pure water, a temperature of 30 °C, and 5 % mol of catalyst. With these optimized conditions in our hands, we studied the VMAR with a variety of substrates (Table 7). In detail, when ethyl, benzyl, and *tert*-butyl esters **7b–d** were used as the substrate in the presence of **10**, then conversions to the corresponding derivatives **8b–d** of 74, 85, and 86 %, respectively (entries 2-4, Table 7), were noted, indicating a lower efficiency compared to methyl ester **7a**. The preference for the *syn* diastereoisomer was respected in all cases, in addition no trace of the α -adducts **9b–d** was detected.

With a view to rationalize these data, we performed molecular mechanics calculations (AMBER force field) in order to investigate the structure of the

²²⁸ Li, C.-J.; Chan, T. -H, *Comprehensive Organic Reactions in Aqueous Media* 2nd ed, John Wiley & Sons, Hoboken, 2007.

complexes between the calix[4]arene catalyst **10** and the α -ketoester substrates **7**.

Table 7. Evaluation of substrate scope for VMAR between TMSOF **6** and ketoesters **7a-l** for VMAR catalyzed by **10** under “on-water conditions”.

Entry ^[a]	7	Product	Time (h)	Yield [%] ^[b]	Dr (<i>anti/syn</i>) ^[c]
1	a	8a	4	99	36/64 (36/64)
2	b	8b	14	74	38/62 (37/63)
3	c	8c	14	86	33/67 (33/67)
4	d	8d	14	85	35/65 (35/65)
5	e	8e	4	99	61/39 (61/39)
6	f	8f	4	99	62/38 (62/38)
7	g	8g	14	99	30/70 (28/72)
8	h	8h	14	36	30/70 (28/72)
9	i	8i	0.3	98	>1/99 (>1/99)
10	j	8j	4	98	5/95 (>1/99)
11	k	8k	14	80	46/54 (46/54)
12	l	8l	4	99	40/60 (40/60)

[a] General conditions: **7** (0.23 mmol), **6** (0.34 mmol) and 5.0 mol % of catalyst **10** in 1 mL of medium at 30°C and under rapid and vigorous magnetic stirring. [b] Combined yield of isolated diastereomers after column chromatography. [c] Determined by ¹H NMR analysis of crude mixture reaction according to literature data^{211,219,229}; in parentheses, dr of the product after column chromatography.

A close inspection of the minimized structure **7a•10** in Figure 66 reveals that the methyl group of ketoester **7a** is included in the aromatic cavity of **10** optimally oriented to establish C-H $\cdots\pi$ interactions (average distance C-H $\cdots\pi^{centroid}$ = 2.76 Å)²²¹ (see Figure 67). In addition, weak H-bonding interactions were detected between two NH₂ groups of **10** and the two carbonyl groups of **7a**, with a mean N \cdots O distance of 3.21 Å. An inspection of the minimized structures of the complexes **7b•10** and **7d•10** (Figure 67) evidenced a lower stabilization of the complexes only due to weak H-bonds between amino and carbonyl groups, while the alkyl groups of the ester moiety of **7b** and **7d** are too large to occupy the calix-cavity of **10**. Thus, in

²²⁹ (a) Evans, D. A.; Burgey, C. S.; Kozłowski, M. C.; Tregay, S. W., *J. Am. Chem. Soc.*, **1999**, *121*, 686; (b) Luo, J.; Wang, H.; Han, X.; Xu, L.-W.; Kwiatkowski, J.; Huang, K.-W.; Lu, Y., *Angew. Chem. Int. Ed.*, **2011**, *50*, 1861.

accordance with previous results, also calixarene catalysts adorned with weak H-bond donors are able to discriminate between different substrates in the VMAR reaction under on-water conditions.

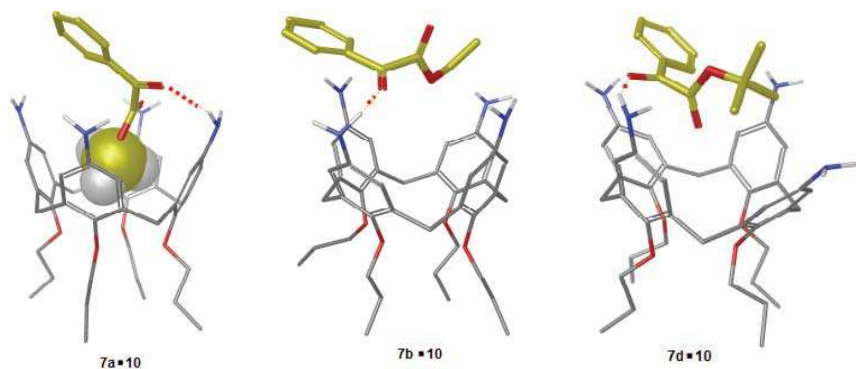


Figure 66. Optimized structures of the **7a·10**, **7b·10** and **7d·10** complexes obtained by molecular mechanics calculations (AMBER force field).

The substitution of the phenyl group of benzoylformate **7a** with a methyl group in acetyl formate **7e** has no influence on the catalytic efficiency of **10**. In fact, the conversion to **8e** was 99 % after 4 h, perfectly matching the value found for the conversion of **7a** to **8a**. Surprisingly, with substrate **7e** a switch of the stereoselectivity was observed, with a 61/39 *anti/syn* ratio (entry 5, Table 7). The model of the complex **7e·10** (Figure 67) shows that **7e** is lying on the upper rim of **10**, establishing H-bonding interactions between carbonyl and amino groups. In the transition state (Figure 67), a ternary complex **6·10·7e** is formed in which the carbonyl group of **7e** is activated by a H-bond with the amino group of **10**, while a proximal amino group forms a H-bond with the oxygen of the silyloxy group of **6**. The ternary complex **6·10·7e** (Figure 67) is further stabilized by C-H... π interactions between the α -methyl group of **7e** and the furan ring of **6**, favoring thus the attack at the activated carbonyl group of **7e** from the back face (as drawn in Figure 67) of **6**. Analogous results were found for the corresponding ethyl acetylformate substrate

7f, which gave similar experimental results (entry 6, Table 7).

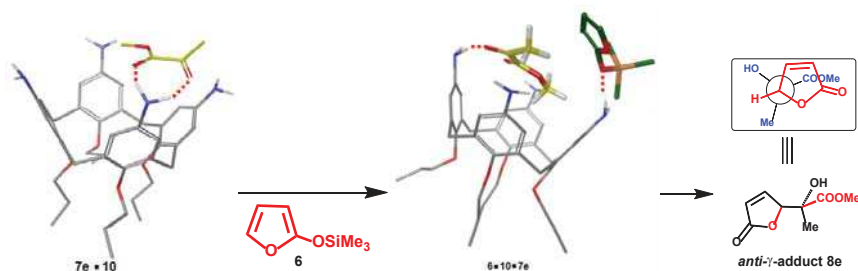


Figure 67. Plausible catalytic cycle for VMAR catalyzed by calixarene **10**. (a) Model of the complex **7e**·**10** obtained by molecular mechanics calculations (AMBER force field). (b) Model of the ternary complex **6**·**10**·**7e** obtained by molecular mechanics calculations (AMBER force field). (c) Proposed transition states for the on water VMAR of **6** and **7e** catalyzed by **10**. (b and c) In green 2-trimethyl silyloxyfuran **6**, in yellow α -keto ester **7e**, the dotted lines in red indicate the hydrogen bonds.

When ethyl 4-cyano-benzoylformate **7i** was reacted with furanone **6** in the presence of catalyst **10** under on-water conditions, a conversion of 99 % was reached after only 36 min. and, surprisingly, a *syn/anti* ratio of 99/1 (entry 9, Table 7) was observed. Analogously, an excellent *syn*-preference was observed with the substrate ethyl 4-nitro-benzoylformate **7j** (entry 10, Table 7), which showed a 99 % conversion to **8j** after 4 h with a *syn/anti* ratio of 95/5. Probably, the high *syn*-preference observed with the substrates **7i** and **7j** are due to more a compact transition state²³⁰ leading to the *syn*-isomer. In fact, a close inspection of the minimized structure of the complex **7i**·**10** (Figure 68a) revealed a multipoint recognition (Figure 68c) of the substrate **7i** in which both polar CN and C=O groups are engaged in H-bonding interactions with proximal amino groups of **10** (Figures 68a and 68c). It is likely that the multipoint H-bonding interactions between **7i** and **10** leads to a higher complex stabilization, providing a more compact transition state after the attack of the silyloxyfuran **6** (Figures 68d,e).

²³⁰ See the outcome of Mukaiyama aldol reaction in aqueous medium: Yamamoto, Y.; Maruyama, K.; Matsumoto, K., *J. Am. Chem. Soc.*, **1983**, *105*, 6963.

In a similar way, the minimized structure of the complex **7j**·**10** (Figure 68b) reveals a multipoint recognition of the substrate **7j** in which both NO₂ and C=O groups are engaged in H-bonding interactions with proximal amino groups of **10** (Figure 68c). Interestingly, when the para position of **7** was occupied by non-H-bond-interacting groups, such as the CH₃ of 4-methyl-benzoylformate **7h**, then the VMAR led to a lower *syn/anti* ratio (70/30, entry 7 in Table 7).

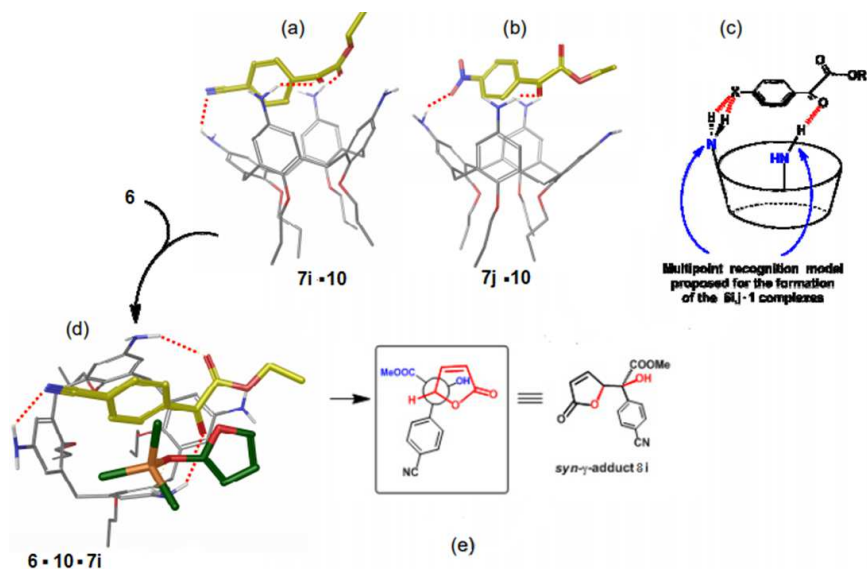


Figure 68. (a and b) Minimized structures (molecular mechanics calculations, AMBER force field) of the **7i**·**10** and **7j**·**10** complexes. (c) Multipoint recognition model proposed for the activation of the substrates **7i** and **7j**. Plausible catalytic cycle for the VMAR catalyzed by calixarene catalyst **10**. (d) Model of the ternary complex **6**·**10**·**7i** obtained by molecular mechanics calculations. (e) Proposed transition states for the on-water VMAR of **6** and **7i** catalyzed by **10**. (a, b and d) In green 2-trimethyl silyloxyfuran **6**, in yellow α -keto esters **7i** and **7j**, the dotted lines in yellow indicate the hydrogen bonds.

At this point, the question arises as to whether the high *syn*-preference observed for **8i** and **8j** (entries 9 and 10 in Table 7) could be alternatively determined by the electron-withdrawing effect of the cyano and nitro groups in **7i** and **7j**. Thus, we

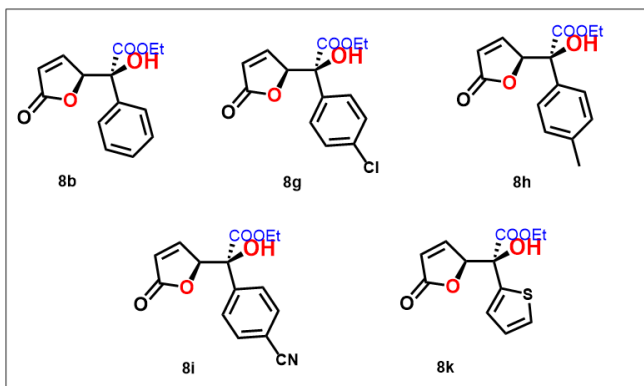
decided to investigate the VMAR on methyl 1,1,1-trifluoropyruvate **7i** bearing an electron-withdrawing trifluoromethyl group. In this instance, the minimized structure indicates that substrate **7i** is too short to match with the multipoint recognition model proposed in Figure 68c, thus predicting a lower *syn*-preference. We observed that after 4 h a 99 % of conversion to **8i** was achieved with a “normal” *syn/anti* ratio of 60/40. Analogously, with ethyl 4-chloro-benzoylformate **7g**, after 14 h a 99 % of conversion to **8g** (entry 7 Table 7) was achieved with a *syn/anti* ratio of 70/30. These results lend a strong support to the multipoint recognition of the substrate **7i** and **7j** leading to a more compact transition state during the attack of silyloxyfuran **6** and determining a higher *syn* preference.

Recyclability of catalyst **10** was investigated using the model reaction between ketoester **7a** and siloxydiene **6** under standard reaction conditions: as can be seen in Figure S4 (Experimental Section), catalytic efficiency, both in terms of yield and diastereoselectivity, was maintained for 5 cycles, setting the basis for future improvements regarding the development of more eco-friendly calixarene-based catalysts.

For γ -butenolides derivatives **8b**, **8g**, **8h**, **8i** and **8k**, crystals suitable for X-ray analysis were obtained²³¹. High-quality diffraction data were collected from frozen crystals with brilliant synchrotron radiation and the structures refinement permitted to assign unambiguously the relative configurations of the *syn* diastereomers of the compounds (crystallographic data and ellipsoid plots are present in Table S1-5 and Figure S9, Experimental Section). For derivatives **8a**, **8c**, **8d**, **8e**, **8f**, **8j** and **8l**, the *syn/anti* stereochemistry was assigned on the basis of the reported NMR spectral data^{211,219,229}.

²³¹ Compound **8i** was crystallized by slow evaporation of its solution in Chloroform/Methanol. Compounds **8b**, **8g**, **8h** and **8k** were firstly subjected to column chromatography to separate their *anti* and *syn* diastereomers; subsequently, *syn* diastereomers were respectively crystallized by slow evaporation of their solution in Hexane/Chloroform/Ethyl Acetate, Hexane/ Chloroform, Hexane/Chloroform and Chloroform. X-Ray analysis was performed by Prof. Geremia and co-workers, Università degli Studi di Trieste.

From a structural point of view, the crystals of these γ -hydroxybutenolides (Scheme 3) showed amazing properties²³². The frameworks of these compounds are equipped with the typical functionalities that can be engaged in processes of molecular



Scheme 3. γ -hydroxybutenolides whose solid state structures have been studied.

recognition through weak interactions^{233,234}. The hydroxyl and carbonyl functional groups and the aromatic or heteroaromatic rings are capable of forming intermolecular networks through hydrogen-bonds, π - π stacking or CH- π interactions. Moreover, they can drive the construction of a crystalline packing. In fact, it was observed that γ -hydroxybutenolides bearing an unsubstituted aromatic or heteroaromatic ring as the side arm show the tendency to assemble in a helical manner. The helical sense depends on the chirality of the molecule and the aromatic residues form an *aromatic zipper* between adjacent homochiral helices. This is an intriguing feature, since significant efforts are addressed to mimicking Nature in the construction of natural helical polymers, such as the double helix of DNA, with focus on the construction and the possibility of helix-sense induction.

²³² De Rosa, M.; La Manna, P.; Soriente, A.; Gaeta, C.; Talotta, C.; Hickey, N.; Geremia, S.; Neri, P., *CrystEngComm*, **2017**, *19*, 5079.

²³³ Grimme, S., *Angew. Chem. Int. Ed.*, **2008**, *47*, 3430.

²³⁴ (a) Desiraju, G. R., *Angew. Chem. Int. Ed. Engl.*, **1995**, *34*, 2311; (b) Desiraju, G. R., *Chem. Commun.*, **1997**, 1745.

Instead, γ -hydroxybutenolides with *para*-substituted aromatic rings exhibit dimers thanks to the O-H \cdots O=C intermolecular hydrogen-bond interactions. When *para* position on the aromatic ring is occupied by a substituent capable of forming strong H-bonding acceptor moiety, such as cyano group, linear chains are exhibited. These results are summarized in Figure 69. Crystal data and refinement details are reported in Table 8 (Experimental Section). Ortep representations of the asymmetric units of the five structures are shown in Figure S9 (Experimental Section).

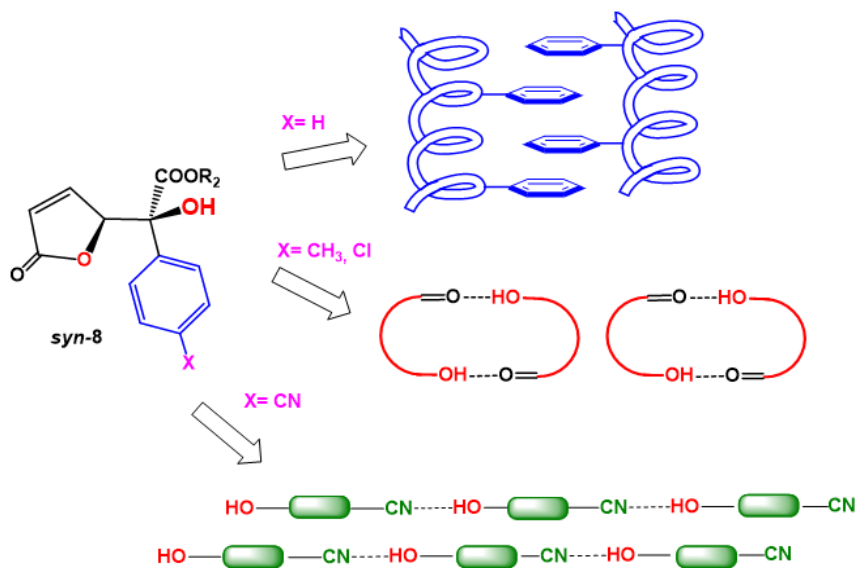


Figure 69. The *p*-substitution on the phenyl ring in **8b**, **8g**, **8h** and **8i** regulates the solid state self-assembly of γ -butenolides in helices, columns of self-assembled dimers or linear chains.

Conclusions

In summary, we have focused our attention, given the lack of methods, on the catalysis of the VMAR under on water conditions. Also, given the hydrophobicity of calixarene macrocycles and the absence of examples in literature concerning the application of calixarenes for the on water catalysis, we have tried to merge these two fields and we developed an efficient protocol for on water VMAR exploiting the aforementioned cyclophanes. So, a variety of α -ketoesters have been reacted with TMSOF in the presence of calixarene macrocycles bearing thioureido and amino moieties under mild conditions, in order to achieve γ -hydroxybutenolides. Results obtained with thioureidocalixarenes show that calixarene can be exploited in on water catalysis. Moreover, surprising outcomes have been achieved exploiting calix[4]arene derivative adorned with amino groups: this macrocycle, despite of bearing weak hydrogen-bond donor moieties, shows to be highly efficient. This can be attributable to “on-water” hydrophobic amplification of non covalent interactions (and of the resulting molecular recognition) and can allow the development of new environmentally-oriented catalytic approaches. It is expectable that the hydrophobicity and the synthetic versatility of calixarene macrocycles could play further important roles for the design of novel supramolecular organocatalysts.

Solid state assembly of five new γ -hydroxybutenolides has been examined and we have found that this self-assembly is regulated by the *para* position on the phenyl ring. Judicious placement of functional groups able to engage in non-covalent interactions could provide the opportunity to drive the crystal packing, thereby building new supramolecular architectures. We also found that racemic compounds **8b** and **8k**, bearing an unsubstituted aromatic (or heteroaromatic) side ring pack in a helical fashion with a specific helical sense related to the chirality of the molecules:

this was an interesting observation, since significant efforts are addressed to mimicking Nature in the construction of natural helical.

3. Asymmetric 1,3-dipolar cycloaddition of nitrones to α,β -unsaturated aldehydes promoted by hexameric resorcinarene capsule

3.1 1,3-Dipolar Cycloadditions

1,3-dipolar cycloaddition (1,3-DC) is a very useful reaction in organic chemistry²³⁵, as attested by the wealth of publications in literature about the argument. The first 1,3-DC was performed by Buchner²³⁶ *et al.*, who reported cycloaddition between diazoacetic ester and α,β -unsaturated aldehydes. Conceived for the first time by Smith²³⁷ and considerably investigated by Huisgens²³⁸ (often this reaction is also named *Huisgens cycloaddition*), 1,3-DC has been exploited to synthesize a broad range of products with biological relevance. Some of this remarkable moieties comprise N-O nucleosides²³⁹, lactams²⁴⁰, key-intermediate in the synthesis of multivalent peptides and amino acids²⁴¹, isoxazolidines²⁴² and sugar-derived isoxazolidines²⁴³, these latter utilized to construct polyfunctional building block for peptidomimetics design²⁴⁴ (Figure 70).

²³⁵ (a) *Synthetic Applications of 1,3-Dipolar Cycloaddition Chemistry Toward Heterocycles and Natural Products*, (eds Padwa, A.; Pearson W. H.), John Wiley & Sons, New York, 2002; (b) Sing, M. S.; Chowdhury, S.; Koley, S., *Tetrahedron*, **2016**, *72*, 1603.

²³⁶ Buchner, E., *Ber. Dtsch. Chem. Ges.*, **1888**, *21*, 2637.

²³⁷ Smith, L. I., *Chem. Rev.*, **1938**, *23*, 193.

²³⁸ Huisgens, R., *Angew. Chem. Int. Ed. Engl.*, **1963**, *2*, 565.

²³⁹ (a) Leggio, A.; Liguori, A.; Maiuolo, L.; Napoli, A.; Procopio, A.; Siciliano, C.; Sindona, G., *J. Chem. Soc., Perkin Trans.*, **1997**, *1*, 3097; (b) Leggio, A.; Liguori, A.; Procopio, A.; Siciliano, C.; Sindona, G., *Tetrahedron Lett.*, **1996**, *37*, 1277

²⁴⁰ (a) Alcalde, B.; Almendros, P.; Alonso, J. M.; Aly, M. F.; Pardo, C.; Sáez, E.; Torres, M. R., *J. Org. Chem.*, **2002**, *67*, 7004; (b) Avalos, M.; Babiano, R.; Cintas, P.; Clemente, F. R.; Gordillo, R.; Jiménez, L.; Palacios, J. C., *J. Org. Chem.*, **2003**, *68*, 6338.

²⁴¹ (a) Pieters, R. J.; Rijkers, D. T. S.; Liskamp, R. M. J., *QSAR Comb. Sci.*, **2007**, *26*, 1181; (b) Kraus, G. A.; Nagy, J. O., *Tetrahedron*, **1985**, *41*, 3537.

²⁴² Pellissier, H., *Tetrahedron*, **2007**, *63*, 3235.

²⁴³ Torrente, S.; Noya, B.; Branchadell, V.; Alonso, R., *J. Org. Chem.*, **2003**, *68*, 4772.

²⁴⁴ Richard, M.; Chapleur, Y.; Pellegrini-Moïse, N., *Carbohydr. Res.*, **2016**, *422*, 24.

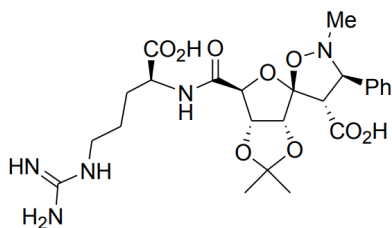


Figure 70. A spiro-sugar isoxazolidine scaffold as polyfunctional building block for peptidomimetics design.

The 1,3-DC involves reaction between two molecules, a dipole and a dipolarophile. The dipole can belong to two classes: the first one includes all dipoles of the allyl anion type, geometrically bent, with four electrons in three parallel p_z orbitals perpendicular to the dipole plane, forming a π system²⁴⁵. The second one comprises dipoles of the allenyl/propargyl anion type, geometrically linear, and also in this case there is a π system formed by four electrons (Figure 71).

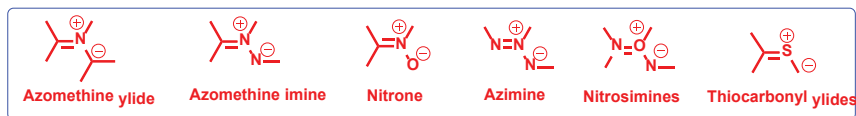


Figure 71. Allyl and allenyl anion types of dipoles for 1,3-DC.

If structure of dipole is defined as an x-y-z structure, in the case of the allyl anion type y can be oxygen, sulfur or nitrogen atom; instead, for the allenyl anion type, this choice is reduced to nitrogen atom. Dipoles can be of various kinds, such as nitrones, azomethine imines, azomethine ylides, nitrosimines, nitrosoxides, carbonyl imines and carbonyl ylides. Dipolarophiles can be electron-poor or electron-rich alkenes (Figure 72).

²⁴⁵ Gothelf, K. V.; Jørgensen, K. A., *Chem. Rev.*, **1998**, *98*, 863.

Dipoles



Dipolarophiles

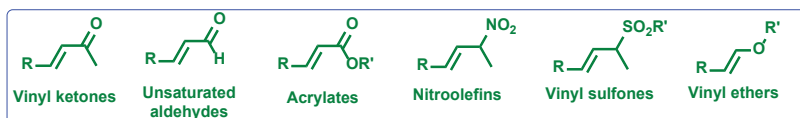


Figure 72. A series of common dipoles and dipolarophiles for 1,3-DC.

The reaction mechanism may be concerted, but that central heteroatom might also stabilize the dipole, leading to a stepwise mechanism (Figure 73).

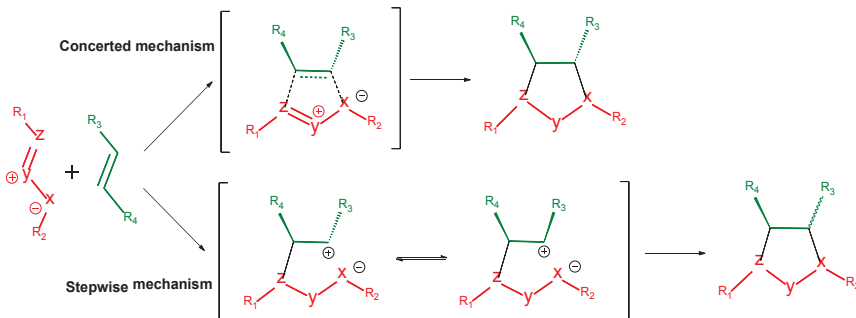


Figure 73. Possible mechanisms for the 1,3-DC.

Frontier molecular orbitals (FMO) of dipole and dipolarophile exert control on the transition state of concerted 1,3-DC reaction. FMO can be involved in three modes: $\text{HOMO}_{\text{dipole}}$ and $\text{LUMO}_{\text{dipolarophile}}$; $\text{HOMO}_{\text{dipolarophile}}$ and $\text{LUMO}_{\text{dipole}}$; the third mode is a combination of the previous ones. Stereoselectivity strongly depends on electronic factors, but also sterical effects may play an important role.

This scenario can seem simple, but exploiting Lewis acids as catalysts, changes of energy in molecular orbitals of dipole and/or dipolarophile because coordination of metal need to be considered (Figure 74).

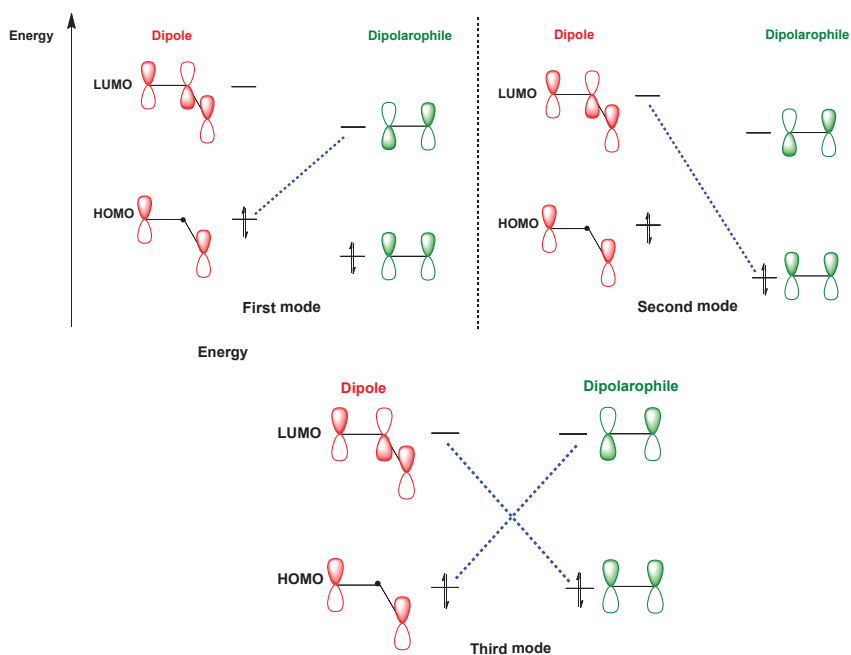


Figure 74. The three main modes in which FMO interact in 1,3-DC.

When asymmetrically 1,2-substituted alkenes (like unsaturated aldehydes) are exploited as dipolarophiles, the attack can occur on either face of π -system, leading to two possible diastereomers, *endo* and *exo*. Generally, *endo* diastereomers arise from a transition state in which nitrogen atom is directed towards the electron withdrawing group of the alkene with a very little stabilization by π -orbital interactions, somehow similarly to Diels-Alder cycloaddition. (Figure 75).

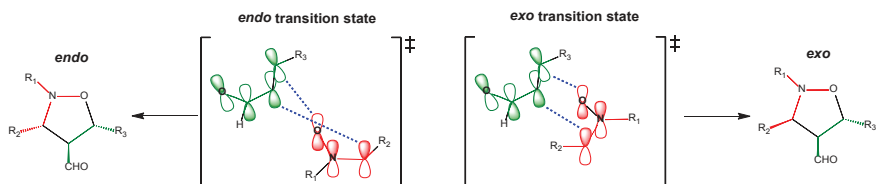


Figure 75. *Endo* and *exo* transition states for the 1,3-DC between nitron and electron-poor alkenes.

Being possible the formation of three stereocenters, eight stereomers are may result. More accurately, two kinds of regioisomers and, for each regioisomer, two kinds of diastereomers, *endo* and *exo*, are possible (Figure 76).

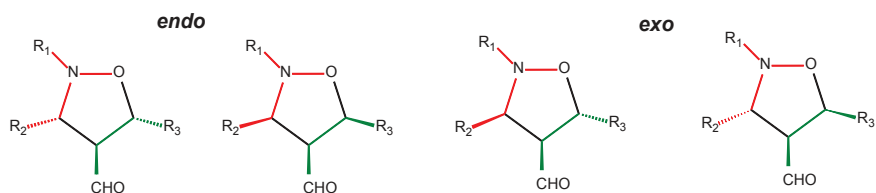


Figure 76. The pairs of enantiomers for *endo* and *exo* regioisomers resulting from the 1,3-DC between electron-poor alkenes and nitrones.

3.1.1 1,3-DC: Synthesis of Isoxazolidines from Nitrones

Unsaturated aldehydes and nitrones involved in 1,3-DC afford isoxazolidines as product. Isoxazolidines are five-membered heterocycles useful as building blocks²⁴⁶ in the synthesis of natural products and they are recurring in alkaloids extracted from marine sponges and fungal metabolites (Figure 77). In organic chemistry they occupy a special place because of the nature of their N-O bond: this latter is labile and it's easy to achieve a ring opening of the molecule under mild conditions to give aminoalcohols²⁴⁷, nitroalcohols²⁴⁸ or also aminocarbonyl compounds²⁴⁹, utilized as intermediates in total synthesis. So, a plethora of methods have been developed to

²⁴⁶ Berthet, M.; Cheviet, T.; Dujardin, G.; Parrot, I.; Martinez, J., *Chem. Rev.*, **2016**, *116*, 15235.

²⁴⁷ (a) Revuelta, J.; Cicchi, S.; Brandi, A., *Tetrahedron Lett.*, **2004**, *45*, 8375; (b) Molander, G. A.; Cavalcanti, L. N., *Org. Lett.*, **2013**, *15*, 3166; (c) Yadav, S.; Taylor, C. M., *J. Org. Chem.*, **2013**, *78*, 5401.

²⁴⁸ Roger, P.-Y.; Durand, A. -C.; Rodriguez, J.; Dulcère, J. -P., *Org. Lett.*, **2004**, *6*, 2027.

²⁴⁹ Dugovic, B.; Fiš'era, L.; Reißig, H.-U., *Eur. J. Org. Chem.*, **2008**, 277.

open isoxazolidine ring with control of the stereoselectivity.

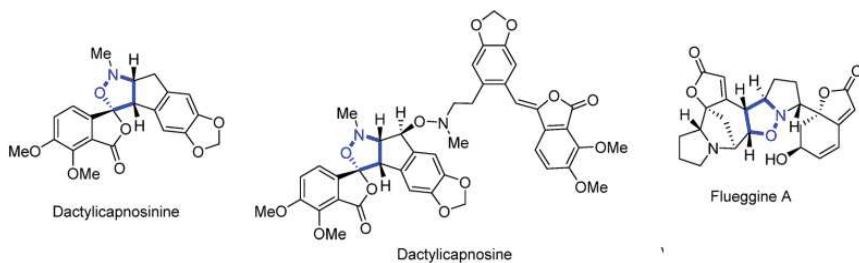


Figure 77. Examples of natural products in which isoxazolidine moiety (in blue) occurs.

Depending on electronic and stereomeric effects, two regioisomers are possible: 3,4- and 3,5-adduct. Typically 3,5-adduct is the preferred one when electron rich substituted alkenes are used and the dominating interactions are between $LUMO_{\text{dipole}}-HOMO_{\text{dipolarophile}}$; these are also known as *inverse-electron-demand cycloadditions* and steric effects also tend to promote the 3,5-cycloadduct (Figure 78), in order to relieve sterical hindrance between the end of the alkene and the C-substituent placed on the nitrone

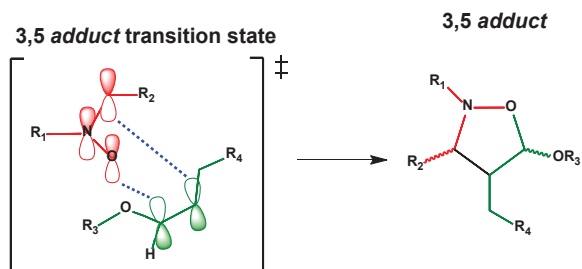


Figure 78. 3,5-cycloadduct resulting from an inverse-electron-demand cycloaddition.

Instead, if electron poor alkenes, such as unsaturated aldehydes, are utilized, 3,4-regioisomer is favored. In this case, interactions between $LUMO_{\text{dipolarophile}}-HOMO_{\text{dipole}}$ are dominating and steric effects hinder the formation of 3,4-cycloadduct. This is called also as *normal-electron-demand cycloaddition*.

From the point of view of stereoselectivity, nitronium can approach unsaturated

aldehydes in an *exo* or *endo* fashion, so two possible types of diastereomers for each regioisomer can be afforded. Moreover, as three stereocenters can be generated, each diastereomer can be obtained as mixture of two enantiomers (Figure 79).

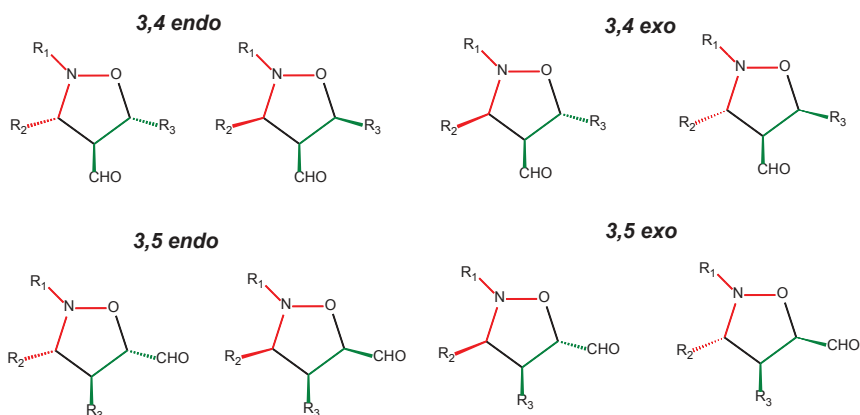


Figure 79. The eight stereoisomers originating from the 1,3-DC of nitrones with unsaturated aldehydes.

Several catalytic systems have been designed to afford isoxazolidines from nitrones. Early systems relied on the use of Lewis acids. Jørgensen group, in 1994²⁵⁰, pioneered TADDOL-Ti based chiral catalysts and in the same year Scheeren²⁵¹ introduced an oxazaborolidinone catalyst which promoted reaction between *C,N*-diphenylnitron and ketene acetals with high ee and dr, but low yield. Later, AlMeBINOL, MgX₂-Ph-BOX, Ni(ClO₄)₂DBFOX, Cu(OTf)₂BOX, Pd-BINAP and Rh based catalysts were introduced²⁵².

A common drawback of the application of metal based catalysts in promoting 1,3-DC of nitrones with electron-poor alkenes arises from the competitive or preferential coordination of Lewis acids to the nitrones, which can be seen as bidentate ligands,

²⁵⁰ Gothelf, K. V.; Jørgensen, K. A., *J. Org. Chem.*, **1994**, *59*, 5687.

²⁵¹ Seerden, J.-P. G.; Reimer, A. W. A. S.; Scheeren, H. W., *Tetrahedron Lett.*, **1994**, *35*, 4419.

²⁵² *Cycloaddition Reactions in Organic Synthesis*, (eds Kobayashi, S. & Jørgensen, K. A.), Wiley-VCH, Weinheim, **2001**.

instead of α,β -unsaturated carbonyl compounds. For this reason, a commonly adopted strategy consisted in the installation on the dipolarophile of an auxiliary oxazolidinone moiety²⁵³.

A more powerful strategy turned out to be based on iminium catalysis²⁵⁴: MacMillan and co-workers developed a series of secondary amines salt, imidazolidinones, able to lower LUMO of the enals without showing a significative coordination to the nitrones (Figure 80). This family of catalysts was further developed and investigated to achieve better performances in terms of recycle of the catalysts²⁵⁵ or greener reaction conditions²⁵⁶.

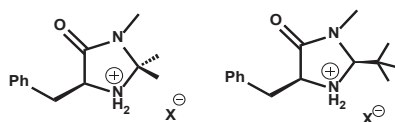


Figure 80. MacMillan's imidazolidinones. Left: first generation; right: second generation.

With this organocatalytic approach collecting success, Jørgensen and Hayashi designed diphenylprolinol TMS ether²⁵⁷ as catalysts for iminium based organocatalysis. Other groups followed iminium based strategy synthesizing hydrazide and silyloxy-aminoalcohols based catalysts²⁵⁸.

Hydrogen bonding catalysis was explored to promote 1,3-DC: Chen group investigated Jacobsen's thiourea as a catalyst²⁵⁹, while Yamamoto team used a *N*-triflyl-phosphoramidate²⁶⁰. Both teams achieved good results in terms of enantioselectivity.

²⁵³ Jensen, K. B.; Gothelf, K. V.; Hazell, R. G.; Jørgensen, K. A., *J. Org. Chem.*, **1997**, *62*, 2471.

²⁵⁴ Jen, W. S.; Wiener, J. J. M.; MacMillan, D. W. C., *J. Am. Chem. Soc.*, **2000**, *122*, 9874.

²⁵⁵ Pagoti, S.; Dutta, D.; Dash, J., *Adv. Synth. Catal.*, **2013**, *355*, 3532.

²⁵⁶ Shen, Z.-L.; Goh, K. K. K.; Wong, C. H. A.; Loo, W.-Y.; Yang, Y.-S.; Lu, J.; Loh, T.-P., *Chem. Commun.*, **2012**, *48*, 5856.

²⁵⁷ Poulsen, P. H.; Vergura, S.; Monteleón, A.; Jørgensen, D. K. B.; Jørgensen, K. A., *J. Am. Chem. Soc.*, **2016**, *138*, 6412.

²⁵⁸ (a) Lemay, M.; Trant, J.; Ogilvie, W., *Tetrahedron*, **2007**, *63*, 11644; (b) Otsuki, T.; Kumagai, J.; Kohari, Y.; Okuyama, Y.; Kwon, E.; Seki, C.; Uwai, K.; Mawatari, Y.; Kobayashi, N.; Iwasa, T.; Tokiwa, M.; Takeshita, M.; Maeda, A.; Hashimoto, A.; Turuga, K.; Nakano, H., *Eur. J. Org. Chem.*, **2015**, 7292.

²⁵⁹ Du, W.; Liu, Y.-K.; Yue, L.; Chen, Y.-C., *Synlett*, **2008**, 2997.

²⁶⁰ Jiao, P.; Nakashima, D.; Yamamoto, H., *Angew. Chem. Int. Ed.*, **2008**, *47*, 2411.

3.2 RESULTS AND DISCUSSION

As just described, the cycloaddition reactions are an effective strategy for the direct access to heterocyclic rings, key components of many compounds with different biological activity. Particularly, the [3+2] dipolar cycloadditions of α,β -unsaturated aldehydes with nitrones lead to the construction of isoxazolidines, which are important building blocks for the construction of β -lactams, amino acids and other biologically active molecules. Furthermore, the reaction can allow the simultaneous formation and the control of three contiguous stereogenic centers in heteroaromatic rings. In Chapter One, we have described how many efforts have been done to develop complex supramolecular structures as nanoreactors for organic reactions, which, thanks to their shape, size, and local environment have been exploited as enzyme mimics. Especially, we have focused our attention on self-assembled hexameric capsules. The supramolecular cage presents a cavity with a volume of approximately 1375 \AA^3 able to host from six to eight chloroform or benzene solvent molecules¹³². Thanks to its ability to accommodate a large number of molecules, the hexameric capsule **15** (Figure 81) has been largely exploited as nanoreactor in a variety of organic reactions^{143,144,145,146} and given its affinity for cationic species, it has been exploited to catalyze a cationic cascade leading to terpene cyclization¹⁴⁰ and an iminium-catalyzed reduction of α,β -unsaturated aldehydes¹⁵⁰.

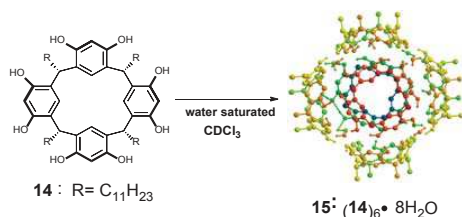
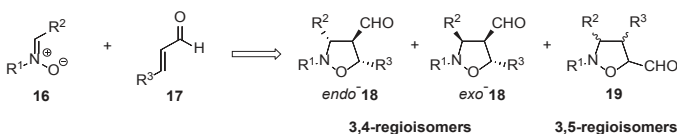


Figure 81. Self-assembly of resorcinarene **14** in water saturated CDCl₃ to give capsule **15**.

Accordingly with the aim of this PhD project concerning the synthesis and the

application of supramolecular scaffolds for biomimetic catalysis, we decided to investigate the 1,3-DC between nitrones and α,β -unsaturated aldehydes affording isoxazolidines inside the self-assembled capsule **15**²⁶¹.

As a model reaction, we started to investigate the cycloaddition between (*E*)-crotonaldehyde **17a** and nitrone **16a** (Table 8). From a mechanistic point of view, the reaction can afford two regioisomers, **18** and **19**, both of which as two diastereomers *endo* and *exo* in two possible enantiomeric forms (Scheme 4).



Scheme 4. 1,3-DC of nitrones **16** to α,β -unsaturated aldehydes **17**.

Based on a preliminary screening of the reaction conditions (see Tables S2–S4 in the Experimental Section), we selected as standard reaction conditions the reaction of **16a** (1 equiv.) with an excess of **17a** (6 equiv.), in the presence of 20 mol% of catalyst **20** and 26 mol% of capsule **15**, in water-saturated CDCl_3 as reaction medium. At first, we evaluated the outcome of the reaction with a series of *L*-proline derivatives **20a–e** as organocatalysts, in the presence of capsule **15** or not (Table 8). The reactions performed without resorcinarene capsule generally showed poor or no conversions (Table 8, entries 1–5). When the reaction was carried out in the presence of the catalyst **20a** significant difference were found with capsule **15** (Table 8, entry 1), in fact, it was observed higher reaction efficiency combined with the superior level of selectivity.

The 4-substituted isoxazolidine cycloadduct **18a** was formed almost exclusively with a diastereo- and enantioselectivity opposite to that observed in the absence of **15**, thus highlighting the key role played by **15** in steering the reaction outcome. These

²⁶¹ La Manna, P.; De Rosa, M.; Talotta, C.; Gaeta, C.; Soriente, A.; Floresta, G.; Rescifina, A.; Neri, P. *Org. Chem. Front.*, DOI: 10.1039/C7QO00942A

results can be attributed to the stabilization of the iminium intermediate by cation- π interactions with the electron-rich aromatic walls of **15**^{138,134,139}, followed by the reaction with nitrene **17a** inside the cavity and finally the release of the less affine reaction product. In order to verify our hypothesis, the same experiment was carried out adding hexamethonium iodide (**HMI**) as a competitive guest for the cavity.^{138,139,134,150} (see Table S4 in the Experimental Section) Under these conditions, the hexamethonium iodide occupying the cavity of the capsule **15** acts as inhibitor lowering both yield and enantiomeric excess.²⁶ Analogously, in presence of the proline derivative **20b** an inverse diastereo- and enantioselectivity for the *endo*-adduct **18a** (Table 8 entry 2) were observed compared to the analogous reaction in the absence of hexameric capsule **15**. The reaction exhibited no significant differences in efficiency compared to **20a** but lower diastereoselectivity (Table 8, entries 1 and 2). Interestingly, the combination of proline benzyl ester **20b** and capsule **15** provided a greater modulation of the enantiomeric excess (Table 8, entry 2). In the presence of proline-*tert*-butyl ester **20c** and capsule **15** the products **18a** and **19a** were formed in modest yield (42%, Table 8, entry 3) with respect to the analogous reaction in presence of proline methyl ester **20a** (88%, Table 8, entry 1).

Table 8. Influence of catalyst structure on the cycloaddition between **16a** and **17a**.

Reaction scheme: **16a** + **17a** $\xrightarrow[\text{CDCl}_3, 30\text{ }^\circ\text{C}]{\text{catalyst } \mathbf{20}, \text{ capsule } \mathbf{15}}$ **endo-18a** + **exo-18a** + **19a**

Entry	20	capsule 15	Yield (%) ^b	<i>endo-18a</i> / <i>exo-18a</i> / <i>19a</i> ^c	ee (%) ^d <i>endo-18a</i> / <i>exo-18a</i>	Δ ee (%) ^d <i>endo-18a</i> / <i>exo-18a</i>
1		No	42	24/67/9	14 (4S)/7 (3R)	—
	20a	Yes	88	86/1/13	43 (4R)/—	57/—
2		No	36	43/57/—	11 (4S)/ 25 (3R)	68/—20
	20b	Yes	89	55/42/3	57 (4R) / 5 (3R)	—
3		No	—	—	—	—
	20c	Yes	42	24/67/9	1 (4R)/—	—
4		No	—	—	—	—
	20d	Yes	18	100/—/—	40 (4R)/—	—
5		No	—	—	—	—
	20e	Yes	90	84/14/2	95 (4R)/8 (3R)	—

^a Reactions were performed on a 0.16 mmol scale using **17a** (1 equiv.), **16a** (6 equiv.), **20** (0.2 equiv.) and capsule **15** (0.26 equiv.) in water saturated CDCl₃ (1.1 mL) under stirring for 4 h at 30 °C. ^b Isolated yield. ^c Determined by ¹H NMR spectroscopy of the crude reaction mixture after removing resorcinarene **14**, according to literature data.^{262,254,258} ^dDetermined by HPLC analysis after reduction to the corresponding alcohol, according to literature data^{262, 254, 258}.

In the case of the hydrochloride salt of the non-esterified proline **20d** the exclusive formation of the *endo-18a* isoxazolidine was observed, but with low yields (18%), and poor enantioselectivity (Table 8, entry 4). On the contrary, the reaction

²⁶² (a) Kano, T.; Hashimoto, T.; Maruoka, K., *J. Am. Chem. Soc.*, **2005**, *127*, 11926; (b) Kanemasa, S.; Ueno, N.; Shirahase, M., *Tetrahedron Lett.*, **2002**, *43*, 657; (c) Wang, X.; Weigl, C.; Doyle, M. P., *J. Am. Chem. Soc.*, **2011**, *133*, 9572.

performed in presence of the free *L*-proline **20e** showed significant differences over the others (Table 8, entry 5); whereas the reaction without the capsule didn't work, in the presence of it the products **18a** were obtained in high yield (90%, Table 8, entry 5). Interestingly, a high regioisomeric **18a/19a** ratio of 98/2 was calculated by integration of ¹H NMR signals of two regioisomers (Table 8, entry 5), and a high *endo*-**18a**/*exo*-**18a** diastereoisomeric ratio of 84/14 was also observed (Table 8, entry 5).

Finally, very high enantioselectivity was obtained (Table 8, entry 5). Additionally, we also noted that the use of an acidic additive¹⁵⁰ resulted in a marked decrease in the reaction performance (see Table 8, entries 4 and 5). In accord with a protocol previously reported by Scarso and Tiefenbacher^{150,143}, evidences for the encapsulation of the reagents were provided by 1D- and 2D-NMR studies (see Figures S16–S20 in the Experimental Section).

Next, we moved to assess the scope of the reaction with several kinds of nitrones and aldehydes using **20e** as the catalyst (Table 9). The reaction appeared quite general with respect to the structure of the nitrones **16** in terms of efficiency and selectivity. When nitrones **16b,c,f** were used as substrates longer reaction times were required in order to obtain satisfactory yields, while a loss of enantioselectivity (Table 9, entries 2,3,6) was observed. Furthermore, the reaction of nitrone **16b** with aldehyde **17a** showed opposite trend in diastereoselectivity with a preference for the *exo* diastereomer (Table 9, entry 2).

We then investigated the structural influence of unsaturated aldehyde on the reaction outcome (Table 9). The reaction with methacrolein **17b** failed to give the cycloaddition products even after prolonged reaction times (Table 9, entry 7). The study conducted with acrolein **17c** resulted in high yield and diastereoselectivity but in significant loss of enantioselectivity. In all the cases, the reaction did not take place in the absence of the capsule.

Table 9. Influence of substituents on the 1,3-DC of nitrones to α,β -unsaturated aldehydes.

Entry ^a	Compounds	R ¹	R ²	R ³	R ⁴	capsule 15	Yield (%) ^b	<i>endo</i> -18/ <i>exo</i> -18/19 ^c	ee (%) ^d <i>endo</i> -18/ <i>exo</i> -18
1	16a, 17a, 18a, 19a	Me	Ph	Me	H	no yes	— 90	— 84/14/2	95 (4R)/0/—
2	16b, 17a, 18b, 19b ^e	Bn	Ph	Me	H	no yes	— 91	— 39/58/3	68 (4R)/39 (3R)/—
3	16c, 17a, 18c, 19c ^e	Bn	4-Me-O-C ₆ H ₄	Me	H	no yes	— 75	— 57/43/—	56 (4R)/50 (3R)/—
4	16d, 17a, 18d, 19d	Me	4-Cl-C ₆ H ₄	Me	H	no yes	— 92	— 94/6/—	94 (4R)/—/—
5	16e, 17a, 18e, 19e	Me	4-Me-C ₆ H ₄	Me	H	no yes	— 91	— 86/10/4	80 (4R)/13 (3R)/—
6	16f, 17a, 18f, 19f ^e	Bn	4-Me-C ₆ H ₄	Me	H	no yes	— 85	— 63/37/—	77 (4R)/50 (3R)/—
7	16a, 17b, 18g, 19g	Me	Ph	H	Me	no yes	— —	— —	— —
8	16b, 17c, 18h, 19h ^e	Bn	Ph	H	H	no yes	— 90	— 87/12/1	— 11 (4R)/8 (3R)
9	16f, 17c, 18i, 19f ^e	Bn	4-Me-C ₆ H ₄	H	H	no yes	— 88	— 90/10/—	— 20 (4S)/—

^a Reactions were performed on a 0.16 mmol scale using **16** (1 equiv.), **17** (6 equiv.), **20e** (0.2 equiv.) and capsule **15** (0.26 equiv.) in water saturated CDCl₃ (1.1 mL) under stirring for 4 h at 30 °C. ^b Isolated yield. ^c Determined by ¹H NMR spectroscopy of the crude reaction mixture after removing resorcinarene **14**, according to literature data.^{254,258,262} ^d Determined by HPLC analysis after reduction to the corresponding alcohol, according to literature data.^{254,258,262} ^e After 72 h reaction time.

Summarizing, these data showed that the hexameric capsule **15** is able to promote the 1,3-DC between nitrones **16** and unsaturated aldehydes **17** leading to the preferential formation of the *endo*-adducts **18** with excellent enantioselectivities. To explain the observed experimental outcome and to get more insight into the reaction mechanism, quantum mechanical studies were conducted²⁶³. The capsule effect on the course of the 1,3-DC reaction between *N*-methyl-*C*-phenyl nitrone **16a**

²⁶³ Quantum mechanical studies were conducted by Prof. A. Rescifina and co-workers, Università degli Studi di Catania.

and (*E*)-crotonaldehyde **17a** in the presence of *L*-proline **20e** as a catalyst, chosen as a representative model, was investigated. The calculations indicated that the hexameric capsule is capable to complex *L*-proline, followed by nitron and aldehyde, suggesting that formation of the iminium intermediate **21** resulting from the condensation reaction between **20e** and **17a** occurs inside the capsule (Figure 82 and Figure 83). The stereoelectronic effects of this supramolecular aggregate is also responsible of the high diastereo- and enantioselectivity exhibited by this cycloaddition.

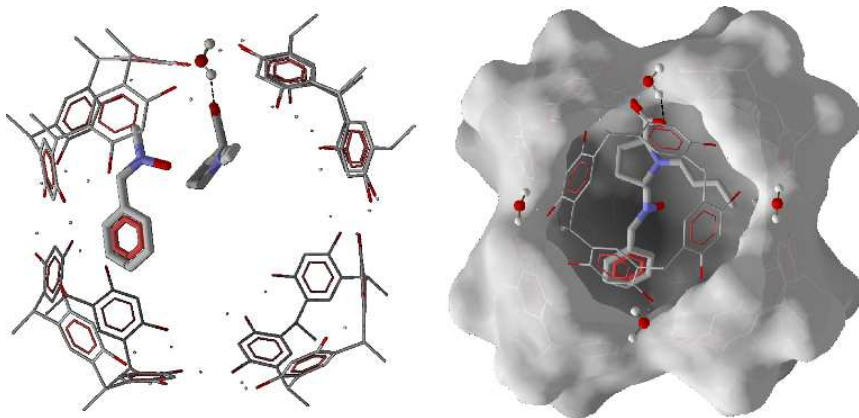


Figure 82. 3D pictures of the complex **16a** and **21** \subset **15**. It is visible the hydrogen bond interaction of the iminium carboxylic moiety with a hydrogen of a water molecule.

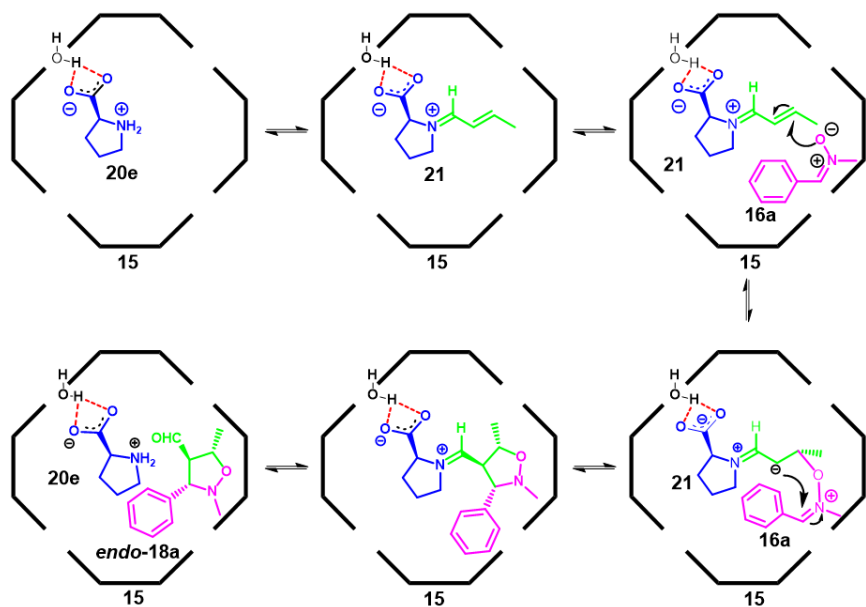


Figure 83. Proposed mechanism for the 1,3-DC between **16a** and **17a** inside the cage **15**. The attack of the iminium intermediate **21** by nitrene **16a** leads to the preferential formation of cycloadduct **endo-18a**.

Experimental evidence of the mechanistic hypotheses inferred by the calculations was given by a series of NMR DOSY and NOESY experiments (see Figures S16-20 in the Experimental Section), which supported our hypothesis.

CONCLUSIONS

We have showed that hexameric resorcinarene capsule **15** is able to promote the 1,3-DC between nitrones and unsaturated aldehydes, so affording isoxazolidines as a valuable product, occurring in several natural compounds. The confined nanoenvironment of this nanoreactor proves to be of fundamental importance for the catalysis of the reaction, since allows, after encapsulation of the substrates, catalysis under mild conditions reaction with excellent selectivity and high yields. Moreover, quantum mechanical investigations show that the importance of the capsule also lies in the fate of the iminium intermediate, as above studies indicate that the formation of the iminium intermediate occurs inside the capsule, which acts as a catalyst for this condensation reaction.

4. FRIEDEL-CRAFTS ALKYLATION INSIDE A SELF-ASSEMBLED RESORCINARENE CAPSULE

4.1 Friedel-Crafts alkylation

The Friedel-Crafts (FC) alkylation can be considered one of the most valuable and versatile C-C bond forming reactions in organic chemistry²⁶⁴, commonly employed both in laboratory and in industrial processes²⁶⁵, due to its capability to functionalize arene and heteroarene moieties with aliphatic groups. Since it was discovered, together with acylation, in 1877 by Charles Friedel and James Crafts²⁶⁶, great efforts were carried out to improve efficiency in terms of milder condition reactions, less catalyst loading and/or possibility of recycling catalyst²⁶⁷. Thus, this reaction has always posed a key step in the transformation of raw starting materials to several kinds of products, from fine chemicals²⁶⁸ to the less valuable high volume products. For example, ethylbenzene²⁶⁹, used essentially as an intermediate material in the manufacture of styrene by a dehydrogenative process, linear alkylbenzenes²⁷⁰, precursors of the related sulfonated derivatives used as surfactants, alkylanilines and alkylphenols²⁷¹, used as antioxidants, dialkylated biaryls²⁷², precursors of dicarboxylic acids, useful in the manufacture of plastic materials, and cumene are produced with a process involving a FC

²⁶⁴ *Friedel-Crafts and Related Reactions*, (ed Olah, G. A.), Wiley, New York, **1963-64**, Vol I-IV,

²⁶⁵ (a) Franck, H.-G.; Stadelhofer, J. W., *Industrial Aromatic Chemistry: Raw Materials, Processes, Products*, Springer-Verlag, Berlin, **1988**; (b) Tyrell, J. A., *Fundamentals of Industrial Chemistry: Pharmaceuticals, Polymers and Business*, Wiley, Hoboken, **2014**.

²⁶⁶ Friedel, C.; Crafts, J. M., *Compt. Rend.*, **1877**, *84*, 1392.

²⁶⁷ Rueping, M.; Nachtsheim, B. J., *Beilstein J. Org. Chem.*, **2010**, *6*, 6.

²⁶⁸ *Pharmaceutical Process Development: Current Chemical and Engineering Challenges*, (eds Blacker, J.; Williams, M. T.), RSC Publishing, Cambridge, **2011**.

²⁶⁹ Perego, C.; Ingallina, P., *Catal. Today*, **2002**, *73*, 3.

²⁷⁰ De Almeida, J. L. G.; Dufaux, M.; Taarit, B. Y.; Naccache, C., *J. Am. Oil Chem. Soc.*, **1994**, *71*, 675.

²⁷¹ Arpe, H.-J., *Industrial Organic Chemistry*, 5th Edition, Wiley-VCH, Weinheim, **2010**.

²⁷² Schaeffgen, J. R., US Pat 4118372, **1975**.

alkylation in liquid phase (AlCl_3 as catalyst) or gas phase (a fixed bed of either a Lewis Acid or a synthetic zeolite catalyst). Other applications linked to large scale hydrocarbon processing concern hydroalkylation processes, which occupy a special role in the fragrance and herbicides industry (Figure 84).

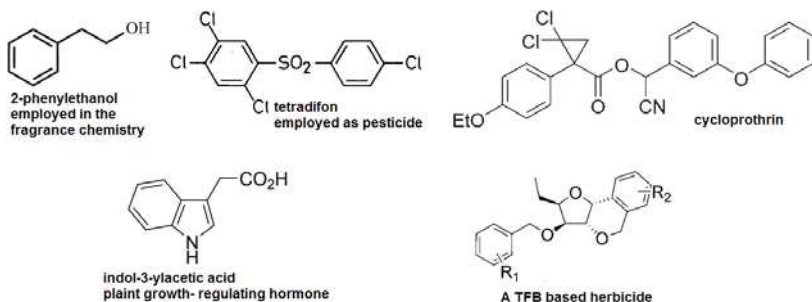


Figure 84. A series of pesticides and fragrance of industrial relevance.

Diarylalkanes, key fragments into synthesis of many fine chemicals and pharmaceuticals²⁷³ (Figure 85), are prepared by Friedel-Crafts methods.

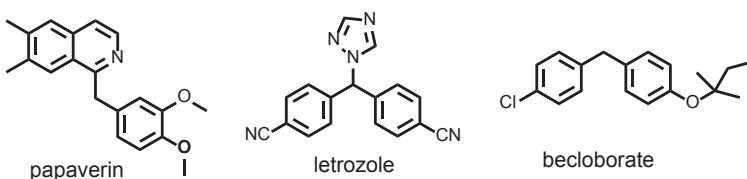


Figure 85. Some diarylalkane-based pharmaceuticals.

²⁷³ (a) Wai, J. S.; Egbertson, M. S.; Payne, L. S.; Fisher, T. E.; Embrey, M. W.; Tran, L. O.; Melamed, J. Y.; Langford, H. M.; Guare, J. P.; Zhuang, L. H.; Grey, V. E.; Vacca, J. P.; Holloway, M. K.; Naylor-Olsen, A. M.; Hazuda, D. J.; Felock, P. J.; Wolfe, A. L.; Stillmock, K. A.; Schleif, W. A.; Gabryelsky, L. J.; Young, S. D., *J. Med. Chem.* **2000**, *43*, 4923; (b) Ohtake, Y.; Sato, T.; Kobayashi, T.; Nishimoto, M.; Taka, N.; Takano, K.; Yamamoto, K.; Ohmori, M.; Yamaguchi, M.; Takami, K.; Yeu, S. Y.; Ahn, K. H.; Matsuoka, H.; Morikawa, K.; Suzuki, M.; Hagita, H.; Ozawa, K.; Yamaguchi, K.; Kato, M.; Ikeda, S. *J. Med. Chem.*, **2012**, *55*, 7828.

Also indoles²⁷⁴, whose chemistry has been far studied and which represent a privileged scaffold present in more than 3000 isolated natural products²⁷⁵ with different biological activities (Figure 86) and molecules recurring in agrochemical and pharmaceutical industry, undergo introduction of alkyl substructures through Friedel-Crafts reaction.

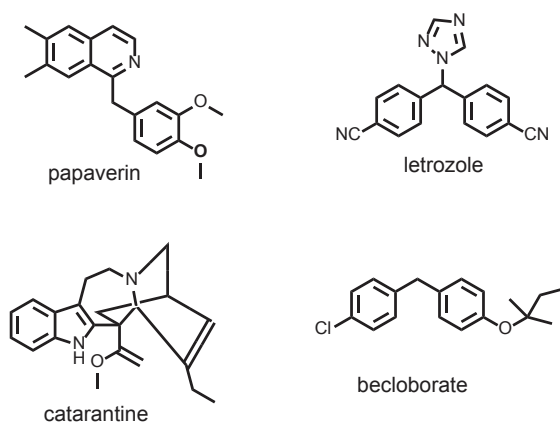


Figure 86. Some isolated natural product with indole framework.

In its original version, AlCl_3 was utilized as catalyst. Figure 87 shows the general mechanism: the reaction starts with the nucleophilic attack of the arene substrate on electrophilic moieties such as alkyl halides, to give the Wheland complex, which evolves to provide the final product.

²⁷⁴ Kaushik, N. K.; Kaushik, N.; Attri, P.; Kumar, N.; Kim, C. H.; Verma, A. K.; Choi, E. H., *Molecules*, **2013**, *18*, 6620.

²⁷⁵ *Catalytic Asymmetric Friedel-Crafts Alkylations*, (eds Bandini, M.; Umani-Ronchi, A.), Wiley-VCH, Weinheim, **2009**.

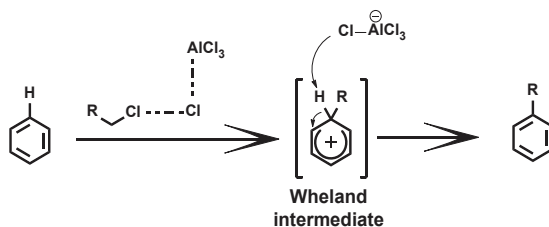


Figure 87. Mechanism for the FC reaction of benzene with alkyl chlorides catalyzed by AlCl_3 .

Other Lewis acids were exploited, such as BeCl_2 , TiCl_4 , SnCl_4 , SbCl_5 , BF_3 , $\text{Sc}(\text{OTf})_3$ or $\text{Cu}(\text{OTf})_2$ complexes²⁷⁶ with appropriate ligands and chiral Al-salen complexes to obtain excellent enantioselectivities and $\text{Mo}(\text{CO})_6$, Brønsted acids²⁷⁷ (sulfuric and hydrofluoric acid) or superacids²⁷⁸, such as triflic acid and imidazolidinones²⁷⁹. In industrial processes, Lewis acids are supported on solids with high porosity, like zeolites²⁸⁰. Generally, FC alkylation requires a stoichiometric amount of Lewis acid catalyst and alkyl chlorides, which unfortunately are a source of undesirable byproducts. With the increasing consciousness about the need of more environmentally friendly and benign methods, new processes were developed, moving towards more *green* catalysts, reactants and solvents. Uemura and co-workers²⁸¹ serendipitously discovered the possibility to exploit alcohols instead of halides as reagents. Investigating conversion of benzyl and alkyl alcohols to the respective chlorides by TeCl_4 in non aromatic solvents they found it occurred with good yields, but when changed solvent using toluene, they found diarylalkanes in high yields. The same result was yielded with catalytic amount of TeCl_4 . Potential

²⁷⁶ Wu, J.; Wang, D.; Wu, F.; Wan, B., *J. Org. Chem.*, **2013**, 78, 5611.

²⁷⁷ (a) You, S.-L.; Cai, Q.; Zeng, M., *Chem. Soc. Rev.*, **2009**, 38, 2190; (b) Yamamoto, Y.; Itonaga, K., *Chem. Eur. J.*, **2008**, 14, 10705.

²⁷⁸ Olah, G. A.; Prakash, G. K. S.; Molnár, A.; Sommer, J., *Superacid Chemistry, Second Edition*, Wiley, Hoboken, **2008**.

²⁷⁹ Paras, N. A.; MacMillan, D. W. C., *J. Am. Chem. Soc.*, **2001**, 123, 4370.

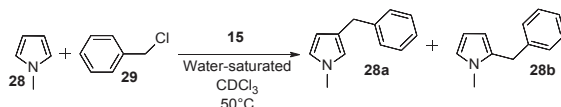
²⁸⁰ Bidart, A. M. F.; Borges, A. P. S.; Nogueira, L.; Lachter, E. R.; Mota, C. J. A., *Catal. Lett.*, **2001**, 75, 155.

²⁸¹ Nishibayashi, Y.; Inada, Y.; Hidai, M.; Uemura, S., *J. Am. Chem. Soc.*, **2002**, 124, 7900.

use of benzyl alcohols in FC alkylation was systematically investigated, with satisfactory results, by Fukuzawa group²⁸², which also used Sc(OTf)₃ as a water and air stable catalyst. In this scenario, Laali and co-workers²⁸³ exploited strategies involving metal triflates in ionic liquids to catalyze FC alkylation and later, Mayr²⁸⁴ group performed this reaction with alkyl halides in water/HFIP. Substrate scope was expanded to include unsaturated aldehydes, epoxides, allyl-substituted frameworks²⁸⁵, and nowadays, nearly all organic compounds exhibiting electrophilic character have been exploited in FC alkylation reactions.

4.2 Results and Discussion

As a part of this PhD project, also aimed at the exploration of the large possibilities offered by catalysis into confined environments, with particular regard to the C-C bond forming reactions, we studied the FC benzylation between aromatic and heteroaromatic compounds and benzyl chloride inside the hexameric capsule formed following the self-assembly of resorcin[4]arene subunits. Firstly, we investigated benzylation reaction between *N*-methylpyrrole (**28**) and benzyl chloride (**29**), with a 26% amount of resorcinarene capsule.



Scheme 5. Benzylation of *N*-methylpyrrole (**28**) with benzylchloride (**29**) promoted by resorcinarene capsule **15**. Possible dibenylation products have been omitted for sake of simplicity.

Low yield (33%) was obtained, also after increasing the amount of electrophile so the reaction was performed with 52% of the capsule (Table 10). In this latter case,

²⁸² Tsuchimoto, T.; Tobita, K.; Hiyama, T.; Fukuzawa, S., *Synlett*, **1996**, 6, 557.

²⁸³ Sarca, D. V.; Laali, K. K., *Green Chem.*, **2006**, 8, 615.

²⁸⁴ Hofmann, M.; Hampel, N.; Kanzian, T.; Mayr, H., *Angew. Chem. Int. Ed.*, **2004**, 43, 5402.

²⁸⁵ Bandini, M.; Melloni, A.; Umani-Ronchi, A., *Angew. Chem. Int. Ed.*, **2004**, 43, 550.

yield was about 81%, with a ratio between 2-benzylpyrrole and 3-benzylpyrrole of 7/93. No trace of dibenzylated products was recognized.

Table 10. Optimization of reaction conditions.

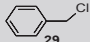
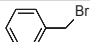
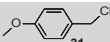
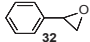
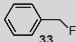
Entry ^a	T(°C)	Eq.of 28	Capsule 15 amount (%)	Yield (%)	Ratio (28a / 28b)
1	30	1.5	0	0	-
2	50	1.5	0	0	-
3	30	1.5	26	20	90/10
4	30	1.5	52	31	93/7
5	50	1.5	52	81	93/7
6	50	2.0	52	62	91/9

^aReaction conditions: **28** (243.9 or 325.2 μ mol), **29** (162.6 μ mol), **14** (254.6 or 509.3 μ mol) in 1.1 mL of water-saturated CDCl₃.

It's a remarkable point that, without capsule or also using resorcinol in place of resorcinarene, no product was achieved²⁸⁶ (Table 10, entries 1-2). With this results in our hand, we decided to exploit the electrophile scope: benzyl bromide (**30**) and *p*-methoxybenzylchloride (**31**) gave high yields. Phenylacetaldehyde was obtained in the case of styrene oxide (**32**), as a result of an isomerization reaction¹⁴⁵ (Table 11). With benzylfluoride (**33**), a slight decrease in yield and regioisomeric ratio was noted. Encapsulation of reagents was demonstrated by a series of 2D NMR experiments (NOESY and DOSY NMR, Figures S15-22 in the Experimental Section). Especially, for *N*-methylpyrrole (**28**), DOSY NMR experiments indicated that this reagent was part of the supramolecular assembly and exchange peaks were observed for the nucleophile *inside* and *outside* the hexameric capsule.

²⁸⁶ Adding NEt₃•BF₄ to the solution containing resorcinarene, nucleophile and electrophile, no yield was achieved; ¹H NMR spectrum of the solution exhibits signals at negative fields, due to the encapsulation of the ammonium salt. See Figure S24 in the Experimental Section.

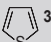
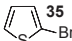
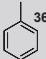
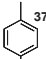
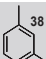
Table 11. Exploration of the electrophiles scope

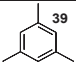
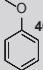
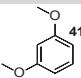
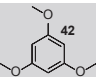
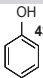
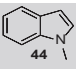
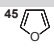
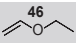
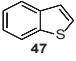
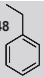
Entry ^a	Electrophile	Yield (%)	Product Ratio (3-regioisomer/2-regioisomer)
1		81	93/7
2		72	91/9
3		77	67/33
4		0	nd
5		75	85/15

^aReaction conditions: electrophile **29-33** (162.6 μ mol, 1 eq.), *N*-methylpyrrole **28** (243.9 μ mol, 1.5 eq.), **14** (509.2 μ mol, 52% mol), T = 50°C, t = 16 h, 1.1 mL of water-saturated CDCl₃.

With the aim to investigate the nucleophile scope, a series of arenes and heteroarenes was exploited in the FC reaction with electrophile **29**. In many cases, high yields were obtained after 16 h (Table 12) and monobenzylated products were selectively achieved; also in these cases, without capsule no products were achieved.

Table 12. Exploration of the nucleophiles scope

Entry ^a	Nucleophile	Yield (%)	Regioisomer ratio ^b
1		82	2 _{regio} 34a /3 _{regio} 34b 60/40
2		91	5 _{regio} 35a /3 _{regio} 35b / 4 _{regio} 35c 90/3/7
3		30	4 _{regio} 36a /2 _{regio} 36b 80/20
4		49	2 _{regio} 37a 100
5		91	4 _{regio} 38a /2 _{regio} 38b /5 _{regio} 38c 92.5/5/2.5

6		92	39a ^d
7		66	4 _{regio} 40a/2 _{regio} 40b 93/7
8		92	4 _{regio} 41a ^e
9		91	42a ^f
10		93	4 _{regio} 43a/2 _{regio} 43b/ 43c ^g 61/35/4
11		81	3 _{regio} 44a/2 _{regio} 44b 80/20
12		0	-
13		0	-
14		83	(2+3) _{regio} 47a +47b /5 _{regio} 47c ^c 91/9
15		32	4 _{regio} 48a/ 2 _{regio} 48b 85/15

^aReaction conditions: electrophile **29** (162.6 μmol, 1 eq.), nucleophile **34-48** (243.9 μmol, 1.5 eq.), **14** (509.2

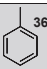
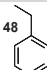
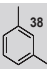
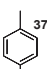
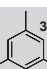
μmol , 52% mol), $T = 50^\circ\text{C}$, 1.1 mL of water-saturated CDCl_3 , $t = 16\text{h}$.^bRegioisomeric ratio was determined by ^1H NMR analysis of the reaction mixture after resorcinarene removal, according with literature data²⁸⁷.^c 2% of side product was obtained.^d 7% of dibenzylated product **39b** was obtained.^e 7% of dibenzylated product **41b** was noted.^f 6% of dibenzylated product **42b** was obtained.^g 4% of dibenzylated product **43c** was obtained.

With ethyl vinyl ether and furan, no formation of product was detectable, but the starting material was fully consumed. This result was due to a probable ring opening of the furan, as the capsule behaves as a weak Brønsted acid, and to acid-catalyzed hydrolysis of the highly reactive vinyl ether to acetaldehyde and corresponding alcohol.

With aromatic hydrocarbons, a linear trend was observed (Table 13). More alkyl substituents were placed on the aromatic ring, more activated was this latter. For example, toluene (**36**) gave a near to quantitative yield after 48 h, while for mesitylene (**39**) only 4 h were sufficient (see Table S8, Experimental Section). Furthermore, the position of these substituents on the ring plays an important role, as can be seen comparing the results of reaction performed with *p*-xylene (**37**) and *m*-xylene (**38**) as nucleophiles.

²⁸⁷ Darbeau, R. W.; White, E. H. *J. Org. Chem.* **1997**, *62*, 8091-8094; Zhang, C.; Gao, X.; Zhang, J.; Peng, X. *Synlett.* **2010**, *2*, 261-265; Kuriyama, M.; Shinozawa, M.; Hamaguchi, N.; Matsuo, S.; Onomu-ra, O. *J. Org. Chem.* **2014**, *79*, 5921-5928; MacDowell, D. W. H.; Jeffries, A. T. *J. Org. Chem.* **1971**, *36*, 1053-1056; Zhang, C.; Gao, X.; Zhang, J.; Peng, X. *Synlett.* **2010**, *2*, 261-265; Vasilopoulos, A.; Zultanski, S. L.; Stahl, S. S. *J. Am. Chem. Soc.* **2017**, *139*, 7705-7708; Nishimoto, Y.; Babu, S. A.; Yasuda, M.; Baba, A. *J. Org. Chem.* **2008**, *73*, 9465-9468; Li, Y.; Xiong, Y.; Li, X.; Ling, X.; Huang, R.; Zhang, X.; Yang, J. *Green. Chem.* **2014**, *16*, 2976-2981; Chahdoura, F.; Pradel, C.; Gómez, M. *Adv. Synth. Catal.* **2013**, *355*, 3648-3660; Li, B.; Leng, K.; Zhang, Y.; Dynes, J. J.; Wang, J.; Hu, Y.; Ma, D.; Shi, Z.; Zhu, L.; Zhang, D.; Sun, Y.; Chrzanowski, M.; Ma, S. *J. Am. Chem. Soc.* **2015**, *137*, 4243-4248; Zhang, J.; Lu, G.; Xu, J.; Sun, H.; Shen, Q. *Org. Lett.* **2016**, *18*, 2860; Tobisu, M.; Takahira, T.; Chatani, N. *Org. Lett.* **2015**, *17*, 4352-4355; Henry, N.; Enguehard-Gueiffier, C.; Thery, I.; Gueiffier, A. *Eur. J. Org. Chem.* **2008**, 4824; Shrestha, S.; Bhattarai, B. R.; Lee, K.-H.; Cho, H. *Bioorganic Med. Chem.* **2007**, *15*, 6535-6548; Yoshida, K.; Narui, R.; Inamoto, T. *Chem. Eur. J.* **2008**, *14*, 9706-9713; Yoon, S.; Hong M. C.; Rhee, H. *J. Org. Chem.* **2014**, *79*, 4206-4211; Porcheddu, A.; Mura, M. G.; De Luca, L.; Pizzetti, M.; Taddei, M. *Org. Lett.* **2012**, *14*, 6112-6115; Galons, H.; Girardeau, J.-F.; Farnoux, C. C.; Miocque, M. *J. Heterocyclic Chem.* **1981**, *18*, 561-563; Lu, M.-Z.; Wang, C.-Q.; Song, S.-J.; Loh, T.-P. *Org. Chem. Front.* **2017**, *4*, 303-307; Jiang, X.; Tang, W.; Xue, D.; Xiao, J.; Wang, C. *ACS Catal.* **2017**, *7*, 1831-1835; Li, Y.; Xiong, Y.; Li, X.; Ling, X.; Huang, R.; Zhang, X.; Yang, J. *Green. Chem.* **2014**, *16*, 2976-2981; Hayashi, R.; Shimizu, A.; Yoshida, J.-i. *J. Am. Chem. Soc.* **2016**, *138*, 8400-8403; Cho, S. H.; Hartwig, J. F. *Chem. Sci.* **2014**, *5*, 694-698; Xia, Y.; Hu, F.; Xia, Y.; Liu, Z.; Ye, F.; Zhang, Y.; Wang, J. *Synthesis* **2017**, *49*, 1073-1086.

Table 13. Investigation of aromatic nucleophiles

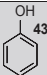
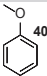
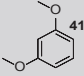
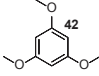
Entry ^a	Nucleophile	Yield (%)	Regioisomer ratio ^b	Time (h)
1		30	2 _{regio} 12a /4 _{regio} 12b 20/80	16
2		32	2 _{regio} 24a /4 _{regio} 24b 15/85	16
3		91	4 _{regio} 38a /2 _{regio} 38b /5 _{regio} 38c 92.5/5/2.5	16
4		49	2 _{regio} 37a 100	16
5		92	39a ^c 100 ^c	16

^aReaction conditions: electrophile **29** (162.6 μmol, 1 eq.), nucleophiles (243.9 μmol, 1.5 eq.), **14** (509.2 μmol, 52% mol), T = 50°C, 1.1 mL of water-saturated CDCl₃, t = 16h.^bRegioisomeric ratio was determined by ¹H NMR analysis of the reaction mixture after resorcinarene removal, according with literature data²⁸⁸.^c 7% of dibenzylated product **39b** was obtained.

The same results were obtained with oxygenated aromatic substrates (Table 14).

²⁸⁸ Darbeau, R. W.; White, E. H. *J. Org. Chem.* **1997**, *62*, 8091-8094; Zhang, C.; Gao, X.; Zhang, J.; Peng, X. *Synlett.* **2010**, *2*, 261-265; Kuriyama, M.; Shinozawa, M.; Hamaguchi, N.; Matsuo, S.; Onomu-ra, O. *J. Org. Chem.* **2014**, *79*, 5921-5928; MacDowell, D. W. H., Jeffries, A. T. *J. Org. Chem.* **1971**, *36*, 1053-1056; Zhang, C.; Gao, X.; Zhang, J.; Peng, X. *Synlett.* **2010**, *2*, 261-265; Vasilopoulos, A.; Zultanski, S. L.; Stahl, S. S. *J. Am. Chem. Soc.* **2017**, *139*, 7705-7708; Nishimoto, Y.; Babu, S. A.; Yasuda, M.; Baba, A. *J. Org. Chem.* **2008**, *73*, 9465-9468; Li, Y.; Xiong, Y.; Li, X.; Ling, X.; Huang, R.; Zhang, X.; Yang, J. *Green. Chem.* **2014**, *16*, 2976-2981; Chahdoura, F.; Pradel, C.; Gómez, M. *Adv. Synth. Catal.* **2013**, *355*, 3648-3660; Li, B.; Leng, K.; Zhang, Y.; Dynes, J. J.; Wang, J.; Hu, Y.; Ma, D.; Shi, Z.; Zhu, L.; Zhang, D.; Sun, Y.; Chrzanowski, M.; Ma, S. *J. Am. Chem. Soc.* **2015**, *137*, 4243-4248; Zhang, J.; Lu, G.; Xu, J.; Sun, H.; Shen, Q. *Org. Lett.* **2016**, *18*, 2860; Tobisu, M.; Takahira, T.; Chatani, N. *Org. Lett.* **2015**, *17*, 4352-4355; Henry, N.; Enguehard-Gueiffier, C.; Thery, I.; Gueiffier, A. *Eur. J. Org. Chem.* **2008**, 4824; Shrestha, S.; Bhattarai, B. R.; Lee, K.-H.; Cho, H. *Bioorganic Med. Chem.* **2007**, *15*, 6535-6548; Yoshida, K.; Narui, R.; Inamoto, T. *Chem. Eur. J.* **2008**, *14*, 9706-9713; Yoon, S.; Hong M. C.; Rhee, H. *J. Org. Chem.* **2014**, *79*, 4206-4211; Porcheddu, A.; Mura, M. G.; De Luca, L.; Pizzetti, M.; Taddei, M. *Org. Lett.* **2012**, *14*, 6112-6115; Galons, H.; Girardeau, J.-F.; Farnoux, C. C.; Miocque, M. *J. Heterocyclic Chem.* **1981**, *18*, 561-563; Lu, M.-Z.; Wang, C.-Q.; Song, S.-J.; Loh, T.-P. *Org. Chem. Front.* **2017**, *4*, 303-307; Jiang, X.; Tang, W.; Xue, D.; Xiao, J.; Wang, C. *ACS Catal.* **2017**, *7*, 1831-1835; Li, Y.; Xiong, Y.; Li, X.; Ling, X.; Huang, R.; Zhang, X.; Yang, J. *Green. Chem.* **2014**, *16*, 2976-2981; Hayashi, R.; Shimizu, A.; Yoshida, J.-i. *J. Am. Chem. Soc.* **2016**, *138*, 8400-8403; Cho, S. H.; Hartwig, J. F. *Chem. Sci.* **2014**, *5*, 694-698; Xia, Y.; Hu, F.; Xia, Y.; Liu, Z.; Ye, F.; Zhang, Y.; Wang, J. *Synthesis* **2017**, *49*, 1073-1086.

Table 14. Investigation of oxygenated aromatic substrates

Entry ^a	Nucleophile	Yield (%)	Regioisomer ratio ^b	Time (h)
1		93	2 _{regio} 19a /4 _{regio} 19b ^c 35.4/60.8	16
2		66	4 _{regio} 16a /2 _{regio} 16b 94/6	16
3		92	4 _{regio} 41a ^d 92.8	16
4		91	18a 93.8	16

^aReaction conditions: 1.5 eq of nucleophile, 1 eq. of **29**, 0.52 eq of **15**, 1.1 mL of water saturated CDCl₃, T = 50°C, t = 16 h. ^bEstimated by ¹H NMR analysis of the reaction mixture after resorcinarene removal.

It is very intriguing, seeing Tables 13 and 14, that better nucleophiles are not necessarily the most reactive ones in this FC alkylation reaction; particularly, mesitylene (**39**) more reactive than *N*-methylpyrrole (**28**), thiophene (**34**), anisole

Table 15. Competition experiments between mesitylene and other nucleophiles

Entry ^a	Conversion of 39 ^b (%)	Nucleophile	Conversion of nucleophile ^b (%)
1	95	34	4.6
2	94.7	40	5.3
3	76.2	41	23.8

^aReaction conditions: 1.5 eq of mesitylene **39**, 1.5 eq. of nucleophile, 1 eq. of **29**, 0.52 eq of **15**, 1.1 mL of water saturated CDCl₃, T = 50°C, t = 16 h. ^bEstimated by ¹H NMR analysis of the reaction mixture after resorcinarene removal.

(**40**) and 1,3 di-methoxybenzene (**41**), in contrast with Mayr scales of nucleophilicity²⁸⁴. While for *N*-methylpyrrole product inhibition was observed²⁸⁹, in

²⁸⁹ Product inhibition experiments were performed with 0.25, 0.5, 0.7 and 1.0 eq. of product. For details see Experimental Section, **Tables S11-S15**.

the other cases this argument can not be accepted, so, competition experiments with mesitylene were performed (Table 15).

As can be seen, mesitylene²⁹⁰ is more reactive than the other three substrates showed in Table 11, probably for its bigger affinity for resorcinarene capsule. So, this affinity modifies the order of nucleophilicity aforementioned and represents an example of how nanoconfined environments can influence common reaction principles.

²⁹⁰ Reaction performed with mesitylene gives maximum conversion after only 4 hours. A table, reporting substrates and the time after which for the nucleophiles maximum conversion is obtained, has been reported in the Experimental Section.

CONCLUSIONS

FC benzylation of several arenes and heteroarenes compounds was performed inside the hexameric resorcinarene capsule **15**. This supramolecular assembly is able to activate the electrophile and at the same time stabilize the resulting cationic intermediate, promoting the attack of the nucleophile at the benzyl moiety of the electrophile. Moreover, affinity of the substrates for the capsule can be exploited to exert a supramolecular control on the reaction. The results here showed can be considered a step forward in the exploitation of the synthetic versatility of the resorcinarene capsule.

5. EXPERIMENTAL SECTION

5.1 General experimental conditions

General methods and materials

Flash chromatography was performed on Merck silica gel (60, 40- 63 μm). All chemicals were reagent grade and were used without further purification. Anhydrous solvents were purchased from Aldrich. Reaction temperatures were measured externally; reactions were monitored by TLC on Merck silica gel plates (0.25 mm) and visualized by UV light and spraying with H_2SO_4 - $\text{Ce}(\text{SO}_4)_2$ or phosphomolybdic acid. NMR spectra were recorded on Bruker Avance- 600 spectrometer [600.13 MHz (^1H) and 150.03 MHz (^{13}C)], Bruker Avance-400 spectrometer [400 (^1H) and 100.57 MHz (^{13}C)], Bruker Avance-300 spectrometer [300 (^1H) and 75.48 MHz (^{13}C)], or Bruker Avance-250 spectrometer [250 (^1H) and 62.80 MHz (^{13}C)]; chemical shifts are reported relative to the residual solvent peak (CHCl_3 : δ 7.26, CDCl_3 : δ 77.23). DOSY experiments were performed on a Bruker Avance-600 spectrometer equipped with 5 mm PABBO BB|19F-1H\D Z-GRD Z114607/0109. The standard Bruker pulse program, ledbpgp2s, employing a double stimulated echo sequence and LED, bipolar gradient pulses for diffusion, and two spoil gradients were utilized. Diffusion times were 150 ms, eddy current delay was 5 ms, gradient recovery delays was 0.2 ms and gradient pulse was 1400 ms. Individual rows of the quasi-2D diffusion databases were phased and baseline corrected. NOESY experiment was performed on Bruker Avance 400 and Bruker Avance 600 spectrometers with D8 value range from 50 to 250 ms. Derivatives: **3**²⁹¹, **5**²⁹¹, **10**²¹⁷, **11a**²²⁵, **11b**²²⁶, **12**²¹⁸, **33**²⁹² were synthesized according to literature procedures.

²⁹¹ Iwamoto, K.; Araki, K.; Shinkai, S.; *Tetrahedron*, **1991**, *47*, 4325.

²⁹² Cox, P.; Terpinski, J.; Lawrynowicz, W. *J. Org. Chem.* **1984**, *49*, 3216.

Melting points were measured with a Stuart melting point apparatus (SMP3). High-resolution mass spectra (HRMS) were acquired using a Bruker solarix XR Fourier transform ion cyclotron resonance mass spectrometer equipped with a 7 T refrigerated actively-shielded superconducting magnet. The samples were ionized in positive ion mode using the ESI ion source (Bruker Daltonik GmbH, Bremen, Germany). The mass range was set to m/z 150-3000. The mass spectra were calibrated externally using a NaTFA solution in positive ion mode. A linear calibration was applied. All final compounds purity was determined by elemental analysis on a Flash EA 1112 Series with Thermal Conductivity Detector, for C, H, N and S. The final compounds was found to be >95% when analyzed. Molecular mechanics calculations was performed with MacroModel-9.0/Maestro-4.1 using AMBER force field²⁹³.

Single crystal diffraction data for the structural determination of compounds **8b**, **8g**, **8h**, **8i** and **8k** were collected with the rotating-crystal method using synchrotron radiation at the XRD1 beam-line of the Elettra Synchrotron, Trieste, Italy. A moist single crystal was attached to a loop and flash-frozen to 100 K in a stream of N₂ vapour. Cryoprotection was not employed. Diffraction images were indexed and integrated using the XDS²⁹⁴ package and the resulting data sets were scaled using XSCALE²⁹⁵. The crystal structures were determined by VLD Phasing with SIR-2014²⁹⁶ and refined with SHELX-14²⁹⁷, operating through the WinGX GUI²⁹⁸. Thermal parameters of all non-hydrogen atoms were refined anisotropically. Hydrogen atoms were placed at the geometrically calculated positions and refined using the riding model. Crystallographic data and refinement details are reported in Table S1-5. HPLC

²⁹³ Macromodel-9.0/Maestro-4.1 program: Mohamadi, F.; Richards, N. G.; Guida, W. C.; Liskamp, R; Lipton, M.; Caufield, C.; Chang, G.; Hendrickson, T.; Still, W. C., *J. Comput. Chem.*, **1990**, *11*, 440.

²⁹⁴ Kabsch, W., *Acta Crystallogr., Sect. D: Biol. Crystallogr.*, **2010**, *66*, 125.

²⁹⁵ Kabsch, W., *Acta Crystallogr., Sect. D: Biol. Crystallogr.* **2010**, *66*, 133.

²⁹⁶ Burla, C. M.; Caliandro, R.; Carrozzini, B.; Cascarano, G. L.; Cuocci, C.; Giacovazzo, C.; Mallamo, M.; Mazzone, A.; Polidori, G., *J. Appl. Crystallogr.*, **2015**, *48*, 306.

²⁹⁷ Sheldrick, G. M., *Acta Cryst.*, **2008**, *A64*, 112.

²⁹⁸ Farrugia, L. J., *J. Appl. Cryst.*, **2012**, *45*, 849.

analysis was performed using a Jasco HPLC system equipped with PU-4180 HPLC pump, 20 μ l loop injector (Rheodyne model 7725i) and MD-4015 Photodiode Array Detector at $\lambda = 210$ or 220 nm. As stationary phases the following Chiralcel columns were used: OD-H (250 x 4.6 mm) and OD guard (50 mm), AD-H (250 x 4.6 mm) and AD guard (50 mm), AS-H (250 x 4.6 mm) and AS guard (50 mm).

Water saturated deuterated chloroform was prepared as reported in literature¹⁵⁰. Resorcinarene **14**¹⁴⁰, nitrones **16a**²⁹⁹, **16b**³⁰⁰, **16c**²⁵⁵, **16d**³⁰¹, **16e**³⁰¹ and **16f**²⁵⁵, catalyst **20d**³⁰² and hexamethonium iodide (HMI)³⁰³ were synthesized according to literature procedures. Percentages of conversions, regioisomeric and diastereomeric ratios of the titles compounds **18a-i** and **19a-i** were determined by ¹H NMR analysis in comparison with literature data^{254,255,258,262}.

5.2 General procedure for On Water catalysis of VMAR in presence of thioureido-calixarene catalysts. A mixture of appropriate α -ketoester **7a-d** (0.22 mmol) and catalyst (0.011 mmol), was stirred in presence of 2-(trimethylsilyloxy)furan (TMSOF) **6** (0.33 mmol) in deionized water (1 mL) as medium. The reaction mixture was kept under magnetic stirring (1400 rpm) at 30 °C for the appropriate time (see Table 3), then was extracted with ethyl acetate (3 x 5 mL). Organic layers were collected and dried over Na₂SO₄, then filtered and evaporated under reduced pressure. Diastereoisomeric ratios and percentage of conversion to γ -adducts **8a**, **8b** and **8d** were determined by integration of the ¹H NMR signals of the crude reaction mixtures in comparison with the literature values.^{179,211,219} In the case of **8c**, crude reaction mixture was purified by flash chromatography on silica gel using a gradient from *n*-

²⁹⁹ Prakash, G. K. S.; Zhang, Z.; Wang, F.; Rahm, M.; Ni, C.; Iulicci, M.; Haiges, R.; Olah, G. A., *Chem. Eur. J.*, **2014**, *20*, 831.

³⁰⁰ Evans, D. A.; Song, H.-J.; Fandrick, K. R., *Org. Lett.*, **2006**, *8*, 3351.

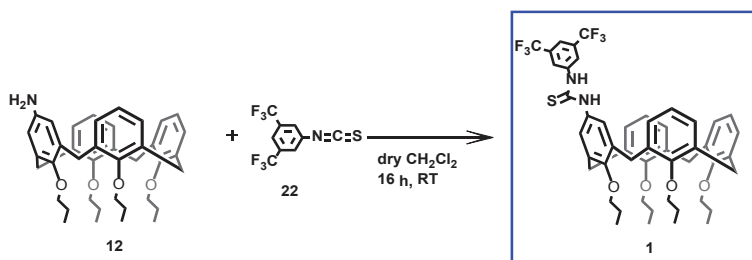
³⁰¹ Tyrrell, E.; Allen, J.; Jones, K.; Beauchet, R., *Synthesis*, **2005**, *14*, 2393.

³⁰² Hamilton PB, *J. Biol. Chem.*, **1952**, *198*, 587.

³⁰³ Engel, R.; Rizzo, J. I.; Montenegro, D.; Leb, J.; Coleman, D.; Hong, C.; Jeanty, H.; Thomas, M., *Chem. Phys. Lipids*, **2009**, *160*, 105.

hexane to a mixture of *n*-hexane/ethyl acetate (90/10) to give *syn* and *anti* diastereomers of **8c**. The relative configuration of **8c** was assigned in analogy to other derivatives **8a**, **8b** and **8d** by comparison of ¹H-NMR chemical shifts of the characteristic -CH and =CH signals of the γ -hydroxybutenolide ring^{179,211,219}.

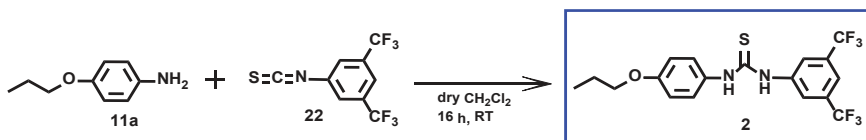
Synthesis of catalyst **1**



To a solution of **12** (0.14 g, 0.23 mmol) in dry CH₂Cl₂ (7 mL), 3,5-bis(trifluoromethyl)phenylisothiocyanate **22** (0.07 g, 0.26 mmol) was added. The reaction mixture was stirred under nitrogen atmosphere for 16 h at RT. The solvent was removed under reduced pressure and the crude mixture was purified by flash chromatography on silica gel (Hexanes/CHCl₃, 80/20) to give the derivative **1** as a light yellow solid (0.16 g, 0.18 mmol, 78.3%). ¹H NMR (250 MHz, CDCl₃, 298 K): δ 0.88-1.14 (overlapped, -OCH₂CH₂CH₃, 12H), 1.86-2.03 (overlapped, -OCH₂CH₂CH₃, 8H), 3.14 (d, *J* = 13.2 Hz, 2H, ArCH₂Ar), 3.17 (d, *J* = 13.2 Hz, 2H, ArCH₂Ar), 3.63-3.75 (overlapped, -OCH₂CH₂CH₃, 4H), 3.98-4.08 (m, -OCH₂CH₂CH₃, 4H), 4.43 (d, *J* = 13.2 Hz, 2H, ArCH₂Ar), 4.49 (d, *J* = 13.2 Hz, 2H, ArCH₂Ar), 5.94 (br t, ArH, 1H), 6.06 (d, ArH, *J* = 7.3 Hz, 2H), 6.18 (s, ArH, 2H), 6.90-7.10 (overlapped, ArH + NH, 7H), 7.61 (s, NH, 1H), 7.71 (s, CF₃ArH, 1H), 7.78 (s, CF₃ArH, 2H). ¹³C NMR (63 MHz, CDCl₃, 298 K): δ 9.7, 10.56, 10.61, 22.8, 23.3, 30.8, 30.9, 76.5, 77.1, 77.3, 119.6, 120.9, 122.4, 124.0, 113

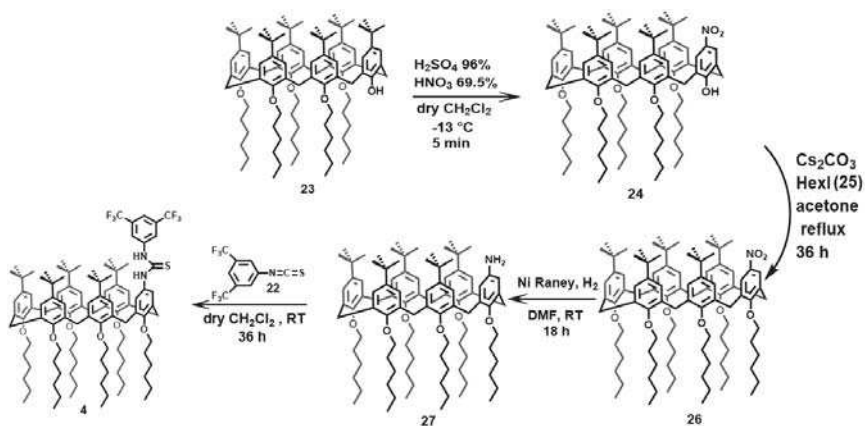
125.1, 126.2, 127.1, 128.5, 128.9, 129.3, 131.4, 133.6, 135.8, 136.3, 136.9, 139.6, 155.1, 155.5, 157.3, 179.1. **HRMS (MALDI-FTICR)**, calcd for $C_{49}H_{52}N_2O_4S$ [$M + H^+$]: 879.36205, found: 879.36198. M.p: 117-118 °C.

Synthesis of catalyst 2

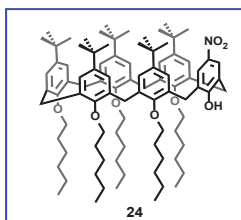


To a solution of **11a** (0.10 g, 0.66 mmol) in dry CH_2Cl_2 (10 mL), 3,5-bis(trifluoromethyl)phenyl isothiocyanate **22** (0.21 g, 0.79 mmol) was added under N_2 . The solution was stirred under nitrogen atmosphere for 16 h at RT. Then, the solvent was removed under reduced pressure and the crude mixture was purified by flash chromatography on silica gel (Hexanes/ $CHCl_3$, 65/35) to give **2** as an other solid (0.22 g, 0.52 mmol, 79.0%). **1H NMR** (250 MHz, $CDCl_3$, 298 K): δ 1.05 (t, $J = 7.4$ Hz, 3H, - $OCH_2CH_2CH_3$), 1.84 (m, 2H, - $OCH_2CH_2CH_3$), 3.95 (t, $J = 6.5$ Hz, 2H, - $OCH_2CH_2CH_3$), 7.00 (d, $J = 8.9$ Hz, 2H, ArH), 7.25 (d, $J = 8.9$ Hz, 2H, ArH), 7.57 (s, 1H, NH), 7.66 (s, 1H, CF_3 ArH), 7.99 (s, 2H, CF_3 ArH), 8.16 (s, 1H, NH). **^{13}C NMR** (63, $CDCl_3$, 298 K): δ 10.4, 22.3, 69.8, 116.1, 119.2, 120.7, 124.4, 127.2, 127.8, 131.0, 131.8, 139.6, 159.2, 180.1. **HRMS (MALDI-FTICR)**, calcd for $C_{18}H_{17}F_6N_2OS$ [$M + H^+$]: 423.09603, found: 423.09608. M.p: 121-122 °C.

Synthesis of catalyst 4



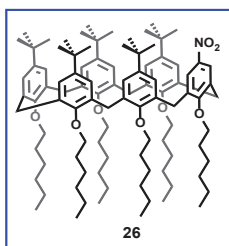
Derivative 24



To a solution of **23** (0.43 g, 0.31 mmol) in dry CH_2Cl_2 (7 mL), at $-13\text{ }^\circ\text{C}$, HNO_3 (69.5%, 0.035 mL) and H_2SO_4 (96%, 0.035 mL) were added under N_2 . After 5 minutes the reaction mixture was quenched with H_2O (20 mL) and extracted with CH_2Cl_2 (3 x 10 mL). The organic layers were collected and dried over Na_2SO_4 , filtered and evaporated under reduced pressure to give a yellow crude solid, which was purified by flash chromatography on silica gel (Hexanes/ CHCl_3 , 70/30) to give derivative **24** as a yellow solid (0.32 g, 0.23 mmol, 74.2%). $^1\text{H NMR}$ (300 MHz, TCDE, 363 K): δ 0.69–

1.65 (overlapped, $-\text{OCH}_2\text{CH}_2\text{CH}_2\text{CH}_2\text{CH}_2\text{CH}_3 + -\text{C}(\text{CH}_3)$, 100H), 3.07-3.76 (overlapped, $-\text{OCH}_2\text{CH}_2\text{CH}_2\text{CH}_2\text{CH}_2\text{CH}_3 + \text{ArCH}_2\text{Ar}$, 22H), 6.64-6.69 (overlapped, ArH, 4H), 6.78 (s, ArH, 2H), 6.91 (s, ArH, 2H), 7.02 (s, ArH, 2H), 7.84 (s, $\text{NO}_2\text{-ArH}$, 2H), 8.62 (bs, OH, 1H). ^{13}C NMR (75 MHz, TCDE, 363 K): δ 13.7, 22.2, 22.3, 22.5, 25.5, 25.6, 29.6, 30.3, 30.5, 31.2, 31.3, 31.4, 31.6, 31.9, 33.8, 72.9, 73.5, 73.8, 124.6, 124.9, 125.8, 126.8, 127.0, 128.1, 129.9, 131.5, 132.8, 133.3, 133.4, 140.3, 144.5, 144.9, 146.4, 151.5, 153.3, 159.4. HRMS (MALDI-FTICR), calcd for $\text{C}_{92}\text{H}_{135}\text{NO}_8\text{K}$ [$M + \text{K}^+$]: 1421.98531, found: 1421.98945. M.p: 181-182°C.

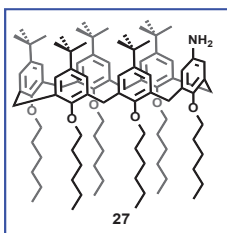
Derivative 26



Cs_2CO_3 (0.75 g, 2.31 mmol) was added to a suspension of derivative **24** (0.32 g, 0.23 mmol) in acetone (20 mL). The reaction mixture was refluxed for 2 hours, then was allowed to cool slowly to room temperature. 1-Iodohexane **25** (0.98 g, 4.62 mmol) was added and the reaction mixture was refluxed for 36 hours, then it was cooled to RT and concentrated under vacuum. The crude product was dissolved in CH_2Cl_2 (50 mL), washed with aqueous 1N HCl (20 mL) and the organic layer was dried over Na_2SO_4 , filtered and the crude product was evaporated to dryness and then purified by flash chromatography on silica gel using a gradient of *n*-Hexane/ CHCl_3 (from 90/10 to 75/25) to give derivative **26** (0.29 g, 0.20 mmol, 87.0 %). ^1H NMR (300 MHz, TCDE, 363 K): δ 0.71-1.80 (overlapped, $-\text{OCH}_2\text{CH}_2\text{CH}_2\text{CH}_2\text{CH}_2\text{CH}_3 + -\text{C}(\text{CH}_3)$, 111H), 3.18-

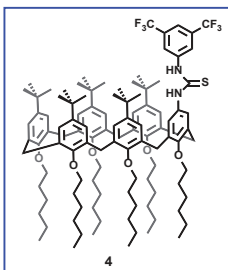
3.80 (overlapped, $-\text{OCH}_2\text{CH}_2\text{CH}_2\text{CH}_2\text{CH}_2\text{CH}_3 + \text{ArCH}_2\text{Ar}$, 24H), 6.58 (bs, ArH, 2H), 6.73 (bs, ArH, 2H), 6.86-7.04 (overlapped, ArH, 6H), 7.56 (s, $\text{NO}_2\text{-ArH}$, 2H). $^{13}\text{C NMR}$ (75 MHz, TCDE, 363 K): δ 13.8, 22.4, 22.5, 25.9, 29.6, 30.1, 30.2, 30.5, 31.2, 31.4, 31.6, 31.7, 31.8, 33.7, 33.8, 33.9, 73.0, 73.3, 73.5, 73.7, 123.2, 124.9, 125.3, 126.2, 126.5, 127.7, 131.2, 132.5, 132.8, 132.9, 133.5, 135.8, 143.6, 145.0, 145.6, 152.8, 153.7, 160.3. **HRMS (MALDI-FTICR)**, calcd for $\text{C}_{98}\text{H}_{147}\text{NO}_8\text{Na}$ [$M + \text{Na}^+$]: 1490.10527, found: 1490.10384. M.p: 243-244 °C.

Derivative 27



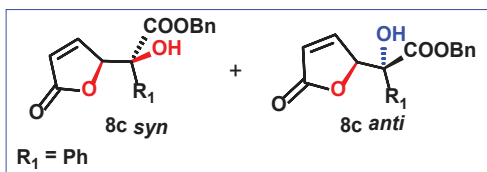
Raney nickel (cat. amounts) was added to a solution of derivative **26** (0.42 g, 0.29 mmol) in hot DMF (230 mL). The resulting black suspension was stirred under H_2 (1 atm) at RT for 18 hours, then was filtered through a celite pad. Concentration of the filtrate to dryness give a crude product, which was purified by flash chromatography on silica gel (Hexanes/ CH_2Cl_2 , 80/20) to give the derivative **27** (0.36 g, 0.25 mmol, 86.2 %). $^1\text{H NMR}$ (300 MHz, TCDE, 363 K): δ 0.39-1.78 (overlapped, $-\text{OCH}_2\text{CH}_2\text{CH}_2\text{CH}_2\text{CH}_2\text{CH}_3 + -\text{C}(\text{CH}_3)$, 111H), 3.63-3.77 (overlapped, $\text{ArCH}_2\text{Ar} + -\text{OCH}_2\text{CH}_2\text{CH}_2\text{CH}_2\text{CH}_2\text{CH}_3$, 24 H), 6.73-7.07 (overlapped, ArH, 12H). $^{13}\text{C NMR}$ (75 MHz, TCDE, 363 K): δ 13.3, 13.4, 25.2, 25.3, 25.4, 29.9, 30.6, 30.9, 31.0, 31.2, 31.4, 33.4, 73.6, 113.5 (*broad*), 125.5 (*broad*), 132.4 (*broad*), 145.0, 145.2, 154.0 (*broad*). **HRMS (ESI-FTICR)**, calcd for $\text{C}_{98}\text{H}_{150}\text{NO}_6$ [$M + \text{H}^+$]: 1438.14915, found: 1438.12274. Decomposes to light red oil at 151.5°C.

Catalyst 4



3,5-bis(trifluoromethyl)phenyl isothiocyanate **22** (0.08 g, 0.30 mmol) was added to a solution of derivative **27** (0.32 g, 0.22 mmol) in dry CH₂Cl₂ (15 mL). The reaction mixture was stirred for 24 hours at RT under N₂ atmosphere, then other isothiocyanate (0.03g, 0.11 mmol) was added. After other 12 hours, solvent was evaporated to give a brown oil, which was purified by flash column chromatography on silica gel (hexanes) to obtain catalyst **4** as a white solid (0.32 g, 0.19 mmol, 86.4 %). **¹H NMR** (300 MHz, TCDE, 363 K): δ 0.31-1.82 (overlapped, -OCH₂CH₂CH₂CH₂CH₂CH₃ + -C(CH₃), 111H), 3.48-3.75 (overlapped, -OCH₂CH₂CH₂CH₂CH₂CH₃ + ArCH₂Ar, 24H), 6.80 -7.42 (overlapped, ArH + CF₃ArH, 13H), 8.10 (s, CF₃ArH, 2H). **¹³C NMR** (75 MHz, TCDE, 363 K): δ 13.7, 22.4, 25.6, 30.0, 31.0, 31.4, 33.8, 126.2 (*broad*), 133.1 (*broad*), 145.6 (*broad*), 154.0 (*broad*). **HRMS (ESI-FTICR)**, calcd for C₁₀₇H₁₅₃F₆N₂O₆S : 1709.13814 [*M* + H⁺], found : 1709.13571. M.p.: 214-215 °C.

Derivative 8c



Prepared according to the general procedure from **7c**, 2-(trimethylsilyloxy)furan **6** and catalyst **1**. The residue was purified by flash column chromatography on silica gel using a gradient from *n*-hexane to a mixture of *n*-hexane/ethyl acetate (90/10) to give *anti* and *syn* diastereomers. *Anti* isomer (isolated as a colorless oil) (0.012 g, 0.037 mmol, 16.7%): ¹H NMR (600 MHz, CDCl₃, 298 K): δ 3.60 (broad, 1H, OH), 5.25 (d, 1H, *J* = 12.1 Hz, CH₂ benz), 5.32 (d, *J* = 12.1 Hz, 1H, CH₂ benz), 5.55 (s, 1H, -CH), 6.10 (dd, *J*₂ = 1.8 Hz, *J*₁ = 5.4 Hz, 1H, =CH), 7.18 (dd, *J*₂ = 1.2 Hz, *J*₁ = 5.4 Hz, 1H, =CH), 7.32-7.37 (overlapped, ArH, 8H), 7.57-7.59 (overlapped, ArH, 2H). ¹³C NMR (150 MHz, CDCl₃, 298 K): δ 69.0, 78.4, 85.8, 124.1, 126.0, 128.75, 128.76, 129.0, 129.1, 129.2, 134.4, 136.8, 152.1, 171.4, 172.4. *Syn* isomer (isolated as a colorless oil) (0.010 g, 0.031 mmol, 14.2%): ¹H NMR (400 MHz, CDCl₃, 298 K): δ 3.88 (s, 1H, OH), 5.28 (d, 1H, *J* = 12.1 Hz, CH₂ benz), 5.34 (d, 1H, *J* = 12.1 Hz, CH₂ benz), 5.78-5.79 (m, 1H, -CH), 6.16 (dd, *J*₂ = 2.0 Hz, *J*₁ = 6.0 Hz, 1H, =CH), 6.95 (dd, *J*₂ = 1.6 Hz, *J*₁ = 5.6 Hz, 1H, =CH), 7.31-7.42 (overlapped, ArH, 8H), 7.66-7.69 (overlapped, ArH, 2H). ¹³C NMR (100 MHz, CDCl₃, 298 K): δ 69.4, 77.6, 86.3, 124.1, 125.7, 128.5, 128.9, 129.0, 129.1, 129.3, 134.5, 136.3, 151.5, 171.7, 172.7.

HRMS (ESI-FTICR), calcd for C₁₉H₁₆O₅Na : 347.08899 [*M* + Na⁺], found : 347.08931.

^1H NMR titrations of **1** with **7a** and **7b**

The following standard procedure was used:

Host solution. A CDCl_3 solution 3.2 mM of catalyst **1** was prepared (2.00 mL). In 0.5 mL of *host solution*, the derivative **7a** was dissolved (*solution 7a*). 0.4 mL of host solution, in a NMR tube, was titrated with *solution 7a* in the concentration range indicated below. [**1**] = 3.2 mM. [**7a**] concentration range during titration: 0.00-2.50 mM. In 0.5 mL of *host solution*, the derivative **7b** was dissolved (*solution 7b*). 0.4 mL of host solution, in a NMR tube, was titrated with *solution 7b* in the concentration range indicated below. [**1**] = 3.2 mM. [**7b**] concentration range during titration: 0.00-2.50 mM.

The titration data were analyzed by nonlinear least-squares fitting procedures³⁰⁴ and in all cases a good fit of the experimental data with the theoretical model confirmed the 1:1 stoichiometry of the complexes.

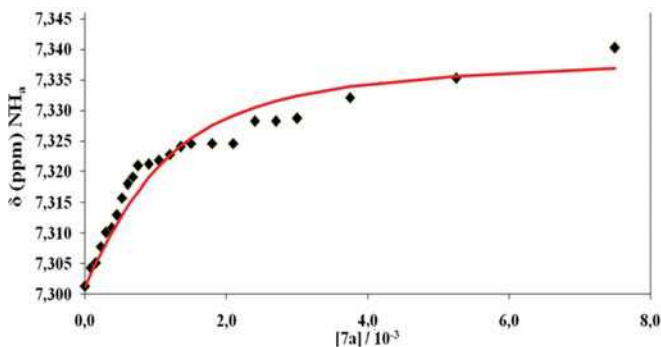


Figure S1. Plot of the chemical shift of NH proton of catalyst **1** (3.2 mM in 0.5 mL CDCl_3 at 298 K) versus $[\mathbf{7a}]/10^{-3}$ at 25 °C in CDCl_3 .

³⁰⁴Connors, K. A. *Binding Constants*; John Wiley & Sons: Chichester, 1987

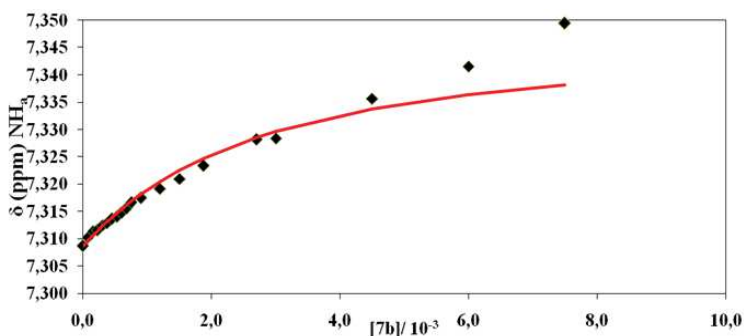


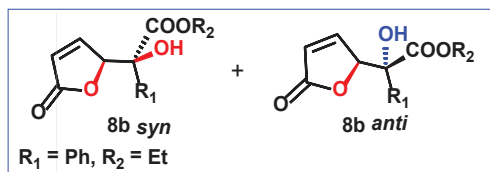
Figure S2. Plot of the chemical shift of NH proton of catalyst **1** (3.2 mM in 0.5 mL CDCl₃ at 298 K) versus [7b]/10⁻³ at 25 °C in CDCl₃.

5.3 General procedure for On water catalysis of VMAR in presence of amino-calixarene catalysts

A mixture of appropriate α -ketoester **7a-l** (0.23 mmol) and catalyst 10–13 (0.011 mmol), was vigorously stirred in presence of 2- (trimethylsilyloxy)furan (TMSOF) **6** (0.053 g, 0.34 mmol) in appropriate solvent (H₂O, D₂O or organic solvent) (1 mL). The reaction mixture was kept under magnetic stirring (1400 rpm) at 30 °C for the appropriate time (see Table 7), then extracted with ethyl acetate (3 x 5 mL), (except for the reaction with α -ketoester **5i** where chloroform was used). Organic layers were collected and dried over Na₂SO₄, then filtered and evaporated under reduced pressure. Diastereoisomeric ratios and percentages of conversion of the γ - adducts **8a-h**, **8j-l** were determined by integration of the ¹H NMR signals of the crude reaction mixtures in comparison with the literature values.^{211,219} The crude reaction mixture was purified by flash chromatography on silica gel to give *syn* and *anti* diastereomers

Derivatives **8a**, **8c**, **8d**, **8e**, **8f**, **8l** were prepared according to the general procedure using the appropriate α -ketoesters, 2-(trimethylsilyloxy)furan **6** and catalyst **10**. The residue was purified by flash chromatography on silica gel (Hexane/EtOAc = 80:20) to give *anti* and *syn* diastereomers. Yields and diastereomeric ratios are listed in Table 7. Spectroscopic data of *anti* and *syn* diastereomers matched those reported in literature^{211,219}.

Derivative 8b

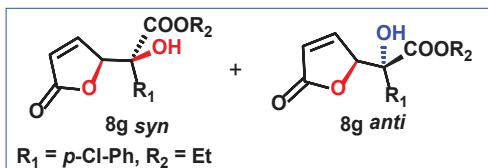


Prepared according to the general procedure using **7b**, 2-(trimethylsilyloxy)furan **6** and in presence of catalyst **10**. The residue was purified by flash chromatography on silica gel (Hexane/EtOAc = 80:20) to give *anti* and *syn* diastereomers. Yield: 74% (combined yield of isolated diastereomers); dr = 38/62 (37/63 after chromatography). *Anti-8b*: Isolated as a white solid. The spectroscopic data for *anti-8b* isomer matched those reported in literature²¹¹.

Syn-8b: Isolated as a white solid. m.p.: 115–116 °C. ¹H NMR (400 MHz, CDCl₃, 298 K): δ = 1.35 (t, 3H, J = 7.1 Hz, -OCH₂CH₃), 3.89 (s, 1H, OH), 4.29–4.43 (m, 2H, -OCH₂CH₃), 5.77 (s, 1H, -CH), 6.16 (d, 1H, J = 5.6 Hz, =CH), 6.96 (d, 1H, J = 6.0 Hz, =CH), 7.39–7.44 (m, 1H, ArH), 7.41 (d, 2H, J = 7.6 Hz, ArH), 7.70 (d, 2H, J = 7.6 Hz, ArH). ¹³C NMR (100 MHz, CDCl₃, 298 K): δ = 14.2 (CH₃), 63.9 (CH₂), 77.4 (C), 86.4 (CH), 124.0 (CH), 125.7 (2C, C_{Ar}H), 129.0 (2C, C_{Ar}H), 129.2 (C_{Ar}H), 136.5 (C_{Ar}C), 151.6 (CH), 171.8 (C), 172.8 (C). HRMS (ESI-FTICR), calcd. for C₁₄H₁₄O₅Na : 285.07334 [M + Na⁺], found :

285.07355. EA (%) for C₁₄H₁₄O₅: calc. C 64.12, H 5.38, found C 64.03, H 5.29.

Derivative 8g

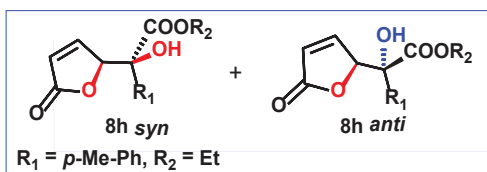


Prepared according to the general procedure using **7g**, 2- (trimethylsilyloxy)furan **6** and catalyst **10**. The residue was purified by flash column chromatography on silica gel (Hexane/EtOAc = 85:15) to give *anti* and *syn* diastereomers. Yield: 99% (combined yield of isolated diastereomers); dr = 30/70 (28/72 after chromatography).

Anti-**8g**: Isolated as a white solid. The spectroscopic data for *anti*-**8g** matched those reported in literature²¹¹.

Syn-**8g**: Isolated as a white solid. m.p.: 124.5–126.0 °C. ¹H NMR (300 MHz, CDCl₃, 298 K): δ = 1.35 (t, 3H, J = 7.2 Hz, -OCH₂CH₃), 3.93 (s, 1H, OH), 4.29-4.43 (m, 2H, OCH₂CH₃), 5.69-5.70 (m, 1H, -CH), 6.18 (dd, 1H, J₂ = 2.1 Hz, J₁ = 5.8 Hz, =CH), 6.95 (dd, 1H, J₂ = 1.5 Hz, J₁ = 5.8 Hz, =CH), 7.39 (d, 2H, J = 8.8 Hz, ArH), 7.65 (d, 2H, J = 8.8 Hz, ArH). ¹³C NMR (75 MHz, CDCl₃, 298 K): δ = 14.2 (CH₃), 64.1 (CH₂), 77.4 (C), 86.2 (CH), 124.3 (CH), 127.3 (2C, C_{Ar}H), 129.2 (2C, C_{Ar}H), 135.0 (C_{Ar}C), 135.4 (C_{Ar}C), 151.2 (CH), 171.4 (C), 172.5 (C). HRMS (ESI-FTICR), calcd for C₁₄H₁₃ClO₅Na: 319.03437 [M + Na⁺], found: 319.03436. EA (%) for C₁₄H₁₃ClO₅: calc. C 56.67, H 4.42; found C 56.75, H 4.33.

Derivative 8h

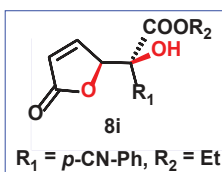


Prepared according to the general procedure from **7h**, 2- (trimethylsilyloxy)furan **6** and catalyst **10**. The residue was purified by flash column chromatography on silica gel (Hexane/EtOAc = 85:15) to give anti and syn diastereomers. Yield: 36% (combined yield of isolated diastereomers); dr = 30/70 (28/72 after chromatography).

Anti-8h: Isolated as a white solid. The spectroscopic data for **anti-8h** diastereomer matched those reported in literature.

Syn-8h: Isolated as a white solid. m.p.: 98-100 °C. ¹H NMR (600 MHz, CDCl₃, 298 K): δ = 1.35 (t, 3H, J = 7.1 Hz, -OCH₂CH₃), 2.37 (s, 3H, -CH₃), 3.86 (bs, 1H, OH), 4.29-4.41 (m, 2H, -OCH₂CH₃), 5.75- 5.76 (m, 1H, -CH), 6.16 (dd, 1H, J₂ = 1.9 Hz, J₁ = 5.8 Hz, =CH), 6.98 (dd, 1H, J₂ = 1.4 Hz, J₁ = 5.8 Hz, =CH), 7.23 (d, 2H, J = 8.1 Hz, ArH), 7.57 (d, 2H, J = 8.3 Hz, ArH). ¹³C NMR (150 MHz, CDCl₃, 298 K): δ = 14.2 (CH₃), 21.2 (CH₃), 63.8 (CH₂), 77.4 (C), 86.4 (CH), 123.9 (CH), 125.5 (2C, C_{Ar}H), 129.7 (2C, C_{Ar}H), 133.5 (Ar-C), 139.1 (Ar-C), 151.7 (CH), 171.9 (C), 172.8 (C). HRMS (ESI-FTICR), calcd for C₁₅H₁₆O₅Na : 299.08899 [M + Na⁺], found : 299.08917. EA (%) for C₁₅H₁₆O₅: calc. C 65.21, H 5.84, found C 65.33, H 5.76.

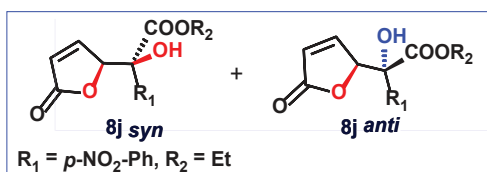
Derivative 8i



Prepared according to the general procedure from **7i**, 2-(trimethylsilyloxy)furan **6** and catalyst **10**. The residue was purified by flash column chromatography on silica gel ($CHCl_3$) to give the single *syn* diastereomer. Yield: 99%, $dr > 1/99$.

Syn-**8i**: Isolated as a white solid. m.p.: 154-155 °C. 1H NMR (400 MHz, $CDCl_3$, 298 K): $\delta = 1.36$ (t, 3H, $J = 7.2$ Hz, $-OCH_2CH_3$), 4.07 (s, 1H, OH), 4.32-4.44 (m, 2H, $-OCH_2CH_3$), 5.70 (br m, 1H, -CH), 6.20 (dd, 1H, $J_2 = 1.9$ Hz, $J_1 = 5.8$ Hz, =CH), 6.91 (dd, 1H, $J_2 = 1.5$ Hz, $J_1 = 5.8$ Hz, =CH), 7.73 (d, 2H, $J = 8.7$ Hz, ArH), 7.87 (d, 2H, $J = 8.7$ Hz, ArH). ^{13}C NMR (100 MHz, $CDCl_3$, 298 K): $\delta = 14.2$ (CH_3), 64.5 (CH_2), 77.4 (C), 85.9 (CH), 113.3 (Ar-CN), 118.3 (CH), 124.6 (2C, C_{ArH}), 126.8 (2C, C_{ArH}), 132.7 (Ar-C), 141.6 (Ar-C), 150.6 (CH), 170.7 (C), 172.2 (C). HRMS (ESI-FTICR), calcd for $C_{15}H_{13}NO_5Na$: 310.06859 [$M + Na^+$], found: 310.06972. EA (%) for $C_{15}H_{13}NO_5$: calc. C, 62.72, H, 4.56, N, 4.88, found C, 62.80, H, 4.47, N, 4.91.

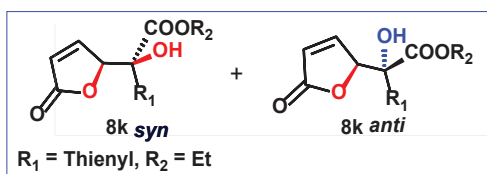
Derivative 8j



Prepared according to the general procedure from **7j**, 2-(trimethylsilyloxy)furan **6**

and catalyst **10**. The residue was purified by flash column chromatography on silica gel (Hexane/EtOAc = 80:20) to give *anti* and *syn* diastereomers. Yield: 98% (combined yield of isolated diastereomers); dr = 5/95 (>1/99 after chromatography). The spectroscopic data for *anti*-**8j** isomer matched those reported in literature²¹¹. Isolated as a yellow oil. The spectroscopic data for *syn*-**8j** isomer matched those reported in literature²¹¹. Isolated as an orange solid.

Derivative 8k



Prepared according to the general procedure from **7k**, 2- (trimethylsilyloxy)furan **6** and catalyst **10**. The residue was purified by flash column chromatography on silica gel (Hexane/EtOAc = 85:15) to give *anti* and *syn* diastereomers. Yield: 80% (combined yield of isolated diastereomers); dr = 46/54 (unchanged after chromatography).

The spectroscopic data for *anti*-**8k** isomer matched those reported in literature²¹¹. Isolated as a yellow oil. *Syn*-**8k**: Isolated as a white solid. m.p.: 95-96 °C. ¹H NMR (300 MHz, CDCl₃, 298 K): δ = 1.37 (t, 3H, J = 7.1 Hz, -OCH₂CH₃), 4.22 (s, 1H, OH), 4.34-4.44 (m, 2H, -OCH₂CH₃), 5.62 (br, 1H, -CH), 6.20 (dd, 1H, J₄ = 2.0 Hz, J₃ = 5.8 Hz, =CH), 7.05 (dd, 1H, J₄ = 3.7 Hz, J₃ = 5.1 Hz, =CH), 7.13 (dd, 1H, J₄ = 1.5 Hz, J₃ = 5.8 Hz, =CH), 7.24-7.26 (m, overlapped with residual signal of CHCl₃ in CDCl₃), 7.34 (dd, 1H, J₄ = 1.2 Hz, J₃ = 5.1 Hz, =CH). ¹³C NMR (75 MHz, CDCl₃, 298 K): δ = 14.1 (CH₃), 64.1 (CH₂), 77.4 (C), 86.4 (CH), 124.1 (CH), 125.3 (CH), 126.6 (CH), 127.8 (CH), 140.5 (C), 151.3 (CH),

170.8 (C), 172.4 (C). HRMS (ESI-FTICR), calcd for C₁₂H₁₂O₅Na: 291.02976 [M + Na⁺], found: 291.02979. EA (%) for C₁₂H₁₂O₅Na: calc. C 53.72, H 4.51, S 11.95, found C 53.81, H 4.45, S 12.83.

Kinetics of VMAR between 7a and 6 in presence of 10 in organic solvents

Medium	Time	Conversion
Toluene	4	39
-----	8	39
-----	14	43
-----	18	45
CH ₂ Cl ₂	4	31
-----	8	38
-----	14	50
-----	18	50
THF	4	25
-----	8	49
-----	14	64

-----	18	64
CH ₃ OH	4	10
-----	8	26
-----	14	70
-----	18	70

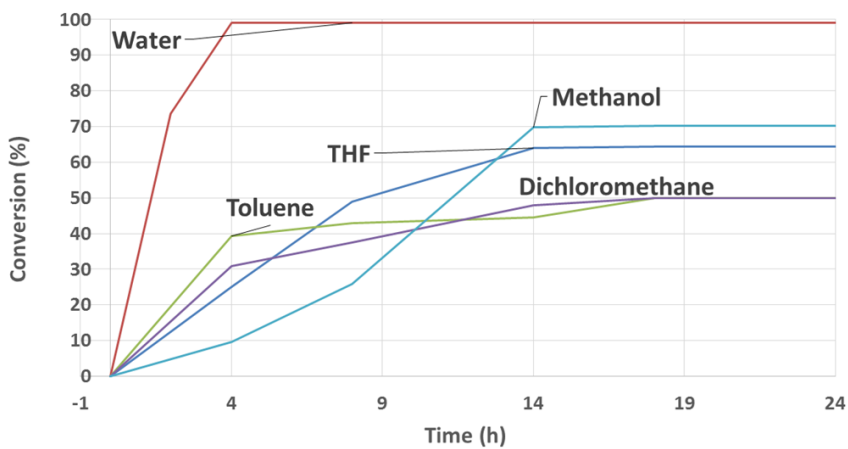


Figure S3. Up: kinetics of the VMAR between ketoester **7a**, silyloxyfuran **6** and catalyst **10** in presence of several organic solvents; bottom: graphical comparison between reaction performed *on water* and *in organic solvents*.

Recycling experiments of the VMAR between **7a** and **6** catalyzed by tetraminocalixarene **10** under optimized reaction conditions.

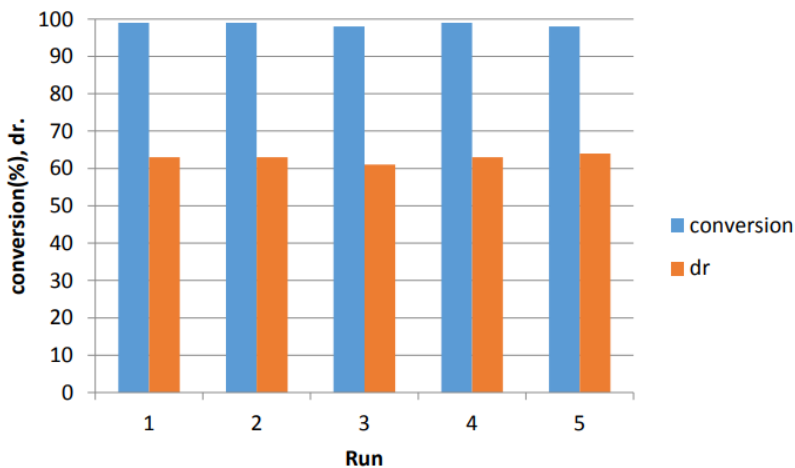


Figure S4. Recycling experiments for the reaction between **6** and **7a** promoted by **10**. As can be seen, catalytic efficiency, both in terms of yield and diastereoselectivity, were maintained for 5 cycles.

¹H NMR titrations of **7a and **7i** with catalyst **10****

The following standard procedure was used. Host solution: a 6.1 mM CDCl₃ solution of catalyst **10** was prepared (1.00 mL). In 0.5 mL of host solution, α -ketoester **7a** was dissolved (solution **7a**). 0.5 mL of host solution, in a NMR tube, was titrated with solution **7a** in the concentration range indicated below. [**10**] = 6.1 mM. [**6a**] range during titration: 0.00-9.40 mM. In 0.5 mL of host solution, derivative **7i** was dissolved (solution **7i**). 0.5 mL of host solution, in a NMR tube, was titrated with solution **6i** in the concentration range indicated below. [**10**] = 6.1mM. [**7i**] range during titration: 0.00-8.98 mM. The titration data were analyzed by nonlinear least-squares fitting procedures³⁰⁴ and in all cases a good fit of the experimental data with the theoretical model confirmed the 1:1 stoichiometry of the complexes.

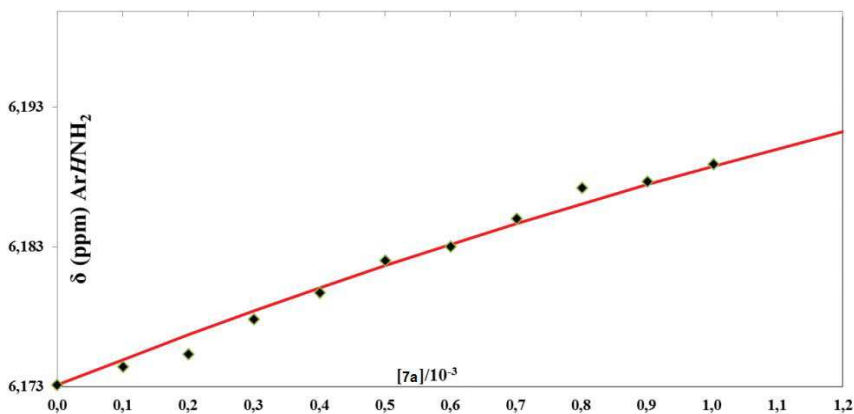


Figure S5. Plot of δ (ppm) for ArHNH₂ proton of **10** as a function of the concentration of **7a** (CDCl₃, 298 K, 400 MHz).

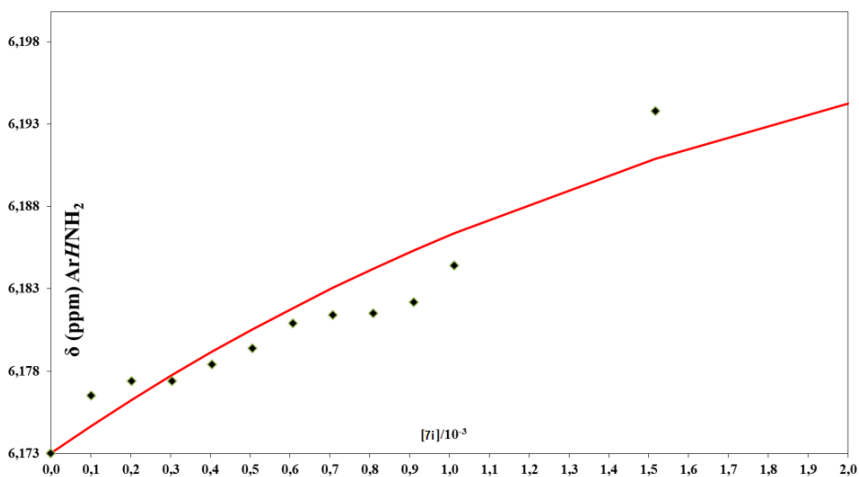


Figure S6. Plot of δ (ppm) for ArHNH₂ proton of **10** as a function of the concentration of **7i** (CDCl₃, 298 K, 400 MHz).

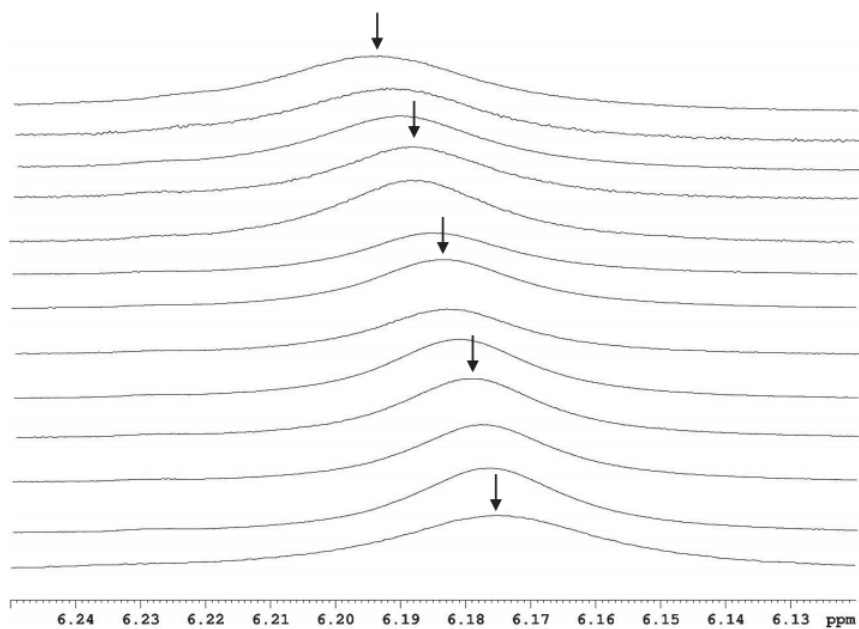


Figure S7. Titration of **10** with **7a**. Aromatic region of the ¹H NMR spectrum (600 MHz, 298 K, CDCl₃) of **10** after addition of **7a** ([**7a**] concentration range during titration: 0.00-9.40 mM, from bottom to top).

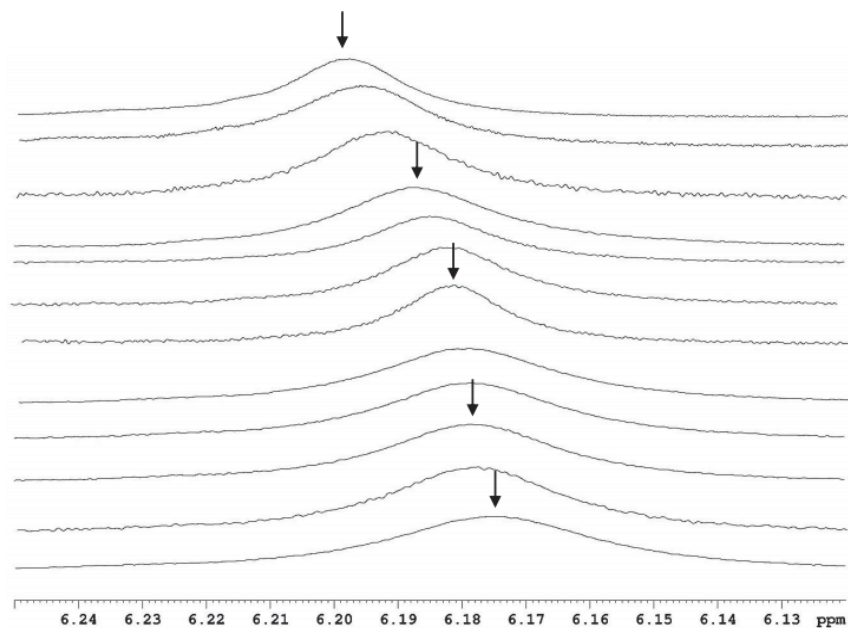


Figure S8. Titration of **10** with **7i**. Aromatic region of the ^1H NMR spectrum (600 MHz, 298 K, CDCl_3) of **10** after addition of **7i** ($[\text{7i}]$ concentration range during titration: 0.00-8.98 mM, from bottom to top).

8b, syn	
diastereomer	
CCDC code	CCDC 1523709
Formula	C ₁₄ H ₁₄ O ₅
Formula weight	262.25
Temperature (K)	100
Wavelength (Å)	0.7
Crystal system	Monoclinic
Space group	P2 ₁ /c
<i>a</i> (Å)	11.8770 (12)
<i>b</i> (Å)	7.9880 (13)
<i>c</i> (Å)	13.7400 (11)
α (°)	90
β (°)	102.046 (3)
γ (°)	90
<i>V</i> (Å ³)	1274.9 (3)
<i>Z</i> , ρ_{calc} (g·mm ⁻³)	4, 1.366
μ (mm ⁻¹)	0.104
<i>F</i> (000)	552
Data collection θ range	2.967 – 29.103
Refl. Collected / unique	20966 / 3399
<i>R</i> _{int}	0.0358
Completeness (%)	99.3
Refinement method	FMLS on <i>F</i> ²
Data/Restraints/Parameters	3399/ 0 / 175
Goof	1.114
<i>R</i> ₁ , <i>wR</i> ₂ [<i>I</i> >2 σ (<i>I</i>)]	0.0425, 0.108
<i>R</i> ₁ , <i>wR</i> ₂ all data	0.0432, 0.1088
Largest. Diff. peak/hole (e. Å ⁻³)	0.457 / -0.345

Table S1. Crystallographic data for compound **8b**, *syn* diastereomer.

8g, syn	
diastereomer	
CCDC code	CCDC 1523706
Formula	C ₁₄ H ₁₃ ClO ₅
Formula weight	296.69
Temperature (K)	100
Wavelength (Å)	0.7
Crystal system	Monoclinic
Space group	P2 ₁ /n
<i>a</i> (Å)	11.6510 (5)
<i>b</i> (Å)	11.4870 (19)
<i>c</i> (Å)	20.733 (2)
α (°)	90
β (°)	104.181 (4)
γ (°)	90
<i>V</i> (Å ³)	2690.2 (5)
<i>Z</i> , ρ_{calc} (g·mm ⁻³)	8, 1.465
μ (mm ⁻¹)	0.282
<i>F</i> (000)	1232
Data collection θ range	1.811 – 29.998
Refl. Collected / unique	50687 / 8125
<i>R</i> _{int}	0.0319
Completeness (%)	98.8
Refinement method	FMLS on <i>F</i> ²
Data/Restraints/Parameters	8125 / 0 / 366
Goof	1.056
<i>R</i> ₁ , <i>wR</i> ₂ [<i>I</i> > 2 σ (<i>I</i>)]	0.0346, 0.0906
<i>R</i> ₁ , <i>wR</i> ₂ all data	0.0359, 0.0918
Largest. Diff. peak/hole (e. Å ⁻³)	0.53 / -0.507

Table S2. Crystallographic data for compound **8g**, *syn* diastereomer.

8h, <i>syn</i> diastereomer	
CCDC code	CCDC 1523708
Formula	C ₁₅ H ₁₈ O ₅
Formula weight	276.28
Temperature (K)	100
Wavelength (Å)	0.7
Crystal system	Monoclinic
Space group	P2 ₁ /n
<i>a</i> (Å)	11.6550 (10)
<i>b</i> (Å)	11.401 (3)
<i>c</i> (Å)	20.9880 (19)
α (°)	90
β (°)	104.186 (2)
γ (°)	90
<i>V</i> (Å ³)	2703.8 (8)
<i>Z</i> , ρ_{calc} (g·mm ⁻³)	8, 1.357
μ (mm ⁻¹)	0.097
<i>F</i> (000)	1168
Data collection θ range	1.807 – 28.218
Ref. Collected / unique	44172 / 6718
<i>R</i> _{int}	0.0294
Completeness (%)	96.2
Refinement method	FMLS on <i>F</i> ²
Data/Restraints/Parameters	6718 / 0 / 368
Goof	1.036
<i>R</i> ₁ , <i>wR</i> ₂ [<i>I</i> > 2 σ (<i>I</i>)]	0.0384, 0.1007
<i>R</i> ₁ , <i>wR</i> ₂ all data	0.0391, 0.1015
Largest. Diff. peak/hole (e. Å ⁻³)	0.471 / -0.244

Table S3. Crystallographic data for compound **8h**, *syn* diastereomer.

8i, <i>syn</i> diastereomer	
CCDC code	CCDC 1523707
Formula	C ₁₅ H ₁₃ N O ₅
Formula weight	287.26
Temperature (K)	100
Wavelength (Å)	0.7
Crystal system	Orthorhombic
Space group	Pn2 ₁ a
a (Å)	10.278 (1)
b (Å)	10.413 (2)
c (Å)	12.405 (1)
α (°)	90
β (°)	90
γ (°)	90
V (Å ³)	1327.6 (2)
Z, ρ _{calc} (g.mm ⁻³)	4, 1.437
μ (mm ⁻¹)	0.104
F (000)	600
Data collection θ range	2.515 – 29.983
Refl. Collected / unique	24594 / 3912
R _{int}	0.0269
Completeness (%)	96.3
Refinement method	FMLS on F ²
Data/Restraints/Parameters	3912 / 0 / 193
Goof	1.056
R ₁ , wR ₂ [I>2σ(I)]	0.0278, 0.0764
R ₁ , wR ₂ all data	0.0277, 0.0767
Is shift su max/mean	0.001 / 0
Largest. Diff. peak/hole (e. Å ³)	0.043 / -0.19
Absoulte structure parameter (Flack)	0.03 (9)

^a Full-matrix least-squares (FMLS) on F²

Table S4. Crystallographic data for compound **8i**, *syn* diastereomer.

8k, <i>syn</i> diastereomer	
CCDC code	CCDC 1523710
Formula	C ₁₂ H ₁₂ S O ₅
Formula weight	268.28
Temperature (K)	100
Wavelength (Å)	0.7
Crystal system	Monoclinic
Space group	P2 ₁ /c
<i>a</i> (Å)	11.4260 (8)
<i>b</i> (Å)	8.0080 (7)
<i>c</i> (Å)	13.8850 (13)
α (°)	90
β (°)	103.063 (6)
γ (°)	90
<i>V</i> (Å ³)	1237.6 (2)
<i>Z</i> , ρ_{calc} (g·mm ⁻³)	4, 1.44
μ (mm ⁻¹)	0.257
<i>F</i> (000)	560
Data collection θ range	1.83 – 28.689
Refl. Collected / unique	19220 / 3168
<i>R</i> _{int}	0.0436
Completeness (%)	99.2
Refinement method	FMLS on <i>F</i> ²
Data/Restraints/Parameters	3168/ 0 / 166
GooF	1.16
<i>R</i> ₁ , w <i>R</i> ₂ [<i>I</i> > 2 σ (<i>I</i>)]	0.0463, 0.12
<i>R</i> ₁ , w <i>R</i> ₂ all data	0.04634, 0.12
Largest. Diff. peak/hole (e. Å ⁻³)	0.384 / -0.839

Table S5. Crystallographic data for compound **8k**, *syn* diastereomer.

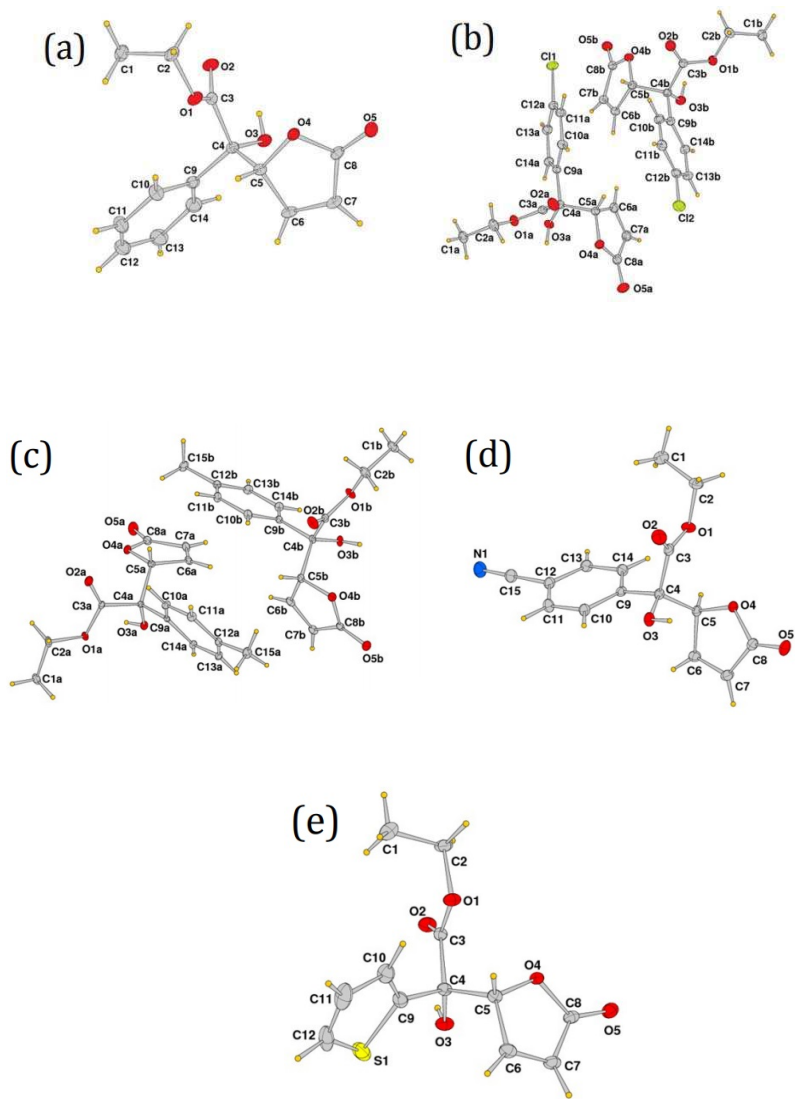


Figure S9. Ellipsoid plots at 50% probability for γ -hydroxybutenolides **8b** (a), **8g** (b), **8h** (c), **8i** (d) and **8k** (e).

5.4 General procedures for the asymmetric 1,3-DC of nitrones to α,β -unsaturated aldehydes promoted by hexameric resorcinarene capsule

The progress of the cycloaddition reaction was controlled after 4 h, 16 h, 48 h and 72 h and was monitored following ^1H NMR signals associated with nitrones. The reaction was stopped after consumption of nitrone or when its conversion reached a plateau. Enantiomeric excess value was determined by HPLC analysis by converting the mixture of isoxazolidines to the corresponding alcohols.

Reaction monitoring

30 μL of the reaction solution in vial was preleved, diluted with 420 μL of CDCl_3 and the reaction progress was monitored by ^1H NMR.

General procedure for 1,3-dipolar cycloaddition reaction without capsule

Catalyst **20** (32.5 μmol , 0.2 eq.) was weighed into 4 mL vial and water saturated deuterated chloroform (1.1 mL) was added. Next, aldehyde **17** (975.6 μmol , 6 eq.) was added, followed by nitrone **16** (162.6 μmol , 1 eq.). The vial was thermostatted at 30 $^\circ\text{C}$ and maintained under vigorous stirring for an appropriate time. The progress of the reaction was monitored by ^1H -NMR analysis by periodically sampling from the reaction mixture at different times. The reaction mixture was concentrated under reduced pressure and purified by flash chromatography on silica gel (Hexane/Ethyl Acetate, from 90:10 to 80:20) to give the title compounds as a mixture of isoxazolidines **18** and **19**. Regioisomeric and diastereomeric ratios were determined by ^1H NMR analysis in comparison with literature data. The determination of enantiomeric purity was performed by HPLC analysis after reduction of the formyl group with NaBH_4 and by comparison with literature^{254,255,258,262}.

General procedure for 1,3-dipolar cycloaddition experiment with capsule

Resorcinarene **14** (281.6 mg, 254.7 μmol , 1.56 eq.) was weighed in a 4 mL vial. Then, 1.1 mL of water saturated deuterated chloroform was added and the mixture was homogenized in an ultrasonic water bath at 40°C for 10 min. To this clear reddish solution, catalyst **20** (32.6 μmol , 0.2 eq.) was added and the solution was stirred at 30°C for 10 minutes. Later, the aldehyde **17** (975.6 μmol , 6 eq.) was added and the reaction mixture was stirred at 30°C for other 10 minutes. Finally, nitrene **16** (162.6 μmol , 1 eq.) was introduced and the reaction system was kept at 30°C under stirring at 1400 rpm for the appropriate time. The reaction was monitored by ^1H NMR analysis taking aliquots of the reaction mixture at various time intervals and diluting with water saturated deuterated chloroform. The reaction was stopped pouring the solution in a 50 mL Eppendorf conical tube and diluting with 0.13% (v/v) DMSO in *n*-hexane (35 mL). The tube was placed in a freezer at -20°C for at least 3 h and successively centrifugated at 1750 rpm for 10 minutes. The diluted reaction mixture was subjected three times to this procedure. Finally, the clear solution was removed and concentrated under reduced pressure. The oily residue thus obtained was purified by flash chromatography on silica gel (Hexane/Ethyl Acetate, from 90:10 to 80:20) to afford the desired title compounds as an inseparable mixture of isoxazolidines **18** and **19**. Regioisomeric and diastereomeric ratios were determined by ^1H NMR analysis via integration of the aldehydic proton signal of the title compounds in comparison with literature data^{254,255,258,262}.

General procedure for reduction of the mixture of isoxazolidine adducts

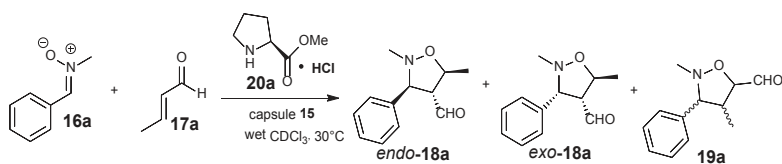
To a solution of compounds **18** and **19** (0.15 mmol) in EtOH (2 mL), NaBH_4 (0.45 mmol, 3 eq.) was added and the resulting mixture was stirred at 30 °C for 75 min. The reaction was quenched by the addition of deionized H_2O (10 mL), then EtOH was

removed under reduced pressure and the residue was extracted with EtOAc (3 x 15 mL). The combined organic phases were dried over Na₂SO₄, filtered and concentrated under reduced pressure. The colorless oil thus obtained was passed through a short plug of silica gel in CH₂Cl₂ to give the corresponding purified alcohols.

Control experiments with different aldehyde/nitrone ratios

A study to optimize the ratio aldehyde/nitrone was performed between aldehyde **17a** and nitrone **16a** in the presence of catalyst **20a**.

Table S6. Optimization of the aldehyde/nitrone ratio^a



Run	17a/ 16a	Capsule 15	Yield (%) ^b	endo-18a:exo-18a: 19a ^c	ee (%) endo- 18a ^d	ee (%) exo- 18a ^d	Δee (%) endo- 18a	Δee (%) exo-18a
1	1/2.2	No	39	50:50:0	11(4S)	24 (3R)		
2	1/2.2	Yes	82	62:25:13	26 (4R)	-	37	24
3	1/1.2	No	45	64:36:0	15(4S)	20(3R)		
4	1/1.2	Yes	83	61:21:18	20(4R)	-	35	20
5	2/1	No	45	49:48:3	11(4S)	20(3R)		
6	2/1	Yes	83	64:28:8	46(4R)	-	57	20
7	4/1	No	44	50:50:0	10(4S)	8(3R)		
8	4/1	Yes	88	69:29:2	57 (4R)	8(3S)	67	16
9	6/1	No	42	24:67:9	14 (4S)	7(3R)		
10	6/1	Yes	88	85:1:14	43(4R)	-	57	7

^aReactions were performed on a 0.16 mmol scale using **20a** (0.2 equiv.) and capsule **15** (0.26 equiv.) in water saturated CDCl₃ (1.1 mL) under stirring for 4h at 30°C.

^b Isolated yield. ^c Determined by ¹H NMR spectroscopy of the crude reaction mixture after removing resorcinarene. ^d Determined by HPLC analysis after borohydride reduction to the corresponding alcohol according to literature data^{254,255,258,262}.

Control experiments on the role played by hexameric resorcinarene capsule **15**

*1,3-dipolar cycloaddition reaction without catalyst **20a***

In a control experiment, the cycloaddition reaction between **17a** and **16a** was performed in the absence of proline catalyst **20a** to assess the catalytic activity of the capsule alone.

Resorcinarene **14** (254.7 μmol , 1.56 eq.) was weighed in a 4 mL vial and water saturated deuterated chloroform (1.1 mL) was added. The mixture was homogenized in an ultrasonic water bath at 40°C for 10 min before adding **17a** (975.6 μmol , 6 eq.). After another 10 minutes at 30 °C, **16a** (162.6 μmol , 1 eq.) was added. The reaction mixture was thermostatted at 30°C and stirred at 1400 rpm for the appropriate time (Table S7). The reaction was stopped by adding *n*-hexane (35mL) containing 0.13% (v/v) DMSO, centrifuged and decanted (need 3 cycles). The conversion, regio- and diastereo-isomeric ratios were determined by ¹H-NMR analysis of the clear reaction solution^{254,255,258,262}. The determination of enantiomeric purity was performed by HPLC analysis after reduction of the formyl group with NaBH₄ and by comparison with literature^{254,255,258,262}.

Table S7. Control reactions with and without proline **20a**

20a	Time (h)	Yield (%)^a	<i>endo-18a:exo-18a: 19a^b</i>	ee (%) <i>endo-18a^c</i>	ee (%) <i>exo-18a^c</i>
No	24	23	14:86:0	0	0
Yes	4	88	85:1:14	43 (4R)	nd

^a Isolated yield. ^b Determined by ¹H NMR spectroscopy of the crude reaction mixture after removing resorcinarene. ^c Determined by HPLC analysis after borohydride reduction to the corresponding alcohol according to literature data^{254,255,258,262}.

This result proves that there is a capsule catalyzed background reaction but with low efficiency, also with prolonged reaction time. Furthermore, no enantioselectivity was found without **20a**.

Control experiment with increasing amount of capsule **15**

In a control experiment, the cycloaddition reaction between **17a** and **16a** was performed in the presence of proline catalyst **20a** and an increased amount of capsule **15** (38 mol%) with respect to **20a**.

Table S8. Comparison between reaction performed with 26% and 38% amount of the capsule

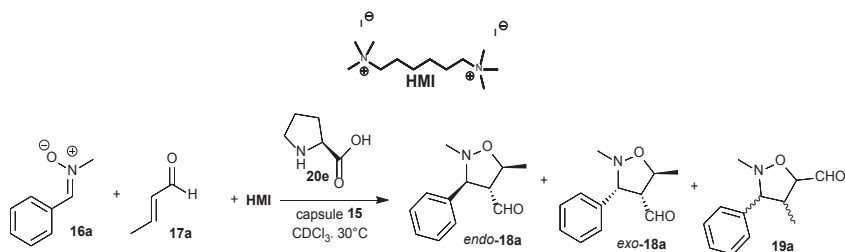
Capsule amount (mol%)	Time (h)	Yield (%) ^b	<i>endo</i> - 18a : <i>exo</i> - 18a : 19a ^c	ee (%) <i>endo</i> - 18a ^d	ee (%) <i>exo</i> - 18a ^d
26%	4	88	85/1/14	43.2 (4 <i>R</i>)	nd
38%	4 ^a	51	52/40/8	53 (4 <i>R</i>)	0

^aAfter 22 h, no changes in conversion, regio- and diastereoselectivity were observed by ¹H NMR analysis.

^bIsolated yield. ^c Determined by ¹H NMR spectroscopy of the crude reaction mixture after removing resorcinarene. ^d Determined by HPLC analysis after borohydride reduction to the corresponding alcohol according to literature data^{254,255,258,262}.

As can be seen in Table S8, increasing amount of capsule **15** leads to a remarkable lower yield, slight decrease in diastereoselectivity and to a light increase in enantioselectivity. This can be explained with a lower probability of **16a**, **20a** and **17a** to meet themselves and so to react inside the capsule.

Control experiment with hexamethonium iodide (HMI) as inhibitor of capsule **15**.



To provide further evidence that the reaction took place within **15**, a control experiment was performed in the presence of a large amount of competitive guest for the capsule as hexamethonium iodide (**HMI**). In fact, Tiefenbacher *et al.*¹⁵⁰ have recently reported that a divalent ammonium salt competes very efficiently with iminium species for encapsulation inside **15**.

To a solution of resorcinarene **14** (254.7 μmol , 1.56 eq.) in water saturated deuterated chloroform (1.1 mL), hexamethonium iodide (**HMI**) (763.8 μmol , 18 eq. respect to resorcinarene capsule) was added. Next, catalyst **20e** (32.6 μmol , 0.2 eq.) was introduced followed by aldehyde **17a** (975.6 μmol , 6 eq.) and, finally, nitron **16a** (162.6 μmol , 1 eq.). The reaction system was kept at 30°C under stirring at 1400 rpm for 4h. The reaction was stopped as specified above.

Table S9. 1,3-cycloaddition reaction with inhibitor **HMI**

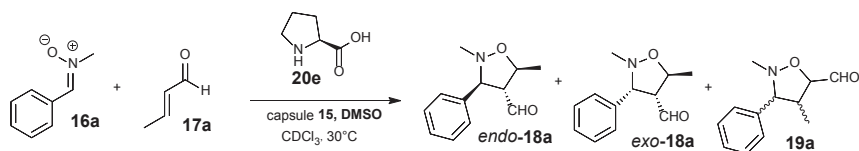
Run	Capsule	Yield(%) ^a	<i>endo-18a:exo-18a:19a</i> ^b	ee (%) <i>endo-18a</i> ^c	ee (%) <i>exo-18a</i> ^c
1	Yes	traces	nd	nd	nd
2	Yes ^d	90	84/14/2	95 (4R)/ 8 (3R)	nd
3	No	traces	nd	nd	nd

^aIsolated yield. ^b Determined by ¹H NMR spectroscopy of the crude reaction mixture after removing resorcinarene. ^c Determined by HPLC analysis after borohydride reduction to the corresponding alcohol according to literature data.^{254,255,258,262} ^dThe reaction was performed without inhibitor **HMI**.

As reported in Table S9, the presence of **HMI** caused the reaction efficiency and selectivity to dramatically decrease to zero in yield (cf entry 1 and 2); the same result was obtained when reaction was performed without capsule. This can be attributed to the blocking of the cavity by **HMI** thus forcing the reaction to be performed outside the capsule.

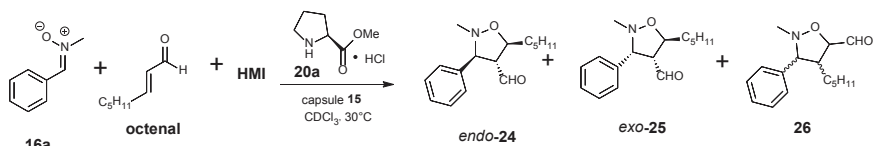
1,3-dipolar cycloaddition in the presence of DMSO

It is reported that DMSO can disrupt the hexameric structure of the capsule thanks to its ability to make hydrogen bonds^{134,150}. So, as a further evidence that the reaction is catalyzed inside the capsule, a reaction in presence of DMSO (90 μ L, 1.27 μ mol) and the capsule (0.42 μ mol) has been performed:



Since catalyst **20e** didn't work without capsule, if catalysis of the reaction is due to the combination of capsule and proline, the reaction with addition of DMSO should not proceed. In fact, with adding DMSO there was no conversion both with capsule or without.

1,3-dipolar cycloaddition with *trans*-2-Octenal



To provide further evidence that the reaction occurs inside the cavity, we performed an additional experiment by using a more elongated aldehyde (2-Octenal) which could prove difficult to enter the host cavity.

When 1,3-dipolar cycloaddition was performed with proline methyl ester hydrochloride **20a** as catalyst (32.5 μmol), octenal (975.6 μmol), nitron **16a** (162.6 μmol) and capsule **15** (26 % mol), no conversion was observed also after 40 h. When the same cycloaddition was performed *without* capsule, 20% conversion was observed by ^1H NMR analysis^{254,255,258,262}. Thus, the unsaturated aldehyde is too large to enter easily inside the capsule, so it is highly improbable the formation of iminium intermediate. Using catalyst **20e**, there was no conversion with or without the capsule.

2D NMR experiments as evidences of encapsulation of reagents inside supramolecular aggregate **15**

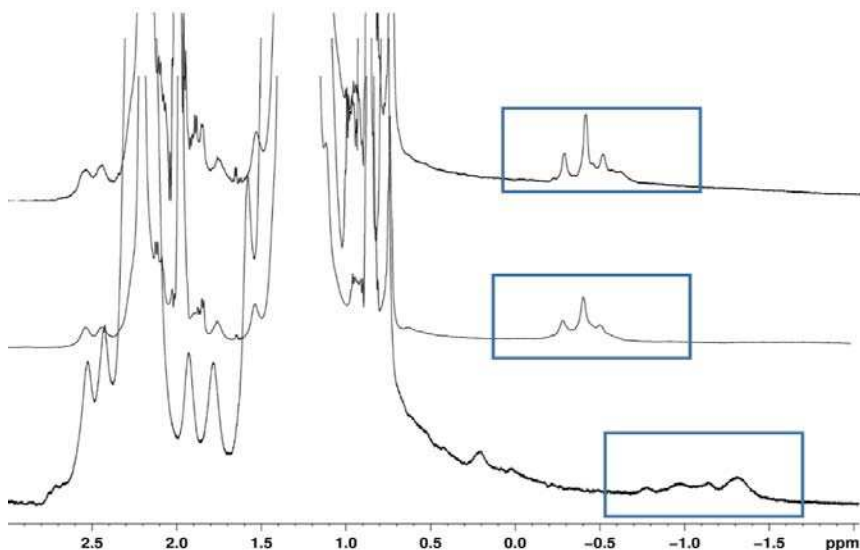


Figure S10. Relevant regions of ^1H NMR spectrum (400 MHz, CDCl_3 , 298 K) showing: L-proline encapsulated (**20e**) (bottom); crotonaldehyde (**17a**) inside the capsule (middle), mixture of **20e** and **17a** (top). As it can be seen, signals pattern at the top is different from patterns at the bottom and middle: this aspect is indicative of the formation of an iminium species, according to Tiefenbacher¹⁵⁰

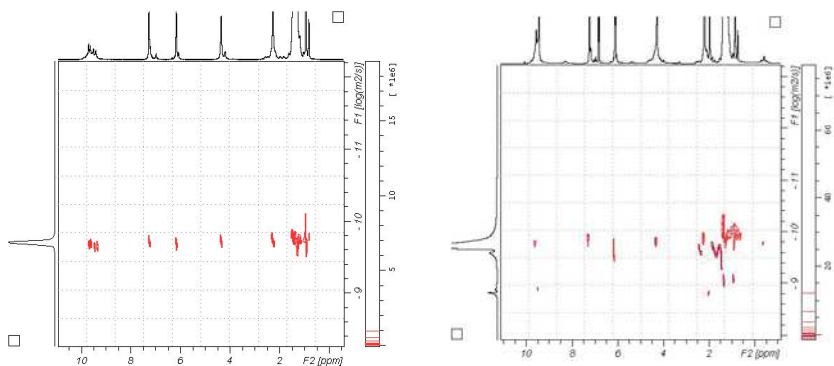


Figure S11. DOSY NMR(600 MHz, CDCl_3 , 298 K) of the capsule **15** at left and of the solution containing capsule **15** and crotonaldehyde **17a** at right.

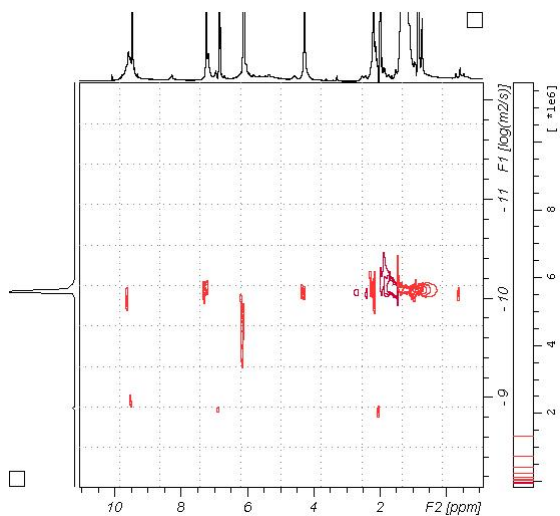


Figure S12. DOSY NMR (600 MHz, CDCl₃, 298 K) of capsule **15** and iminium species **21**.

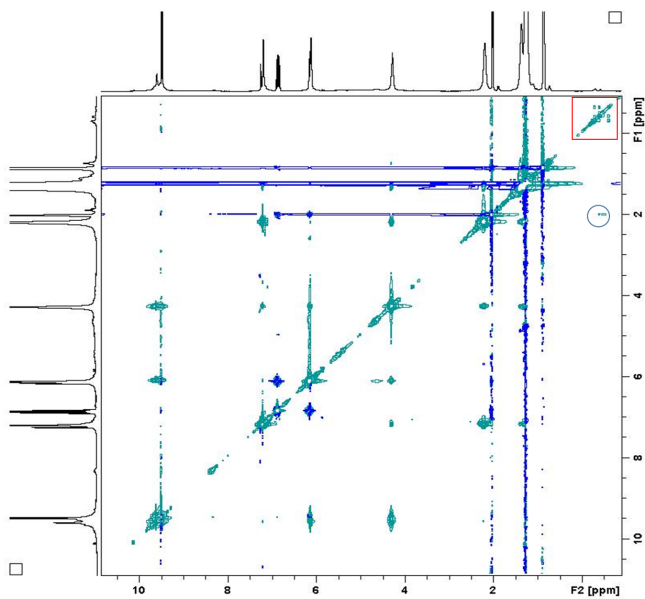


Figure S13. NOESY NMR (400 MHz, 298 K, CDCl₃) of the capsule **15** and iminium species **21**. Exchange peaks

in red square and green circle are showed enlarged in the following figures.

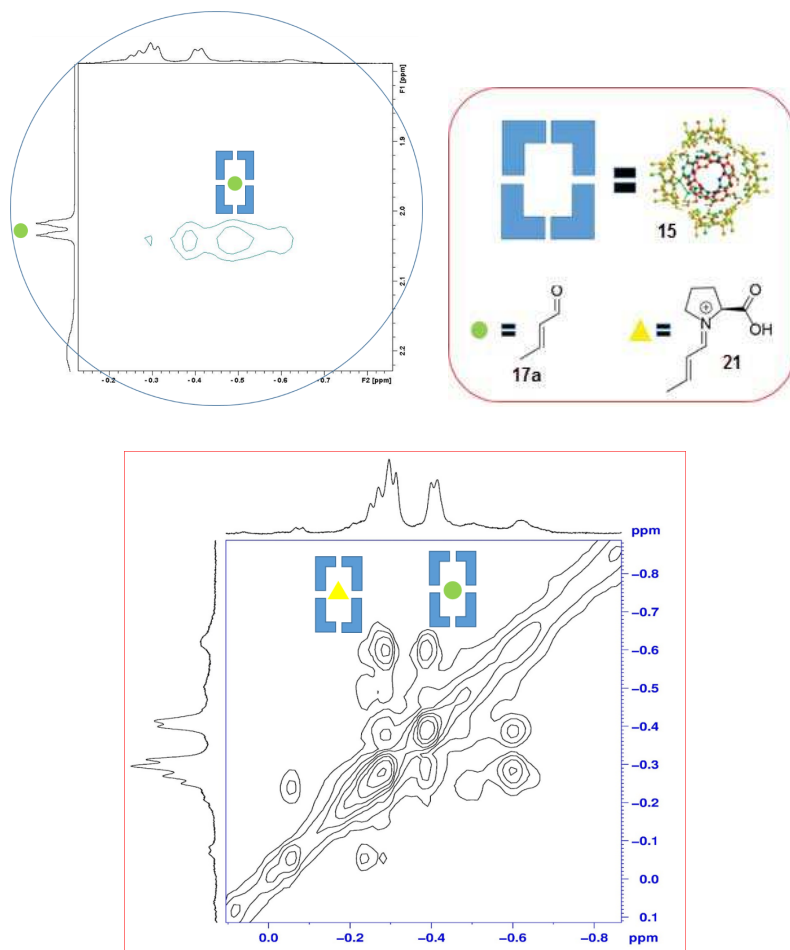


Figure S14. Selected expansions of NOESY NMR spectrum in **Figure S13**. Exchange peaks between aldehyde **17a** *outside* and *inside* the capsule **15** (top) and aldehyde **17a** and iminium species **21** (bottom) are visible.

5.5 General procedures for the FC alkylation inside a self-assembled resorcinarene capsule

General procedure for FC alkylation with capsule 15

Resorcinarene **14** (563.2 mg, 509.3 μmol , 3.12 eq.) was weighed in a 4 mL vial. Then, 1.1 mL of water saturated deuterated chloroform was added and the mixture was homogenized in an ultrasonic water bath at 40°C for 10 min. To this clear yellowish solution, nucleophile (243.9 μmol , 1.5 eq.) was added and the solution was stirred at 30°C for 10 minutes. Later, the electrophile **17** (162.6 μmol , 1.0 eq.) was added and the reaction mixture was vigorously stirred (1400 rpm) at 50°C for the appropriate time. The reaction was monitored by ^1H NMR analysis taking aliquots of the reaction mixture (50 μL) at various time intervals and diluting with water saturated chloroform. The reaction was stopped pouring the solution in a 50 mL Eppendorf conical tube and diluting with 0.13% (v/v) DMSO in *n*-hexane (35 mL). The tube was placed in a freezer at -20°C for at least 3 h and successively centrifugated at 1750 rpm for 10 minutes. The diluted reaction mixture was subjected three times to this process of centrifugation/dilution with *n*-hexane. Finally, the clear solution was removed and concentrated under reduced pressure. The oily residue thus obtained was purified by flash chromatography on silica gel or basic alumina to afford the desired title compounds. Regioisomeric ratios were determined by ^1H NMR analysis via integration of proton signals of the title compounds in comparison with literature data²⁸⁷.

General procedure for FC alkylation without capsule

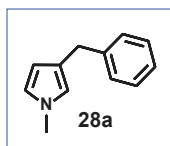
Nucleophile (243.9 μmol , 1.5 eq.) was added into a 4 mL vial containing 1.1 mL of water saturated deuterated chloroform. After stirring the solution for 10 minutes at 30°C, electrophile (162.6 μmol , 1.0 eq.) was added and the solution was vigorously

stirred (1400 rpm) at 50°C for the appropriate time. The progress of the reaction was monitored by $^1\text{H-NMR}$ analysis by periodically sampling from the reaction system at different times.

General procedure for FC alkylation competition experiments

Nucleophile (anisole, thiophene or 1,3-dimethoxybenzene) (243.9 μmol , 1.5 eq.) was added into a 4 mL vial containing 1.1 mL of water saturated deuterated chloroform and resorcinarene (**14**) (563.2 mg, 509.3 μmol). After stirring the solution for 10 minutes at 30°C, mesytilene (243.9 μmol) was added and the solution was stirred for other 10 minutes. Lately, benzyl chloride (162.6 μmol , 1.0 eq.) was added and the solution was vigorously stirred (1400 rpm) at 50°C for the appropriate time. The progress of the reaction was monitored by $^1\text{H-NMR}$ analysis by periodically taking aliquots from the reaction system at different times.

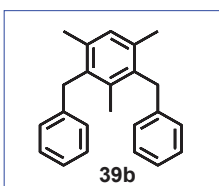
Derivative 28a



Obtained as a clear oil, following general procedure described above for the FC alkylation inside the capsule using *N*-methylpyrrole (**28**) as nucleophile. Purification of the residue after removal of most of the resorcinarene was carried out by column chromatography on basica lumina (Hexane, 95/5 Hexane/ CH_2Cl_2) to give a mixture of regioisomers, mainly constituted by **28a** (96% **28a**, 4% **28b**). Total yield: 22.8 mg, 81%. For the major regioisomer, $^1\text{H NMR}$ (300 MHz, CDCl_3 , 298 K): δ 3.59 (s, 3H, N-CH_3), 3.81 (s, 2H, CH_2 benzylic), 5.97 (t, $J = 2.1$ Hz, 1H, $\text{ArH}_{\text{pyrrole}}$), 6.34 (s, 1H, $\text{ArH}_{\text{pyrrole}}$), 6.52 (t, $J = 2.4$ Hz, 1H, $\text{ArH}_{\text{pyrrole}}$), 7.14-7.28 (m, 5H, $\text{ArH}_{\text{benzylic}}$). $^{13}\text{C NMR}$ (100 MHz,

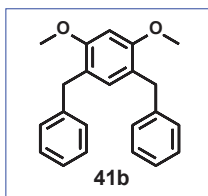
CDCl₃, 298 K): δ 33.8, 36.3, 108.9, 120.1, 122.0, 123.7, 125.9, 128.5, 128.9, 142.7. For the minor regioisomer: ¹H NMR (300 MHz, CDCl₃, 298 K): δ 3.42 (s, 3H, N-CH₃), 3.94 (s, 2H, CH₂ benzylic), 5.90 (s, 1H, ArH_{pyrrole}), 6.07 (t, *J* = 2.9 Hz, 1H, ArH_{pyrrole}), 6.6 (t, *J* = 2.4 Hz, 1H, ArH_{pyrrole}), 7.14-7.30 (m, 5H, ArH_{benzylic}). ¹³C NMR (73 MHz, CDCl₃, 298 K): δ 32.9, 33.9, 77.2, 106.8, 108.2, 126.4, 128.7, 131.5, 139.5. ESI-MS (*m/z*): 171.7 [M+H]⁺.

Derivative 39b



Obtained as a clear oil, following general procedure described above for the FC alkylation inside the capsule using mesitylene (**39**) as a nucleophile. Product has been isolated by semipreparative TLC on silica gel (99.5/0.25/0.25 Hexane/Et₂O/AcOEt) with a yield of 3.4 mg. ¹H NMR (250 MHz, CDCl₃, 298 K): δ 2.1 (s, 3H, ArCH₃), 2.2 (s, 6H, ArCH₃), 4.1 (s, 4H, -CH₂ benzylic), 7.0-7.2 (m, 10H, ArH); ¹³C NMR (62.5 MHz, CDCl₃, 298 K): δ 20.5, 29.9, 35.6, 125.8, 128.0, 128.5, 130.1, 134.9, 135.3, 136.5, 140.4. HRMS-ESI (*m/z*): 323.17708 [M+Na]⁺.

Derivative 41b



Obtained as a clear oil, following general procedure described above for the FC alkylation inside the capsule using 1,3 dimethoxybenzene (**41**) as a nucleophile. Product has been isolated by semipreparative TLC on silica gel (99/1 Hexane/Et₂O) with a yield of 3.2 mg. **¹H NMR** (300 MHz, CDCl₃, 298 K): δ 3.8 (s, 6H, -OCH₃), 3.9 (s, 4H, -CH₂ benzylic), 6.5 (s, 1H, ArH), 6.8 (s, 1H, ArH), 7.14-7.23 (m, 10H, ArH); **¹³C NMR** (72.88 MHz, CDCl₃, 298 K): δ 35.4, 55.9, 95.8, 121.3, 125.7, 128.3, 128.8, 132.3, 141.8, 156.9. **HRMS-ESI** (m/z): 341.15097 [M+Na]⁺.


Capsule 15

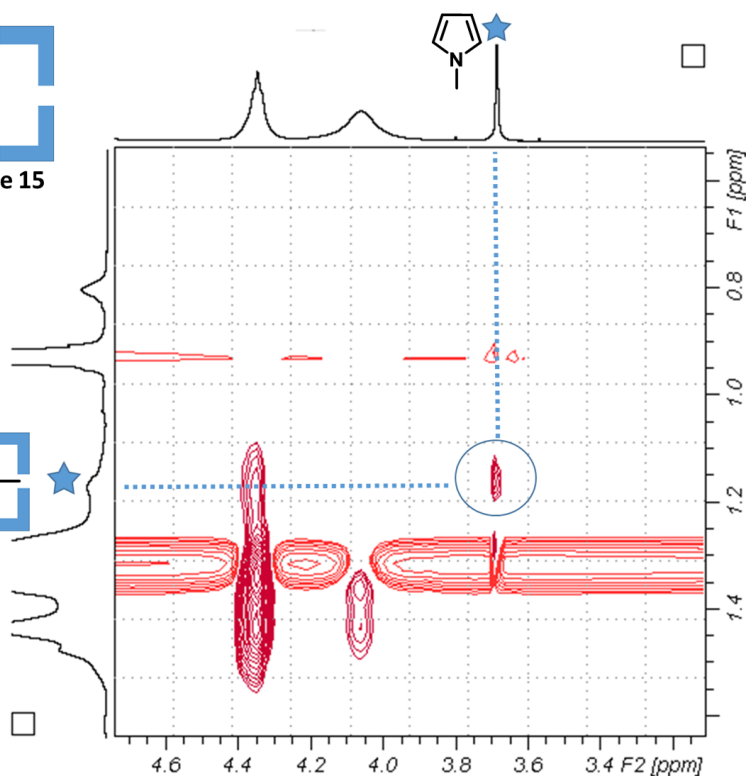
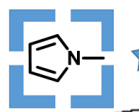


Figure S15. Relevant region of NOESY NMR (400 MHz, $CDCl_3$, 298 K), $d_8 = 250$ ms, spectrum of the mixture of capsule **15** and **28**. Exchange peak between $N-CH_3$ of **28**, outside (3.67 ppm approximately) and inside (1.18 ppm) the capsule **15** (top) is visible.

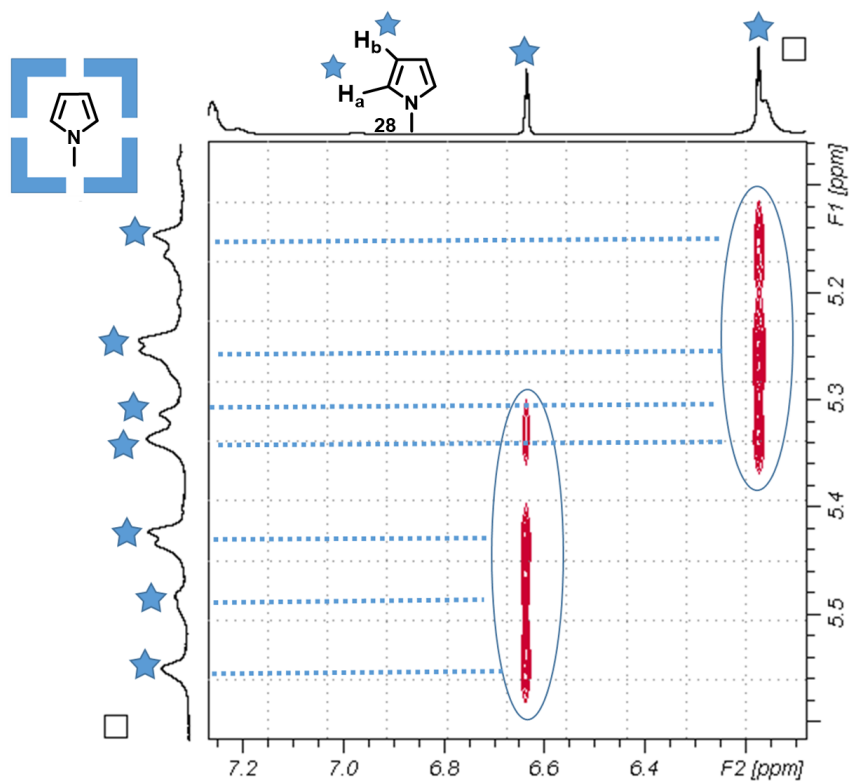


Figure S16. Relevant region of NOESY NMR (400 MHz, CDCl₃, 298 K), d8 = 250 ms, spectrum of mixture of capsule **15** and **28**. Exchange peaks between aromatic protons of **28** *outside* the capsule and *inside* the capsule are visible and are indicated with blue stars.

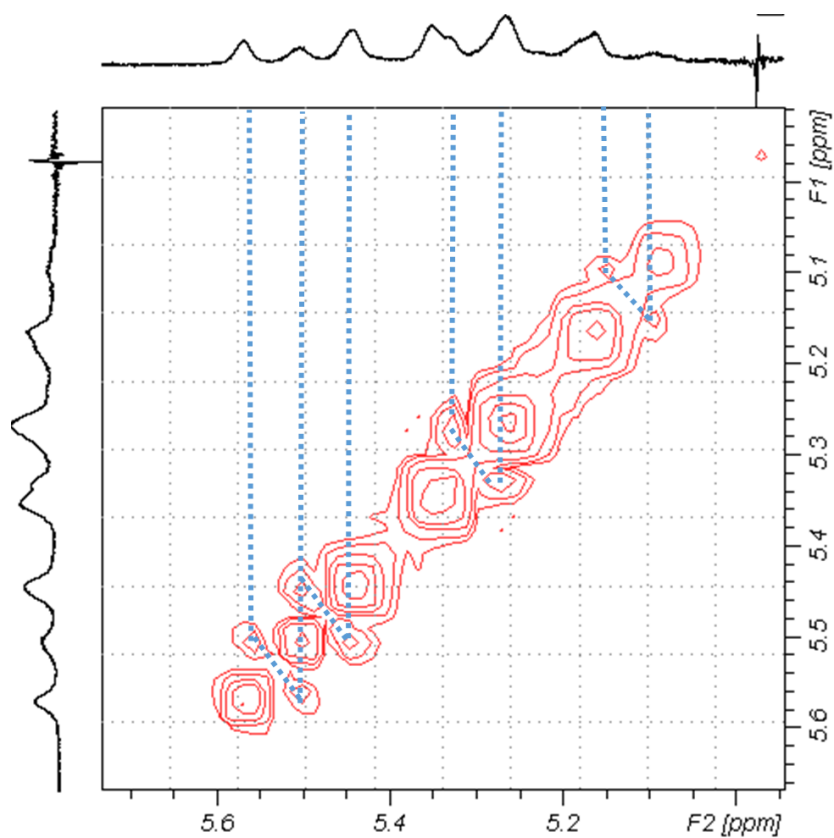


Figure S17. Relevant region of COSY NMR (400 MHz, CDCl₃, 298 K) experiment performed on the mixture of capsule **15** and **28**. As can be seen, the pattern of peaks present in the range 5.1-5.6 ppm shows couplings involving two sets of protons.

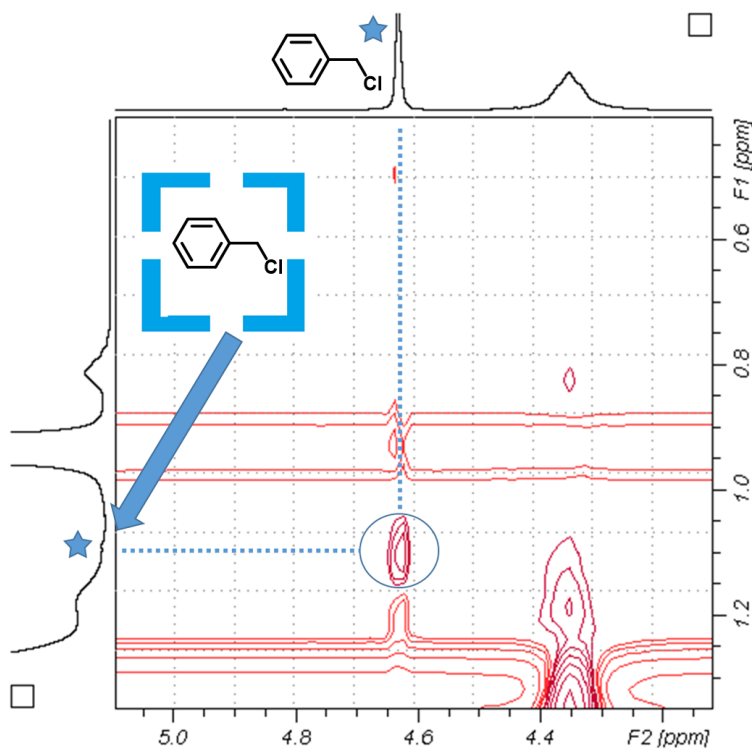


Figure S18. Relevant region of NOESY NMR (600 MHz, CDCl_3 , 298 K) experiment performed on the mixture of capsule **15** and benzyl chloride (**29**). As can be seen, an exchange peak involving CH_2 benzylic protons is visible (indicated with blue star)

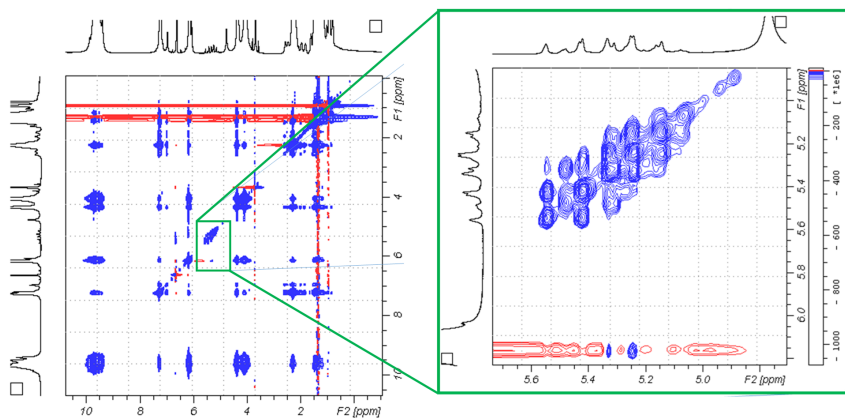


Figure S19. NOESY NMR (600 MHz, CDCl₃, 298 K), d8 = 250 ms, performed on the solution of resorcinarene capsule **15** and *N*-methylpyrrole (**28**). Aromatic proton of pyrrole shows exchange with a set of signals between 5 and 5.6 ppm. This complex pattern, indicative of the presence of diastereoisotopic protons and/or the presence of diverse amounts of pyrrole in the capsules, is shown to be aligned with capsule signals in the following DOSY NMR experiment in **Figure S20**.

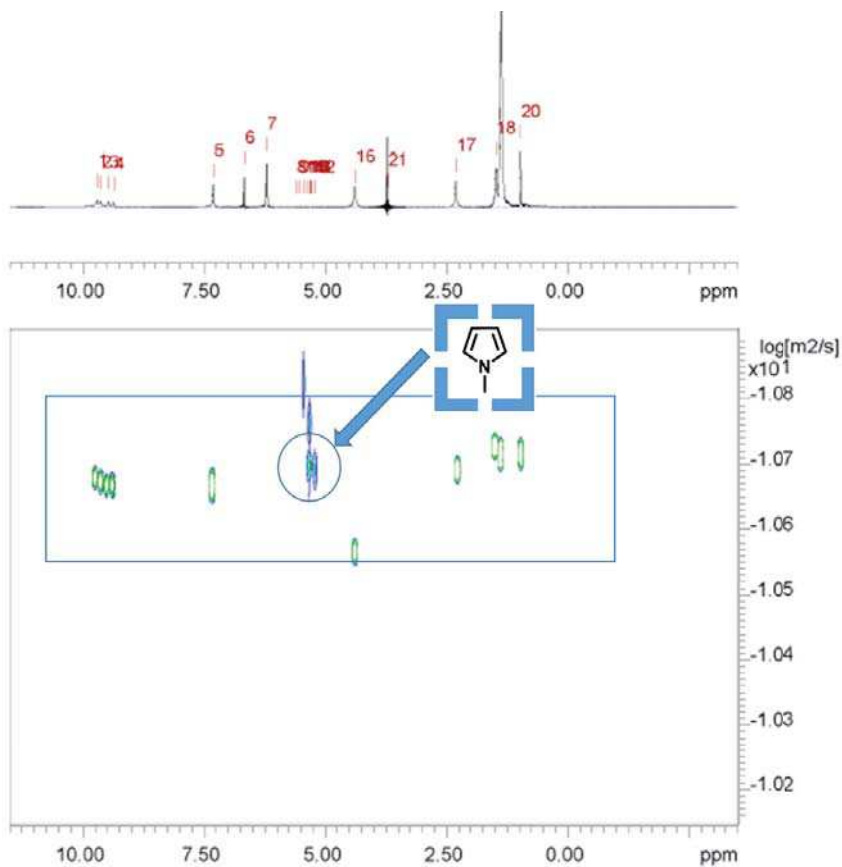


Figure S20. DOSY NMR (600 MHz, CDCl_3 , 298 K) of the solution of resorcinarene capsule **15** and *N*-methylpyrrole (**28**). As can be seen, peaks of signals pattern associated to inside aromatic protons (in the blue circle) of the nucleophile are almost aligned with capsule signals in the rectangle; this, with NOESY experiments illustrated before, turns out to be a proof of the encapsulation of the reagent.

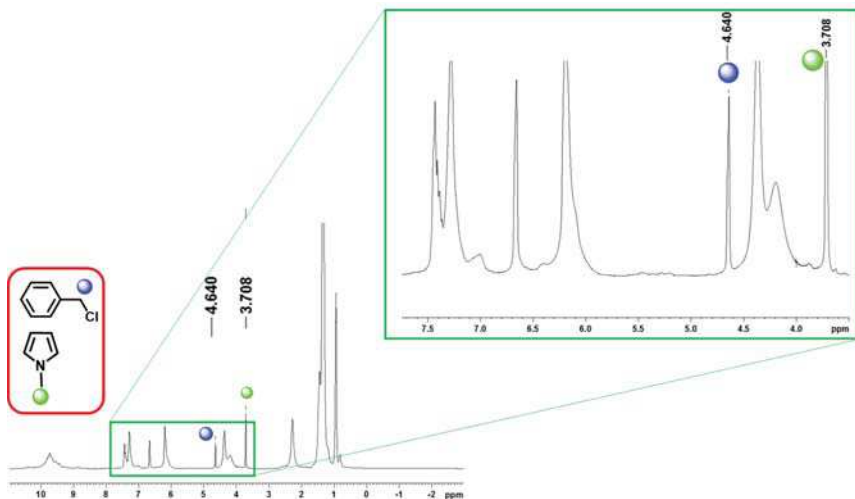


Figure S21. ^1H NMR (400 MHz, CDCl_3 , 298 K) of the solution containing hexameric resorcinarene capsule **15**, *N*-methylpyrrole (**28**) and benzyl chloride (**29**) (in the same ratio used in the model reaction). As can be seen, the signal pattern associated with aromatic protons of encapsulated nucleophile is absent, indicating that adding benzyl chloride this latter begins to react with nucleophile *inside* the capsule, so leading to the disappearance of signals attributed to this latter.

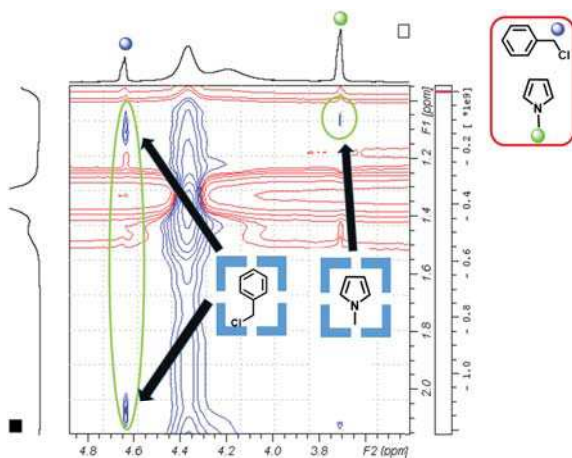
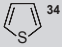
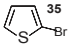
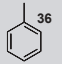
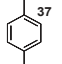
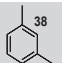
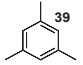
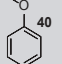
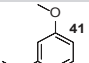
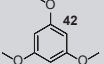
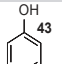
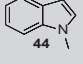
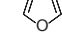


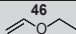
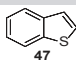
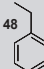
Figure S22. NOESY NMR (400 MHz, CDCl_3 , 298 K), $d_8 = 250$ ms, of the mixture of benzyl chloride (**29**) and *N*-methylpyrrole (**28**) in presence of the capsule **15**. Exchange peaks attributed to the electrophile *inside*

160

(probably diastereotopic benzylic protons) are visible at 4.62 ppm, along with those of the nucleophile, at 3.67 ppm.

Table S10. Exploitation of the nucleophiles for the FC reaction. Time is reported to obtain maximum conversion for the substrates present in the table.

Entry ^a	Nucleophile	Yield (%)	Regioisomer ratio ^b	Time (h)
1		82	2 _{regio} 34a /3 _{regio} 34b 60/40	24
2		91	5 _{regio} 35a /3 _{regio} 35b /4 _{regio} 35c 90/3/7	16
3		90	4 _{regio} 36a /2 _{regio} 36b 80/20	48
4		91	2 _{regio} 37a 100	48
5		91	4 _{regio} 38a /2 _{regio} 38b /5 _{regio} 38c 92.5/5/2.5	16
6		92	39a 93 ^c	4
7		93	4 _{regio} 40a /2 _{regio} 40b 93/7	48
8		92	4 _{regio} 41a 93 ^d	16
9		91	42a 94 ^e	16
10		93	4 _{regio} 19a /2 _{regio} 19b / 19c 61/35/4 ^f	16
11		81	3 _{regio} 20a /2 _{regio} 20b 80/20	16
12		0	-	16

13		0	-	16
14		83	2+3 _{regio} 47a + 47b / 5 _{regio} 23c 91/9	24
15		90	4 _{regio} 48a / 2 _{regio} 48b 85/15	48

^aReaction conditions: electrophile **29** (162.6 μ mol, 1 eq.), nucleophile **34-48** (243.9 μ mol, 1.5 eq.), **14** (509.2 μ mol, 52% mol), T = 50°C, 1.1 mL of water-saturated CDCl₃, t = 16h.^bRegioisomeric ratio was determined by ¹H NMR analysis of the reaction mixture after resorcinarene removal, according with literature data. ^c 7% of dibenzylated product **39b**. ^d 7% of dibenzylated product **41b**. ^e 6% of dibenzylated product **42b**. ^f 4% of dibenzylated product **43c**.

Table S11. Product inhibition experiments for the FC alkylation between *N*-methylpyrrole (**28**) and benzyl chloride (**29**) performed in the presence of the capsule **15** with 0.25 eq. of product **28a** + **28b** (37 mM) as starting material.

Time (h)	0	2	4	6	20	24
Conversion (mM)	40.7	51.7	64.6	73.1	86.4	90

Table S12. Product inhibition experiments for the FC alkylation between *N*-methylpyrrole (**28**) and benzyl chloride (**29**) performed in the presence of the capsule **15** with 0.5 eq. of product **28a** + **28b** (74 mM) as starting material.

Time (h)	0	2	4	6	20	24
Conversion (mM)	74	85.7	93.3	95.9	100.6	101.1

Table S13. Product inhibition experiments for the FC alkylation between *N*-methylpyrrole (**28**) and benzyl chloride (**29**) performed in the presence of the capsule **15** with 0.7 eq. of product **28a** + **28b** (103.4 mM) as starting material.

Time (h)	0	2	4	6	20	24
Conversion (mM)	103.4	103.4	104.4	106.5	109.4	110

Table S14. Product inhibition experiments for the FC alkylation between *N*-methylpyrrole (**28**) and benzyl chloride (**29**) performed in the presence of the capsule **15** with 1.0 eq. of product **28a** + **28b** (147.8 mM) as starting material.

Time (h)	0	2	4	6	20	24
Conversion (mM)	147.8	147.8	148.6	150.1	152.6	153.2

Table S15. Conversions for model reaction between nucleophile (**28**) and electrophile (**29**) (no amount of product **28a** + **28b** was added as starting material) in presence of the capsule **15**.

Time (h)	0	2	4	6	20	24
Conversion (mM)	0	57.6	69.9	73.9	138.7	147.8

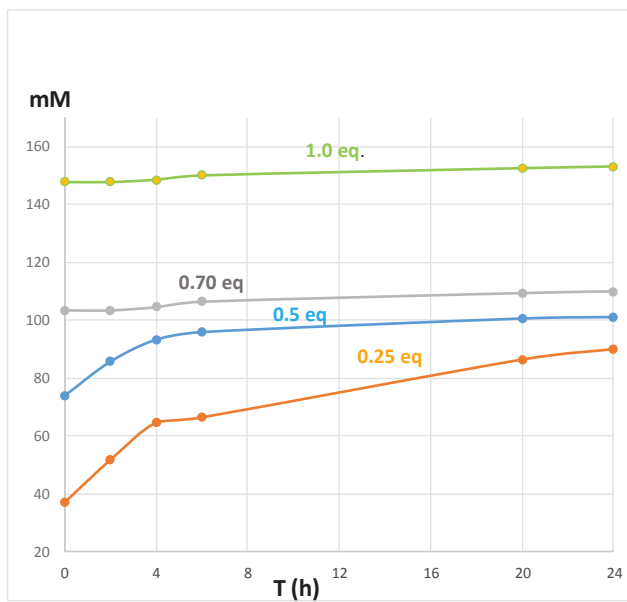


Figure S23. Plot of data for the product inhibition experiments summarized in **Tables S11-14**. As can be seen, bigger is the initial product added to the solution of capsule **15**, *N*-methylpyrrole (**28**) and benzylchloride (**29**), bigger is the decrease in the conversion of the FC reaction.

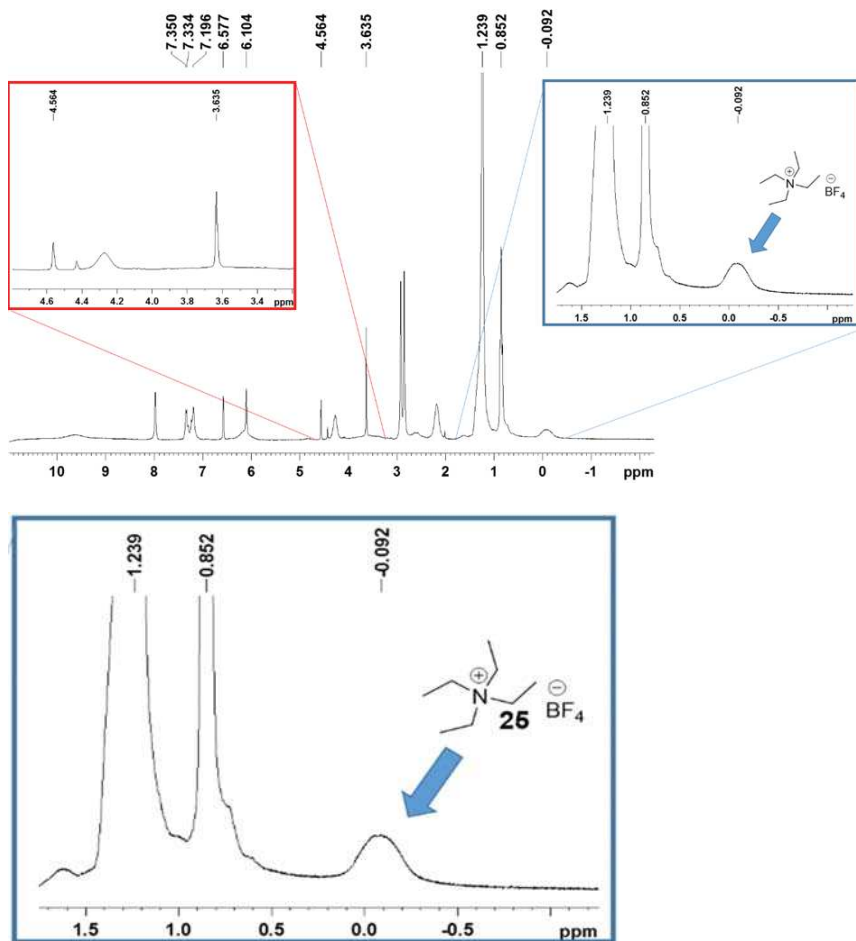


Figure S24. ^1H NMR Spectrum (300 MHz, CDCl_3 , 298 K) of the solution (inhibition experiment) containing **28** (1.5 eq), **29** (1 eq) and capsule **15** (0.52 eq) in presence of $\text{NEt}_4^+\text{BF}_4^-$ (10 eq respect to the resorcinarene capsule, 0.84 mmol). In the red square is visible the absence of signals of products. In the blue square (expanded zone of the NMR spectrum to the bottom), signal relative to encapsulation of salt is present.

The work contained within this thesis is partially described in the following publications:

“Exploiting the hydrophobicity of calixarene macrocycles for catalysis under on-water conditions”

De Rosa, M.; La Manna, P.; Soriente, A.; Gaeta, C.; Talotta, C.; Neri, P., *RSC Adv.*, **2016**, *6*, 91846.

“A simple Tetraminocalix[4]arene as a Highly Efficient Catalyst under On-Water Conditions through Hydrophobic Amplification of Weak Hydrogen Bonds”

De Rosa, M.; La Manna, P.; Soriente, A.; Gaeta, C.; Talotta, C.; Hickey, N.; Geremia, S.; Neri, P., *Chem. Eur. J.*, **2017**, *23*, 7142.

“Supramolecular synthons in the gamma-hydroxybutenolides”

De Rosa, M.; La Manna, P.; Soriente, A.; Gaeta, C.; Talotta, C.; Hickey, N.; Geremia, S.; Neri, P., *CrystEngComm*, **2017**, *19*, 5079.

“The hexameric resorcinarene capsule as an artificial enzyme: ruling the regio and stereochemistry of a 1,3-dipolar cycloaddition between nitrones and unsaturated aldehydes”

La Manna, P.; De Rosa, M.; Talotta, C.; Gaeta, C.; Soriente, A.; Floresta, G.; Rescifina, A.; Neri, P., *Org. Chem. Front.*, Accepted. DOI: 10.1039/C7QO00942A